CYPRUS UNIVERSITY OF TECHNOLOGY
FACULTY OF ENGINEERING AND TECHNOLOGY
DEPARTMENT OF CIVIL ENGINEERING AND GEOMATICS

ESTIMATING EVAPOTRANSPIRATION FOR ANNUAL CROPS IN CYPRUS USING REMOTE SENSING

PAPADAVID CH. GIORGOS

A Dissertation Submitted
in Partial Fulfillment of the Requirements for the Degree of

Doctor of Philosophy

LIMASSOL, 2011

APPROVAL PAGE

Doctor of Philosophy Dissertation

ESTIMATING EVAPOTRANSPIRATION FOR ANNUAL CROPS IN CYPRUS USING REMOTE SENSING

Presented by

Papadavid Ch. Giorgos

Research Supervisor _____
Dr. Hadjimitsis Diofantos

Committee Member (Chairperson) _____
Dr. Loukas Athanasios

Committee Member _____
Dr. Toulios Leonidas

Committee Member _____
Dr. Michaelides Silas

Committee Member _____
Dr. Akylas Evangelos

Cyprus University of Technology

January, 2012

This PhD Thesis is dedicated to my family Katerina, Maria-Eleni and my forthcoming daughter. Their help and understanding was precious for the completion of this project.

ACKNOWLEDGEMENTS

This research project was made possible by the financial support by the Cyprus Research Promotion Foundation, the European Union (Structural Funds) and the Cyprus University of Technology for their funding support. Their contribution is gratefully acknowledged.

I am extremely grateful to my supervisor Associate Professor Diofantos G. Hadjimitsis. His moral support and contribution to this project is inestimable. His guidelines at the impassable points of this Thesis were my 'crutches' to go through.

I am particularly indebted to the Remote Sensing Laboratory of the CUT for providing me with the resources to undertake the ground measurements in the Mandria village, Paphos. Many thanks are also given to the Mandria community and especially Mr. Mitas, for providing me access to their fields and cultivations.

Thanks are also due to Mr Athos Agapiou and Mr Kyriacos Themistocleous for their technical support during this Thesis.

The author is grateful to Katerina Kousoulou and Eirini Charalambous for their support in the writing procedure of this Thesis.

Finally I would like to express my sincere thanks to my Director in Agricultural Research Institute, Dr Dora Chimonidou, for providing me the opportunity to proceed with this PhD thesis, while her preceding Director thought that such thesis was "impossible".

The specific PhD Thesis has been funded by the Cyprus Government and E.U. Structural Funds (ΠΕΝΕΚ/ΕΝΙΣΧ/0308/13 for SUSTAINABLE DEVELOPMENT) through Cyprus Research Promotion Foundation. The project proposal ranked the first place among many other proposals and has been reviewed as an '*ambitious project that could assist Cypriot agriculture'*.

TABLE OF CONTENTS

LIST OF FIGURES

LIST OF TABLES

LIST OF NOTATIONS AND ABBREVIATIONS

NOTATIONS

a – albedo (dimensionless)

C_p – specific heat capacity of the air (J kg^{-1} K^{-1})

d – zero plane displacement height (m)

d – correction coefficient accounting for variation in the sun-to earth distance

dT (K) – temperature difference ($T_a - T_s$) where a is for the air and s is for the foliage

E_0 – solar irradiance at the top of the atmosphere

e – emissivity

e_a – actual vapour pressure (kPa)

ETc – crop evapotranspiration (mm/day)

ETc_{inst} – instantaneous ET (mm/hr)

ET_r - reference crop evapotranspiration (mm/day)

ET_r (24h) – total reference evapotranspiration of the day in mm/day

f(u) - wind speed function

G – soil heat flux (W.m-2),

H – sensible heat flux (W m^{-2}).

H – sensible heat flux (W.m-2)

$K1$ – calibration constant = 666.09 ($W * m^{-2} * ster^{-1} \mu m^{-1}$)

$K2$ – calibration constant = 1282.71 (^{o}Kelvin)

k – von Karman's constant, 0.41 (dimensionless)

K↓ – incoming solar radiation (W/m^2)

K_c - crop coefficient (dimensionless)

L* net longwave radiation (W/m^2)

LAI_{active} – active (sunlit) leaf area index (m^2 (leaf area) / m^2 (soil surface)

LE – latent heat flux from evapotranspiration (W/m^2)

L_λ – spectral radiance ($W * m^{-2} * ster^{-1} \mu m^{-1}$)

L_{ts} – spectral radiance at the sensor

ρ_{ts} – reflectance at the top of the atmosphere

r_{ah} – aerodynamic resistance to heat transport (s/m)

r_l – bulk stomatal resistance of the well-illuminated leaf (s/m)

$R_{L\uparrow}$ – outgoing longwave radiation (W/m^2)

R_n – net radiation (W/m^2)

R_{n24} - 24-h averaged net radiation (W/m^2)

R_{nl} – net outgoing longwave radiation (W/m^2)

r_s – (bulk) surface resistance (s/m)

R_s – incoming shortwave radiation (W/m^2)

T – temperature (^oC or K)

T_s – surface temperature (^oC or K)

U – wind speed (m/s)

u_* – the friction velocity (m/s)

u_2 -wind speed at 2 m height (m/s)

u_x – wind speed (m/s) at height z_x

z_1 and z_2 – heights above the zero plane displacement (d) of the vegetation (m)

z_h – roughness length governing transfer of heat and vapour (m)

z_{om} – momentum roughness length (m)

γ – thermodynamic psychrometric constant (kPa / K)

Δ – slope of the saturated vapor pressure temperature relationship (kPa / K1)

ε_o – surface thermal emissivity (dimensionless)

θ_0 – solar zenith angle (rad)

λ – latent heat of vaporisation of water (J / kg)

λET – latent heat flux (W/m^2)

ρ – air density (kg/m^3),

P - atmospheric pressure (hPa)

ρtg – target reflectance at the ground

ρ_w - water density (kg/m^3),

σ – Stefan-Boltzmann constant ($5.67E^{-08}$ W m^{-2} K^{-4})

ABBREVIATIONS

NDVI – Normalised Difference Vegetation Index

VI – Vegetation Indices

WDD – Water Development Department

NIR – Near Infra Red

SAVI – Soil Adjusted Vegetation Index

WDVI - Weighted Difference Vegetation Index

RSR- Relative Spectral Response

ETM – Enhanced Thematic Mapper

TM – Thematic Mapper

MSS – Multi Spectral Scanner

LAI – Leaf Area Index

SEBAL – Surface Energy Balance Algorithm for Land

CYSEBAL – Modified Surface Energy Balance Algorithm for Land

EB – Energy Balance

MODIS- Moderate Resolution Imaging Spectroradiometer

SWIR – Short Wave Infra Red

PAR – Photosynthetic Active Radiation

SEBI - Surface Energy Balance Index

CWSI - Crop Water Stress Index

SUMMARY

This thesis provides a novel method for estimating crop evapotranspiration (ETc) on a systematic basis using remote sensing techniques. The major aims of the project are to provide accurate estimations of crop evapotranspiration spatially and to create a method where potential users could monitor irrigation water management through ETc estimation, in the future. Landsat-5 TM and Landsat-7 ETM+ images of the area of interest were transformed into crop evapotranspiration maps, in order to retrieve the value of evapotranspiration for each crop.

To reach this goal, ground truth data, meteorological data, remotely sensed data, modelling techniques and energy balance algorithms were employed and combined. Following the phenological stages of each crop, semi-empirical models were developed, regarding the crop canopy factors of each crop. Vegetation Indices were created from spectroradiometric measurements during crops phenological stages. These indices were used to describe the crop canopy factors, namely Leaf Area Index (LAI) and Crop Height (CH). The developed semi-empirical models were found to have strong correlation coefficients. The models were evaluated with very satisfactory results. The models were finally used to modify the algorithms decided to be used in this project, SEBAL and Penman-Monteith adapted to satellite data.

The direct application of the two crop evapotranspiration algorithms has provided close results but with statistically significant difference. When employing the semi-empirical models, for modifying the two algorithms, the results were even closer and without any significant difference. Maps of crop evapotranspiration were created from the satellite images and the corresponding values were retrieved. The method is applicable for any other satellites with different temporal, spatial and spectral resolution.

INTRODUCTION

Water resources include surface water, groundwater, inland water, rivers, lakes, coastal waters and aquifers (Chave, 2001). Water resources are essential to production in primary, secondary and tertiary sectors, as well as to household consumption (UNESCO, 2006). Throughout the years, overexploitation of water resources has led to their degradation and depletion globally. Regarding water quantity, freshwater use increased six-fold within the 20th century while 50% of global wetlands were lost (UN, 2008). In European countries, statistical evidence shows increased pressure on water resources and a decline in their quantity and quality over recent years (SIWI, 2002). Total water abstraction in Europe is expected to decrease by more than 10 % between 2000 and 2030 (EEA, 2007). Climate change is expected to reduce water availability and increase irrigation withdrawals in Mediterranean river basins. Under mid-range assumptions on temperature and precipitation changes, water availability is expected to decline in southern and south-eastern Europe (by 10 % or more in some river basins by 2030). Agriculture is expected to remain the largest water user in the Mediterranean countries, with more irrigation and warmer and dryer growing seasons resulting from climate change (EEA, 2007).

Agriculture occupies 44% of the EU territory and is by far the largest water user in Europe (Massarutto, 2003); it accounts for about one-third of the total water abstraction in Europe, used mostly for irrigation.. Due to its geographic orientation, Europe experiences a wide variability of climates, ranging from the temperate climates of the north to the arid climates around the Mediterranean Sea, which implies diverse farming patterns and crops grown. The importance of irrigation thus increases from north to south, being an essential input for farming in most of the arid and semi-arid regions (Zoumides and Zachariades, 2009). Water withdrawal for irrigation is the largest share of overall water abstraction in southern Europe and will continue to be in future. Continuously improving efficiency in irrigation water use decreases water withdrawal per unit irrigated, but the savings are offset by an increase in the utilized irrigated area, leading to an increase of more than 15% in withdrawals for agriculture (utilized irrigated area is assumed to expand by more than 20% by 2030). However, even if the area under irrigation remains constant over the next 30 years, changing climate conditions alone are estimated to increase irrigation requirements by around 5%. Thus negative changes in water availability are expected to take place especially in northern parts of Europe (Figure 1) (Loukas et al., 2007; 2008).

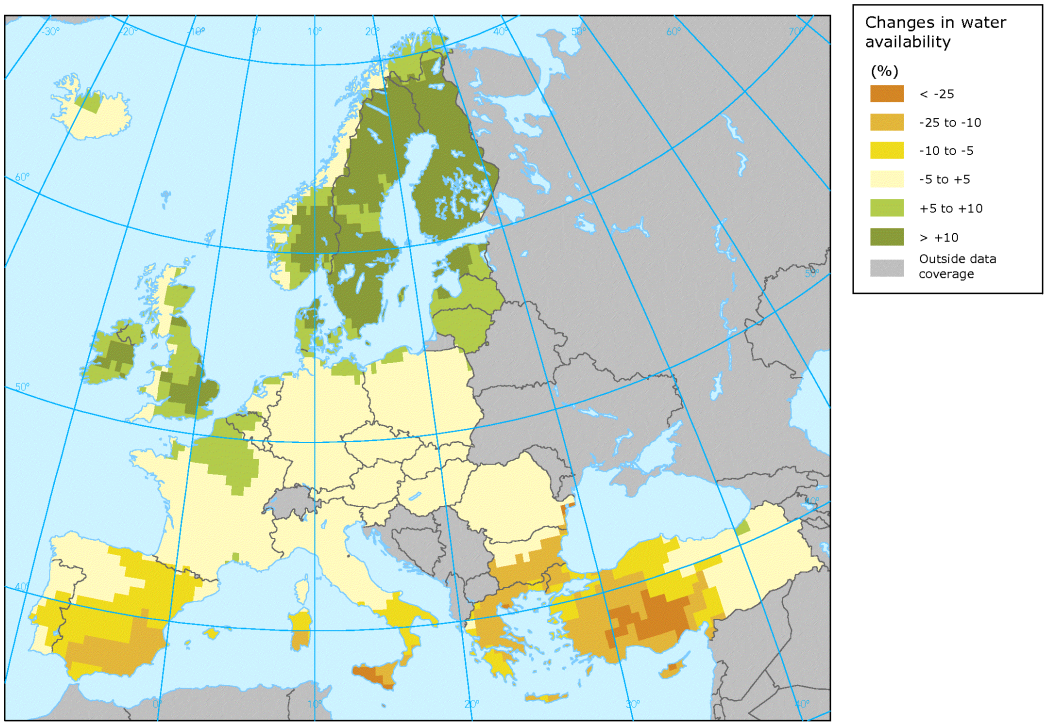

Figure 1: Anticipated changes in water availability by 2030 (EEA, 2007)

In Southern Europe, irrigation accounts for a large proportion of total water usage (83% in Greece, 69% in Cyprus, 69% in Spain, 57% in Italy and 52% in Portugal), whereas, it accounts for less than 10% in the North (Berbel et al., 2007). The constantly rising demand for water revealed its relative shortage, while the absence of integrated policies along with poor management initiated an intensive debate about its sustainable use (Gómez-Limón and Riesgo, 2004). Climate change is expected to put additional pressure on water resources, particularly in the arid and semi-arid regions (EEA, 2007); sustainable water management is therefore an important ingredient of policies for adaptation to climate change. In response to the deterioration of water resources, the European Commission implemented new policies in order to contribute to sustainable, balanced and equitable water use (EC, 2000). Cyprus, as a full member of the EU, bears the obligation to comply with the corresponding policies.

1. Current situation of Agricultural Water Demand in Cyprus

Cyprus is the third largest island in the Mediterranean Sea, with an area around 9251 km^2, population around 754 000, and average annual precipitation around 490-520 mm. During the last century, it was observed that the climate changed with precipitation reducing at a rate of 1mm per year, where the temperature increased by 0,5°C. (EEA, 2007) The reduction in precipitation and the increase in temperature had an adverse impact on the availability of the natural water resources, which were reduced by 40% from the estimates made in 1970 at the

preparation of the Cyprus Water Master Plan (Zoumides and Zachariades, 2009). Extreme climatic phenomena, especially droughts, are more frequent than before, causing water shortage and scarcity, and adverse effects on the economy and the environment. Cyprus has developed and implemented a National Water Master Plan which was prepared in the 1970's, based on the meteorological data available at the time, covering the period 1900-1970. After implementing the Master Plan it was realized that the available water resources were by 40% less than originally estimated causing a water crisis (WDD, 2008). The water crisis caused by the climate change forced the Government to revise the original policy on water resources management plans, which envisaged, among others, the introduction of seawater desalination by the years 2005-2010 and the re-allocation of cultivations in Cyprus for better irrigation water management. As it is known, 69 % of the total water consumption is allocated for irrigation purposes in the Agricultural sector (Zoumides and Bruggeman, 2010). The thought of better irrigation water management based on scientific data is very promising in order to avoid over-waste of water and support a sustainable scheme of irrigation in Agriculture (Loukas et al., 2007; 2008).

Agriculture was considered as the backbone of the Cypriot economy during the 1960s and 1970s, reaching 18% of Gross Domestic Product (GDP) and 20% of total employment in the mid-1960s; however, as Cyprus gradually became service-dominated, the contribution of agriculture has decreased dramatically, and currently accounts for about 2% of GDP and 7% of the total workforce. Despite such decreases the agriculture still remains the dominant water user in the country using 69 % of the total water consumption; 69 % of the Agricultural Water Demand (Figure 2) corresponds to 182.4 Million m^3 (MCM) and is distributed as follows:

- Irrigated Agriculture 174.4 MCM
    - Major Government Irrigation Schemes 100.1 MCM
    - Outside Government Irrigation Schemes 74.3 MCM
- Animal Husbandry 8 MCM

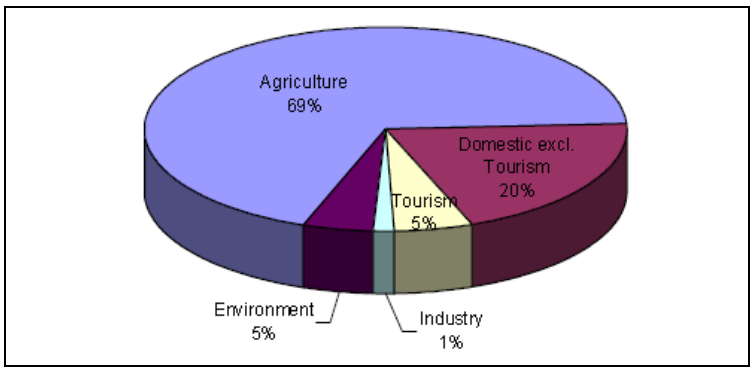

Figure 2. Distribution of Water Demand in Cyprus (WDD 2008)

Agricultural water supply is provided either through government irrigation schemes (55 %) or through private boreholes (45%). Figure 3 shows water demand by sector and anticipated sources used. While domestic water supply is provided by the government to all municipalities at a universal price that covers the full operating costs, farmers purchase water at subsidized prices, a scheme that was politically decided to support agriculture especially in disadvantageous and mountainous areas. It is estimated that most aquifers are overexploited by 40 % of their natural (sustainable) replenishment rate (Demetriou and Georgiou, 2004). In general, water use efficiency in private irrigated land is lower precisely because control and monitoring of groundwater exploitation is difficult or deficient. Currently irrigation water is priced at €0,17 per m^3 and covers about 77 % of financial costs (Zoumides and Zachariades, 2009).

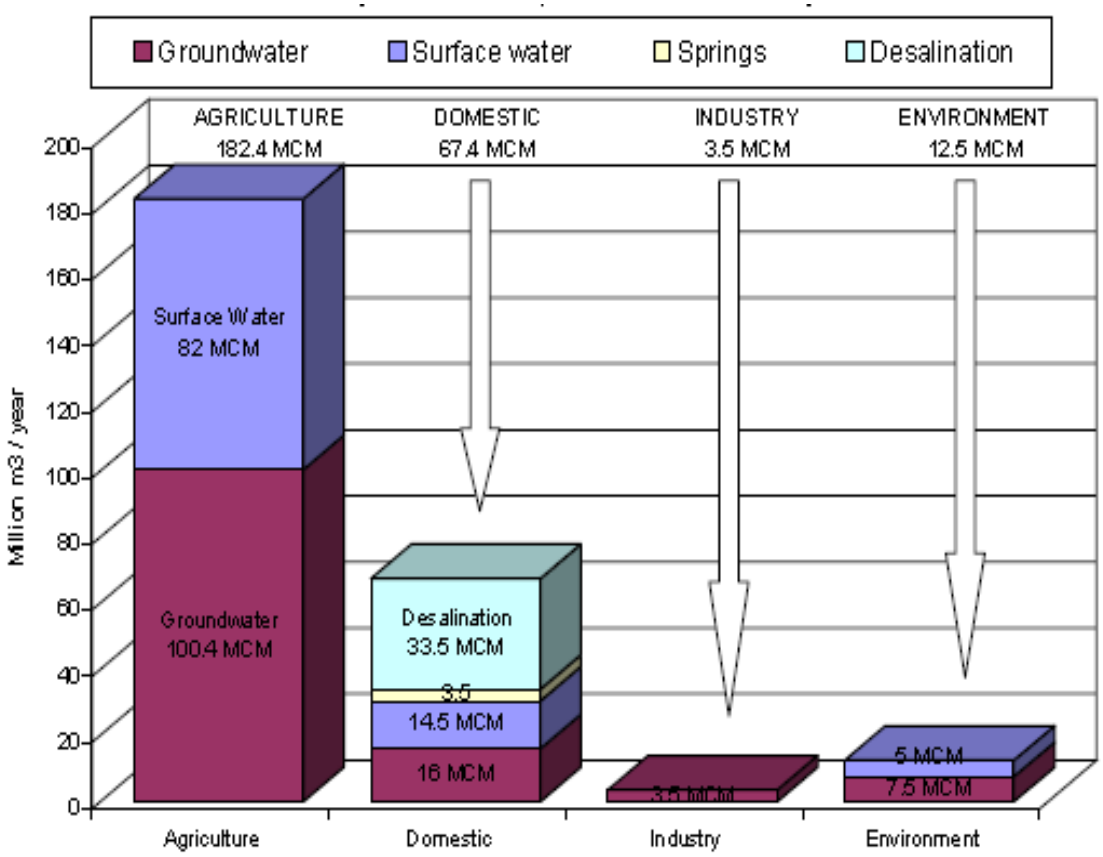

Figure 3. Water demand by sector and anticipated sources used (WDD 2008)

Consecutively, the low cost of water encouraged the cultivation of high-value and water-demanding crops. The increase in the price of water will have different repercussions depending on a variety of factors. First of all, without subsidized water, there will be a two-dimensional loss in competitiveness of some crops (Markou and Papadavid, 2008), domestic competition between crops and competition from foreign markets as regards exported agricultural products. Other factors may include scale of farming (i.e. small compared to large scale farming), labour costs and profitability of crops. In this rational, policy makers should direct agricultural procedure to the direction of the nonwater-demanding crops and scientific data are needed to support their decision. One of the targets of this thesis is to provide such data to policy makers for boosting a sustainable scheme of irrigation management. Nonetheless, most farmers are driven by the net economic benefit of agricultural products rather than the cost of water (Markou and Papadavid, 2008).

Table 1 shows how irrigation water is allocated to permanent and annual crops in Cyprus, while Table 2 shows the total irrigated areas for each group of crops.

Table 1. Water demand in Agriculture (WDD 2008)

	Water demand in MCM Million m^3			
	Major Government Irrigation Schemes	**Outside Government Irrigation Schemes**	**Total**	**%**
Permanent Crops				
Citrus	35,2	16,7	51,9	32%
Deciduous	4,8	12,5	17,3	11%
Olives	5,1	3,4	8,5	5%
Table Grapes	2,7	2,7	5,4	3%
Bananas	3,2	0,01	3,21	2%
Remaining demand		9,5	9,5	6%
Total Permanent	**51**	**44,8**	**95,8**	**59%**
Annual Crops				
Fodders	4,1	7,3	11,4	7%
Potatoes	10,5	2,3	12,8	8%
Greenhouses	2,6	0,3	2,9	2%
Open Field Vegatables	18,8	19,6	38,4	24%
Total Annual	36	29,5	65,5	41%
GRAND TOTAL(MCM)	**87**	**74,3**	**161,3**	
(+)Losses 15%	**100,1**	**-**	**174,4**	
TOTAL(%)	**57%**	**43%**		**100%**

Table 2 illustrates that permanent crops possess 56 % of the total area while they absorb 59% of the total water allocated to the Agricultural Sector. Annual crops possess 44 % and absorb 41%, respectively.

Table 2. Irrigated areas in Cyprus per group of crops (WDD 2008)

	Irrigated Areas in Decars			
	Outside Government Irrigation Schemes	**Major Government Irrigation Schemes**	**Total decars**	**%**
Permanent Crops				
Citrus	47 662	23 177	70 839	26%
Deciduous	6 483	18 326	24 809	9%
Olives	11 375	8 472	19 847	7%
Table Grapes	10 438	9 636	20 074	7%
Bananas	2 899	10	2 909	1%
Remaining demand		14 000(estimated)	14 000	5%
Total Permanent	**78 857**	**73 621**	**15 2478**	**56%**
Annual Crops				
Fodders	2 377	6 260	8 637	3%
Potatoes	35 457	7 241	42 698	16%
Greenhouses	2 893	315	3 208	1%
Open Field Vegetables	31 354	32 827	64 181	24%
Total Annual	**72 081**	**46643**	**118 724**	**44%**
GRAND TOTAL (MCM)	**150 938**	**120 264**	**27 1202**	**100%**

The Major Government Irrigation Schemes (Figure 4) are: Pafos, Chrysochou (Chrysochou, Pomos, Ag. Marina), Akrotiri West, Yermasoyia – Polemidhia, Vasilikos – Pendaskinos – Alaminos/Mazotos – Kiti/Pervolia, Kokkinokhoria, Kalopanayiotis, Xyliatos, Vyzakia, Lympia and Avdimou/Paramali. The Major Government Irrigation Schemes consume, including estimated 15 % network losses, 100.1 million m^3 annually, reaching 57 % of the total Agricultural Water Demand. The Government has invested considerablyin these projects, as they are of major importance for the overall economy of Cyprus (Zoumides and Bruggeman, 2010).

Figure 4. Cyprus Major water works (WDD 2008)

2. Opportunities of remote sensing for estimating crop evapotranspiration (ETc)

It is essential to understand how much water is being used by crops in different areas of an irrigation project in order to establish irrigation efficiency, so as to achieve sustainable and improved water use efficiency. Especially in Cyprus, there is a need for an effective method of establishing crop water use in large irrigation projects so that crop demand can be accurately met by supply in order to eliminate problems such as lack of up to date information on the cropped area, evaporative demand in the agricultural fields and water supply. For most of the irrigation projects, irrigation is managed and supplied on the basis of historic precedence and the existing conventional data collection for determining the irrigation demand is not adequate and effective for large areas.

However, satellite remotely sensed data can be used to accurately identify cropped areas in irrigated fields. If this information is combined with some other auxiliary local climatic and crop data, it is possible to identify the seasonal crop water demand in the fields (Loukas 2004; D'Urso et al., 2006; Telis et al., 2007; Hadjimitsis et al., 2008, Papadavid et al., 2009; 2011). Inefficient irrigation practices due to lack of effective data for irrigation purposes cause a negative effect on water resources. Remotely sensed data is becoming an important tool in

agriculture. The challenges for the operational application of remote sensing techniques are of great importance in terms of economic values. Today remote sensing fits in almost all of the scientific branches of agronomy providing on time and reliable data regarding the subject used for.

3. Problem statement

The Intergovernmental Panel on Climate Change identified the Mediterranean as one of the regions that is likely to experience a decrease in water resources due to climate change (Kundzewicz, 2007). Giorgi (2006) also showed that the Mediterranean region is a hotspot of climate change. Cyprus has already experienced a decrease in precipitation in the recent past. A regional analysis of the changes in precipitation found a statistically significant step change in the 1916-2000 annual precipitation time series between the hydrologic years 1968/69 and 1971/72, with a 15-25% reduction in precipitation for the last 30 years of the 20th century (Rossel, 2001).

Data from the Cyprus Meteorological Service (CMS, 2010; 2011) give an average annual precipitation over the government controlled area of Cyprus of 541 mm for 1901/02-1969/70 and 466 mm for the 1970/71-2009/10 period (Bruggeman et al. 2011). This decrease in precipitation has resulted in an even greater decrease in the country's water resources. A recent study by the Ministry of Agriculture, Natural Resources and Environment (Vakakis et al., 2010), which addressed the future of agriculture in Cyprus, indicated that climate change is likely to increase irrigation water demands, reduce yields and increase soil degradation. On the other hand, the Water Development Department's (WDD) review of the country's water policy for the implementation of articles 11, 13, and 15 of the European Water Framework Directive (WFD) recommended a 15% reduction in irrigation water demand (Karavokyris et al., 2010).

Since there is great probability that the climate parameters will continue to change with further decrease in the precipitation and further increase in the temperature (Zoumides and Bruggeman, 2010), the need for a suitable and cost-effective method of estimating crop water requirements seem to be indispensable. For this reason, a collaboration of the Agricultural Research Institute of Cyprus and the Cyprus University of Technology was co-funded by the Regional Development Fund of the EU and Cyprus Government through the Research Promotion Foundation, to provide a sound method and an operational tool for estimating crop

evapotranspiration on a regular basis. To support this PhD thesis, Remote Sensing and Statistical techniques along with established crop evapotranspiration (ETc) algorithms were employed.

Estimating ETc based on remote sensing is being used almost all over the world because of the benefits that remote sensing offers: huge amount of raw data for low cost and synoptic coverage. It is worth to mention that a Landsat 5 TM or 7 ETM+ image covers almost the whole island of Cyprus and its spatial resolution is fine regarding hydrological studies (Alexandrides, 2003). The study area is located in Mandria village, in Pafos district (Southwest Cyprus) which is the main agricultural area of the district of Pafos and absorbs the biggest share regarding irrigation water (26%) of the major irrigation schemes of Cyprus (Table 3).

Pafos and Kokkinochoria areas are dominant in water demand and are absorbing almost half of water demand (48%) in Cyprus. They are the basic areas for producing the main annual crops in Cyprus such as potatoes (*Solanum tuberosum*), beans (*Phaseolous vulgaris*), chickpeas (*Cicer arietinum*) and groundnuts (*Arachis hypogaea)* which are the target crops of this research. Special characteristics of the area of interest and selected crops are presented in the next chapters.

Table 3. Water demand per group of crops and major irrigation scheme (WDD 2008)

	Pafos	**Chrysochou/Argaka**	**Pomos**	**Agia Marina**	**Akrotiri West**	**Yermasoyia Polemidia**	**Vasilikos**	**Kokkinochoria**	**Kalopanayiotis**	**Xyliatos**	**Vyzakia**	**Lympia**	**Avdimou/Paramali**	**Total**	**%**
Permanent Crops	**Water Demand in MCM**														
Citrus	6,91	4,34	0,67	0,31	2,17	13,4	3,2	4	0,06	0,11	0,08	0,02	0	**35,2**	41%
Deciduous	1,67	0,67	0,1	0,12	0,59	0,31	0,22	0,17	0,24	0,6	0,06	0,05	0	**4,8**	6%
Olives	0,4	0,47	0,04	0,05	0,32	0,08	1,4	1,64	0,04	0,4	0,23	0,06	0	**5,1**	6%
Table Grapes	0,6	0,04	0	0	0,56	0,47	0,03	0	0	0	0	0	1,01	**2,7**	3%
Bananas	3,13	0,01	0,03	0,02	0	0	0	0	0	0	0	0	0	**3,2**	4%
Total Permanent	**12,7**	**5,5**	**0,8**	**0,5**	**3,6**	**14,2**	**4,9**	**5,8**	**0,3**	**1,1**	**0,4**	**0,1**	**1**	**51,1**	59%
Annual Crops															
Fodders	1,13	0,14	0,01	0	0,35	0,1	2,16	0,17	0	0	0	0	0	**4,1**	5%
Potatoes	*	*	*	*	*	*	*	10,5	*	*	*	*	*	**10,5**	12%
Greenhouses	0,78	0,06	0,08	0,12	0,24	0,26	0,73	0,33	0	0,01	0,01	0	0	**2,60**	3%
Open Field Vegetables	8,4	1,26	0,06	0,07	0,84	1	4,36	2,58	0,01	0,08	0,08	0,02	0	**18,8**	22%
Total Annual	**10,3**	**1,5**	**0,2**	**0,2**	**1,4**	**1,4**	**7,3**	**13,5**	**0**	**0,1**	**0,1**	**0**	**0**	**35,9**	**41%**
GRAND TOTAL	**23**	**7**	**1**	**0,7**	**5,1**	**15,6**	**12,1**	**19,4**	**0,4**	**1,2**	**0,5**	**0,2**	**1**	**87**	100 %
Plus Losses (15%)	26,5	8	1,1	0,8	5,8	17,9	13,9	22,3	0,4	1,4	0,5	0,2	1,2	**100**	
(%)of the Total	26	8	1	1	6	18	14	22	0,4	1	1	0,2	1	100	

The objectives of this thesis are to provide a literature review regarding remote sensing techniques on estimating ETc, obtain the spectral signatures of each crop, modify some of the most widely used evapotranspiration algorithms and finally establish a methodology of estimating ETc which methodology could be used as a tool for providing data to irrigation policy makers, on a regular basis.

The arrangement of this thesis is as shown below:

- Chapter 1: Review and Basics on estimating evapotranspiration. In this Chapter a description of how remote sensing techniques are used in order to estimate ETc is presented.

- Chapter 2: Materials and Methods. In this chapter, an outline of the materials and methods required to reach the goals are described.

- Chapter 3: Ground data: In this chapter, field spectroscopy and optical properties of vegetation basics are described. Then a description of how ground measurements were conducted and how these measurements can support this study is explicated.

- Chapter 4: Modeling Vegetation Indices (VI) to Leaf Area Index (LAI) and Crop Height (CH). In this Chapter, modeling techniques are used to correlate and evaluate measured crop canopy factors (LAI and CH) to VI produced from remotely sensed data.

- Chapter 5: Results of ETc algorithms applications and modifications with ground models. In this Chapter the results of the method are illustrated and tested. Two ETc algorithms are applied and then modified with the semi-empirical models developed in Chapter 4 to test if the algorithms can increase accuracy.

- Chapter 6: Discussion and Conclusions. In this chapter, the author discusses advantages and disadvantages of the method adopted, opportunities and future work that conclude from this Thesis, and finally, how this innovative procedure-method can be used from Water Authorities in Cyprus to assure that irrigation water availability will remain sustainable. Original research contribution of this Thesis is highlighted.

CHAPTER 1: REVIEW AND BASICS

This chapter describes how remote sensing techniques are used to estimate ETc. A review and a critical assessment of the main ETc algorithms based on the Energy Balance Equilibrium are illustrated with emphasis on their main characteristics regarding their application.

1.1. Literature Review

1.1.1. Crop evapotranspiration

Evapotranspiration, the means for exploiting irrigation water, is referred to as the combination of two different processes, where in the first water is lost from the soil and plant surfaces by evaporation and in the second from the crop by transpiration (Allen et al., 2000). Evapotranspiration constitutes a major component of the hydrological cycle and its estimation demands auxiliary meteorological data (Telis et al., 2007). Several formulas have been developed by scientists to calculate evapotranspiration (French et al., 2008). The ETc is a basic and crucial parameter for climate studies, weather forecasts and weather modeling, hydrological surveys, ecological monitoring and water resource management (Hoedjes et al., 2008).

In the past decades, the estimation of ETc combining conventional meteorological ground measurements with remotely-sensed data has been widely studied and several methods have been developed for this purpose (Tsouni, 2003). An accurate estimation of the ETc is necessary for hydrological resources management and irrigation scheduling (Caselles et al., 1987; Carlson et al., 1989; D'Urso et al., 1995; Tsuni et al., 2003; Hoedjes et al., 2008 ; Papadavid et al., 2011). Crop evapotranspiration rate is highly important for identification of crop stress due to crop disease, water deficiency, insect infestation and other problems but mainly for estimating the exact potential needs of crops for best yields.

In general, water depletion methods - such as lysimeters - are the most accurate methods for estimating ETc, though they require more time, high costs and more man-power. Other methods are preferred due to the convenience they offer using readily available metrological data. The most acceptable and widely used methods as found in the literature are the computational ones that use meteorological parameters in order to estimate the ETc of

different crops (Telis et al., 2007; Rogers et al., 2007). If lysimeters are not available, the estimation of evapotranspiration is difficult to calculate, because the actual evapotranspiration depends on various factors and varies considerably with time and space (D'Urso et al., 2006). Thus, a number of semi-empirical methods have been developed by scientists worldwide over the last 50 years, in order to estimate the evapotranspiration from different climatic variables (Courault et al., 2005). Recently, a breadth of mathematical equations and modelling is recommended (D'Urso et al., 1995; Aaron et al., 1996 ; Tsuni et al., 2003; Hoedjes et al., 2008). Bastiaanssen (2005) has proposed a widely accepted relationship for estimating evapotranspiration. This relationship can be used for defining the crop coefficients as a function of:

-climate data (temperature, relative humidity, solar radiation and wind speed)
-crop parameters such as the surface albedo, the leaf area index (LAI)
- crop height (related to the surface aerodynamic roughness)

However, some other researchers have shown that crop coefficients are greatly influenced by canopy development and vegetation coverage. Roerink et al. (1997), based on the fact that these parameters directly affect the reflectance of crops, has demonstrated that it is possible to establish a correlation between multi-spectral measurements of canopy reflectance and corresponding ETc values. Therefore, remotely sensed reflectance values can be used in combination with other detailed information for estimating ETc of different crops. These days, the potentiality of remote sensing techniques in ETc estimation and water resource management has been widely acknowledged (Papadavid et al., 2010).

1.1.2. Remote sensing for ETc estimation

Remote sensing for hydrological purposes is used to improve farm-level irrigation management. The possibility for monitoring irrigation demand from space is catalytic for policy makers. The increased accuracy can lead to a reduction on the water for irrigation and improve water reservoirs management. In addition, on a micro-economic level, at the producers' level, improved irrigation management can have a positive effect on the economics of the farm. It has been found that saving irrigation water through remote sensing techniques could diminish farm irrigation cost which reaches 25% of the total costs and increases the margin of net profit (Papadavid et al., 2011).

A consistent effort has been made in the field of agricultural research to improve the understanding of physical processes involved in an irrigation system (Feddes et al., 1988; Menenti, 1989). With the water resources shortage being a basic issue for many countries, management of the available water resources is one of the greatest challenges of the 21st century. The agricultural sector is one of the major consumers of water, accounting for more than 70% of the world's fresh water. Thus, the use of irrigation water plays a significant part in increasing land productivity (Ahmad et al., 2008). According to Azzali et al. (2001), the spreading of modeling techniques using distributed parameters has largely encouraged the use of input data from remote sensing with the support of GIS systems for manipulating large data sets in irrigation water management, while Menteti et al. (1989), D'Urso et al. (1992), Bastiaanssen (2000), Ambast et al. (2006) and Papadavid et al. (2011) have indicated the potentiality of multispectral satellite images for the appraisal of irrigation management. Estimation of crop water parameters using remote sensing techniques is an expanding research field and development trends have been progressing since 1970s (Jackson et al., 1977; Seguin and Itier, 1983). Since then, remote sensing has played an increasing role in the field of hydrology and especially water management. The integration of remotely sensed data with auxiliary ground truth data for obtaining better results is common in literature. (Bastiaanssen et al., 1998; Bastiaanssen et al., 2003; Ambast et al., 2006; Minaccapili et al. 2008). It is considered that the resolution in time and space of remotely sensed data is vital in water management (Schultz et al., 2001). The rationalistic use of surface water and the monitoring of consumptive use of water by applying remote sensing techniques has been a topic of great interest for irrigation water policy makers (Tasumi et al., 2003).

The use of remote sensed data is very useful for the deployment of water strategies because it can offer a huge amount of information in short time, compared to conventional methods. Besides convenience and time reducing, remotely sensed data lessens the costs for data acquisition, especially when the area is extended (Thiruvengadachari et al., 1997). Ambast et al. (2006) have shown that the application of remote sensing data in irrigation is of high importance because it supports management of irrigation and is a powerful tool in the hands of policy makers. The potentiality of remote sensing techniques in irrigation and water resource management has been widely acknowledged. It has been found that research in ETc is directed towards energy balance algorithms that use remote sensing directly to calculate input parameters and, by combining empirical relationships to physical models, to estimate the energy budget components (Courault et al., 2005; Bastiaanssen, 2005; Minaccapili et al.,

2008; Papadavid et al., 2010). All the remote sensing models of this category are characterized by several approximations and need detailed experimental validations. Multispectral images are used to infer ETc, which is the main input for water balance methods-models. For estimations of ET, ground truth data (Leaf Area Index, crop height) and meteorological data (air temperature, wind speed, humidity) is needed to support this approach. In nearly every application of water balance model, knowledge of spatial variations in meteorological conditions is needed (Moran et al., 1997).

1.2. The Energy Balance (EB) theory

Energy Balance (EB) algorithms are based on the rationale that ETc is a change of the state of water using available energy in the environment for vaporization (Su et al., 2005). Remote sensing based EB algorithms convert satellite sensed radiances into land surface characteristics such as albedo, leaf area index, vegetation indices, surface roughness, surface emissivity, and surface temperature to estimate ET as a "residual" of the land surface energy balance equation:

$$Rn = G + H + LE$$

where:

- *Rn* is the net radiation resulting from the budget of shortwave and longwave incoming and emitted radiation (W m^{-2})
- *LE* is the latent heat flux from evapotranspiration (W m^{-2})
- *G* is the soil heat flux (W m^{-2})
- *H* is the sensible heat flux (W m^{-2}).
- *LE* is converted to ET (mm h-1 or mm d-1) by dividing it by the latent heat of vaporization (λv, ~2.45 MJ kg-1).

Net radiation and soil heat flux, the latter beinga function of *Rn* and vegetation indices (Daughtry et al., 1990; Chavez et al., 2005), may be estimated using meteorological measurements (Allen et al., 1998) and by incorporating spatially distributed reflected and emitted radiation (Kustas et al., 1989; Daughtry et al., 1990) as:

$$Rn = (1 - a)R_s + e_\alpha \sigma T_a^{\,4} - e_s \sigma T_s^{\,4}$$

where:

- α is surface albedo
- R_s is incoming shortwave radiation (W m^{-2})
- σ is the Stefan-Boltzmann constant ($5.67E^{-08}$ W m^{-2} K^{-4})
- e is emissivity
- *T* is temperature (Kelvin) with subscripts *a* and *s* for air and surface, respectively.

T_s is the remotely sensed radiometric surface temperature, which is obtained after correcting the brightness temperature imagery for atmospheric effects and surface emissivity.

Some early applications of remote sensing based EB models (Brown and Rosenberg, 1973; Stone and Horton, 1974; Idso et al., 1975; Jackson et al., 1977) proposed to use surface temperature derived from remotely sensed data (thermal band) to estimate regional ETc in the form:

$$LE = Rn - G - \frac{p_a C_p (T_s - T_a)}{r_{ah}}$$

where:

- ρ_a is air density (kg m^{-3})
- C_p is specific heat capacity of the air (J kg^{-1} K^{-1})
- r_{ah} is aerodynamic resistance for heat transfer (s m^{-1})

T_s and T_a are expressed in Kelvin (K). Brown and Rosenberg (1973) and Brown (1974) used the surface radiometric temperature and air temperature difference (*Ts* - *Ta*) and the aerodynamic resistance (r_{ah}) to estimate *H*, where the canopy or surface temperature was obtained from remotely sensed radiometric temperature using thermal scanners having a bandwidth mostly in the range of 10 to 12 μm. Later, Rosenberg et al. (1983) incorporated the surface aerodynamic temperature term (T_o) in the *H* model, instead of *Ts*, considering that the temperature gradient (for *H*) was a gradient between the air temperature within the canopy (at a height equal to the zero plane displacement plus the roughness length for heat transfer) and the air temperature above the canopy (at a height where wind speed was measured or height for r_{ah}). They indicated that for partially vegetated areas and water-stressed biomass, the radiometric and aerodynamic temperatures of the surface were not equal.

Accurate estimates of *H* are very difficult to achieve using a direct, absolute equation for *H* when T_s is used instead of T_o and atmospheric effects and surface emissivity are not considered properly. In such cases, *H* prediction errors have been reported to be around 100 W m^{-2} (Chavez and Neale, 2003), which could affect negatively the procedure for estimating ETc. Consequently, more recent EB models differ mainly in the manner in which *H* is estimated (Bastiannesen et al., 2005). These models include: the Surface Energy Balance Algorithm for Land (SEBAL) developed by Bastiannesen et al., (1998) that uses hot and cold pixels within the satellite images to develop an empirical temperature difference equation; the Surface Energy Balance Index (SEBI) developed by Menenti et al., (2003) based on the contrast between wet and dry areas; the Simplified Surface Energy Balance Index (S-SEBI) developed by Roerink et al., (2000) and the Surface Energy Balance System (SEBS) developed by Su, (2002).

1.2.1. The Surface Energy Balance algorithms SEBI, SEBS, and S-SEBI

SEBI, proposed by Menenti et al., (2003) and Choudhury (1994), is based on the Crop Water Stress Index (CWSI) (Jackson et al., 1981) concept in which the surface meteorological scaling of CWSI is replaced with planetary boundary layer scaling. It uses the contrast between wet and dry areas appearing within a remotely sensed scene to derive ET from the relative evaporative fraction (Λ). The 'Λ' is calculated by relating surface temperature observations to theoretical upper and lower bounds on the difference between *Ts* and *Ta* (Menenti et al., 2003). The evaporative fraction (Λ), as utilized by Bastiaanssen et al. (1998), is defined as the ratio of latent heat flux to the available energy ($\Lambda E = R_n - G$) and is assumed to remain nearly constant during the day. SEBS was developed using the SEBI concept (Su, 2002); it uses a dynamic model for aerodynamic roughness length for heat (see also, Su et al., 2001), bulk atmospheric similarity (Brutsaert, 1975) and Monin-Obukhov similarity theories to estimate regional ETc, and atmospheric surface layer scaling for estimating ETc at local scale. SEBS requires theoretically defined wet and dry boundary conditions to estimate *H*. Under dry conditions, the calculation of H_{dry} is set to the *AE* as evaporation becomes zero due to the limitation of water availability and H_{wet} is calculated using Penman-Monteith parameterization (Monteith, 1981). The main limitation with SEBS is that it requires aerodynamic roughness height. A potential weakness in the SEBS approach is the neglect of heat flux absorption along the temperature profile when extrapolating to and from the blending layer. The absorption, over a dry condition, can be large and disrupts the assumption of a smooth *T* gradient that conveys the *H* flux estimate all the way to the mixing height. This

results in an overstatement of the surface temperature for the dry condition and must be accounted for somehow empirically. S-SEBI is a simplified method derived from SEBS to estimate surface fluxes from remote sensing data (Roerink et al., 2000). Consequently, this model is based on Λ and the contrast between the areas with extreme wet and dry temperature. A disadvantage of this method may be that it requires extreme T_s values, which cannot always be found on every image. However, the major advantages of this method are that it is a simpler method that does not need additional meteorological data and it does not require roughness length as in the case of SEBS.

1.2.2. SEBAL (Surface Energy Balance Algorithm for Land) methodology for estimating ETc

SEBAL was originally developed and tested by Bastiaanssen (Bastiaanssen, 1995; Bastiaanssen, 2000; Bastiaanssen et al., 2003). Briefly, SEBAL is essentially a single source model that solves the EB for *LE* as a residual. R_n and *G* are calculated based on *Ts* and reflectance-derived values for albedo, vegetation indices, LAI and surface emissivity. *H* is estimated using the bulk aerodynamic resistance model and a procedure that assumes a linear relationship between the aerodynamic near-surface temperature - air temperature difference (*dT*) and T_s calculated from extreme pixels. Basically, extreme pixels showing cold and hot spots are selected to develop a linear relationship between *dT* and T_s, where the *dT* parameter eliminates the need for T_a and knowledge of T_o. The procedure presumes that there is no *H* from the wet pixel and there is no evaporation from the dry pixel. SEBAL first computes *H* at extreme dry (hottest) and wet (coldest) locations because *H* is not known for all other pixels. This eliminates the need to install expensive instruments to determine *H*. Thus, a linear relationship between the temperature difference and the surface temperature (T_0) is developed to describe the spatial distribution of the temperature difference which is a function of *H.*

It also provides for some bias compensation for errors in R_n and *G*. At the pixel with cold condition, *H* is assumed non-existent ($H_{cold} = 0$), and at the hot pixel, *LE* is commonly set to zero, which in turn allows $H_{hot} = (R_n - G)$ *hot*. Then $dT_{cold} = 0$, and dT_{hot} can be obtained by inverting the bulk aerodynamic resistance equation. The *dT* artifice is expected to compensate for bias in surface temperature estimates due to atmospheric correction and it does not assume that radiometric and aerodynamic temperatures are equivalent. SEBAL has been tested extensively in different parts of the world (Bastiannesen et al., 2005). Table 1.1 shows the worldwide applications of SEBAL.

Table 1.1. Validation of Surface Energy Balance Algorithm for Land (SEBAL)-Based Evapotranspiration (ET) Fluxes at Field Scale using Different Measurement Techniques (Bastiaanssen et al., 2005)

Field instrument	Country	Landscape	Source
Drainage Iysimeter	U.S	Irrigated native sedge forage	Morse et al. (2000), Allen et al. (2002)
Weighing Iysimeter	U.S	irrigated sugar beet	Trezza (2002), Tasumi (2003), Allen et al. (2002)
Bowen ratio	Egypt	Playas and desert surfaces	Bastiaanssen and Menenti (1990)
Bowen ratio	Spain	Rainfed crops	Pelgrum and Bastiaanssen (1996)
Bowen ratio	Kenya	Savannah	Farah (2001)
Bowen ratio	France	Alfalfa wheat	Jacob et al. (2002)
Eddy correlation	Spain	Sunflower Rainfed and irrigated crops	Pelgrum and Bastiaanssen (1996)
Eddy correlation	China	Irrigated maize and deserts	Wang et al. (1995)
Eddy correlation	Niger	Savannah tiger bush	Roerink (1995)
Eddy correlation	Netherlands	Forest pastures	Bastiaanssen and Roozekrans (2003)
Eddy correlation	New Mexico	Riparian vegetation	Unpublished
Eddy correlation	Oklahoma	Pastures	Schmugge et al. (2003)
Scintillometer	Turkey	Irrigated crops	Kite and Droogers (2000)
Scintillometer	Netherlands	Grassland	Kohsiek et al. (2002)
Scintillometer	Sri Lanka	Palm trees and rice	Hamakumara et al. (2003)
Scintillometer	France	Sunflower wheat, bare soil	Legouarde et al. (2002)
Scintillometer	Morocco	Olives	Van den Kroonenberg A. (2003)
Scintillometer	Botswana	Savannah	Timmemans et al. (2003)

1.2.3. FAO Penman-Monteith adapted to satellite data model for estimating ETc

The FAO Penman-Monteith adapted to satellite data model needs both meteorological and remotely sensed data to be applied. The equation is used to estimate ET_c under assumptions and relies on the direct application of the Penman-Monteith equation (Monteith, 1965) also based on EB theory, with canopy parameters estimated from satellite imagery (D' Urso, 2001; D'Urso et al., 2006; Minaccapili et al., 2008; Agapiou et al., 2009; Papadavid et al., 2010). The method also needs empirical equations for describing the crop canopy factors (like SEBAL), namely albedo, crop height and LAI.

$$ETc = \frac{86400}{\lambda}\left[\frac{\Delta(R_n - G) + c_p p_a (e_s - e_a)/r_{ah}}{\Delta + \gamma(1 + r_s / r_{ah})}\right]$$

where:

- ETc is the crop evapotranspiration (mm/day)
- Δ represents the slope of the saturated vapor pressure temperature relationship (kPa / K1)
- R_n is the net solar radiation (W/m^2)
- G Soil Heat flux (W/m^2)
- c_p is the air specific heat (J/kg K)
- ρa is the air density (kg / m^3)
- e_s is the saturated vapor pressure (kPa)
- e_a is the actual vapour pressure (kPa)
- r_{ah} is the aerodynamic resistance (s/m)
- r_s is the surface resistance (s/m)
- λ is the latent heat of vaporisation of water (J / kg)
- γ is the thermodynamic psychrometric constant (kPa / K)

In 1948, Penman (Penman 1948) combined the energy balance with the mass transfer method and derived an equation to compute the evaporation from an open water surface from standard meteorological records of sunshine, temperature, humidity and wind speed (Agapiou et al., 2009; Papadavid et al., 2010). This combination method was further developed by many researchers and extended to cropped surfaces by introducing resistance factors (Rijtema, 1965; Smith, 1992; Allen et al., 1998). The resistance nomenclature distinguishes between aerodynamic resistance and surface resistance factors. The surface resistance parameters are often combined into one parameter, the 'bulk' surface resistance parameter which operates in series with the aerodynamic resistance (Monteith and Unsworth, 1990). The surface resistance, r_s, describes the resistance of vapour flow through stomata openings, total leaf area and soil surface. The aerodynamic resistance, r_{ah}, describes the resistance from the vegetation upward and involves friction from air flowing over vegetative surfaces. Although the exchange process in a vegetation layer is too complex to be fully described by the two resistance factors, good correlations can be obtained between measured and calculated evapotranspiration rates (D'Urso et al., 2006).

The transfer of heat and water vapor from the evaporating surface into the air above the canopy is determined by the aerodynamic resistance r_{ah},. In most practical applications, the r_{ah}, is calculated as a function of crop height *hc* (m) and wind speed *U* (m/s) (Allen et al., 1998, 2000, 2007; Brutsaert, 1982; D'Urso, 2001). Zero displacement heights and roughness lengths have to be considered when the surface is covered by vegetation thus several empirical equations have been developed for this purpose (FAO 1998). The 'bulk' surface resistance describes the resistance of vapor flow through the transpiring crop and evaporating soil-vegetated surface (Monteith and Unsworth, 1990).

1.3. Overview

In many EB models, T_s is one of the key boundary conditions for estimating spatially distributed ETc. Numerous remote sensing satellites provide thermal images that can be used to derive T_s. However, the spatial resolutions of these thermal images are nearly always coarser than that acquired in other wavelengths such as visible, near-infrared (NIR), and shortwave-infrared (SWIR) (Alexandridis, 2003). Further, the time interval between successive satellite overpasses (repeat cycle) over the same geographic area varies from satellite to satellite. For more frequent coverage, the spatial resolution of the acquired images becomes coarser. For example, the Landsat 5 Thematic Mapper (TM) satellite has a repeat cycle of 16 days with 30 to 120 m spatial resolution, compared with daily coverage of MODIS (Moderate Resolution Imaging Spectroradiometer) with 250 to 1000 m. The ETc maps derived from remote sensing data acquired by satellite-based sensors with daily coverage such as MODIS and Advanced Very High Resolution Radiometer (AVHRR) are not sufficient to satisfy most agricultural management needs as their pixel size is larger than individual fields, causing significant errors in ETc estimation at the field scale (Tasumi et al., 2006). The errors in the estimated ETc are partly due to the presence of mixed pixels, such as pixels with land/vegetation types with significant differences in cover, roughness, and/or moisture content (Kustas et al., 2004). This condition is more common in arid and semi arid regions where fully irrigated fields are usually surrounded by extremely dry landscape.

One main drawback of EB methods is that they rely on the presence of extreme T_s (hot and cold or dry and wet) pixels in the imagery (Tasumi et al., 2006). Without the presence of high water use crops in the imagery, these methods may under scale if not adjusted to the true potential surface temperature range, thus leading to errors in the spatial ETc estimation. Other

errors with the EB models may relate to the spatial validity of weather station data, such as air temperature, dew point temperature, and wind speed, in highly advective arid and semi-arid regions, as well as the sub-models used to derive LAI, crop height, and fraction cover from remote sensing data.

Reliable regional ETc estimates are essential to improve spatial crop water management. Land surface energy balance models, using remote sensing data from ground, airborne, or satellite platforms at different spatial resolutions, have been found to be promising for mapping daily and seasonal ETc at a regional scale. Although remote sensing based ETc models have been shown to have the potential to accurately estimate regional ETc, there are opportunities to further improve these models testing the equations used to estimate LAI and crop height for their accuracy under current agro-meteorological and soil conditions. As it was recently shown (Edward et al., 2010), improving the quality of the models used to describe the canopy factors such as LAI and Crop Height can increase the accuracy of the algorithms. The procedure can be considered as a modification of the algorithm since the idea is to adapt the algorithm to the local conditions. This procedure has been followed in this thesis in an attempt to test if the modification to the local conditions can really improve the results of specific algorithms.

In Chapter 5, SEBAL and Penman-Monteith adapted to satellite data models are employed and modified to estimate ETc for the specific crops. Under the specific simplifications and assumptions of each model, the author applies and modifies two of the most important algorithms (SEBAL and Penman-Monteith adapted to satellite data) with the use of semi-empirical equations for crop canopy factors, which were produced using ground truth data. This is important according to the literature, since each model uses empirical equations (based on the theory which makes them semi-empirical) to describe the canopy factors.

CHAPTER 2: MATERIALS AND METHODS

In this chapter, an outline of the materials and methods required to reach the goals described in Introduction are described. The area of interest is described and the methodology is presented and illustrated in a holistic diagram.

2.1. Area of Interest

The study area is located in the area of Mandria village (x=456182, y=3840861; WGS84, UTM 36^0 N), in the vicinity of Paphos International Airport (Figure 2.1). The project area lying in the southwest of Cyprus is a coastal strip between Kouklia and Yeroskipou villages. The area is a coastal plain with seaward slope of about 2% and it consists of deep fertile soils made of old fine deposits. The area is dissected by three major rivers, the Ezousa, Xeropotamos and Diarizos.

The selected area is a traditionally agricultural area with a diversity of annual and perennial cultivations and is irrigated by Asprokremnos Dam, one of the biggest dams of Cyprus. The storage capacity of the Dam is 51 Million Cubic Meters (MCM) gross, and is situated on the Xeropotamos river. The Dam is designed for carry-over storage. The total average supply for agricultural purposes every year is estimated up to 22 MCM. Other water resources in the area are the 24 boreholes drilled in the gravel aquifers of the major river beds which have potential extraction of about 10 MCM of water and the coastal aquifer with a total supply of 4 MCM of water. The calculated reliability factor of water supply is above 92%.

The area is almost at sea level (altitude 15 m) and is characterized by mild climate which provides the opportunity for early production of leafy and annual crops. The uniform and moderate temperatures, attributed to the permanent sea breeze of the area, and the relative humidity, are conductive to the early production of fruits and vegetables, for which the reputation of the area is known all over Cyprus. Cereals are also cultivated in the area. A typical Mediterranean climate prevails in the area of interest, with hot dry summers from June to September and cool winters from December to March, during which much of the annual

rainfall occurs with an average record of 425mm. Nevertheless, irrigation is indispensable for any appreciable agricultural development in the area.

There are four types of ownership in the area with the following distribution: private individually owned (35%), private community owned (45%), government owned (15%) owned by religious institutes (5%). As it generally occurs in Cyprus, the plots have irregular shape and size with the average area of the agricultural plots of the area reaching 1.2 ha. Morphologically, the area is a flat terrain of about 30 km^2. The type of soil that is dominant in the area is the Cambisol (calcic and chromic types) (Figure 2.2).

Figure 2.1. Area of Interest marked (Landsat 5TM satellite image)

Figure 2.2. Example of soils at the area of interest

A Cambisol is a soil at the beginning of soil formation with weak horizon differentiation and mostly brownish discoloration or structure formation in the soil profile. Most of these soils make good agricultural land and are intensively used. Cambisols in temperate climates are among the most productive soils on earth. The soil texture is loamy to clayey. Signs of beginning clay illuviation may be detectable in the cambic horizon but the clay content is normally highest in the A-horizon. The soil of the experimental site is calcareous, characterized by a deep brown color, and having a rather heavy to very heavy structure. Table 2.1 is projecting the soil texture of the area for two different points, A and B, in two different depth points; 20cm and 50cm. The soil texture was measured by the Agricultural Research Institute of Cyprus for the year of 2009 for the needs of the specific research. The main method of irrigation applied in the area is with sprinklers, due to its morphology, soils and cultivations.

Table 2.1. Soil texture analysis in the area of interest

	CLAY	SILT	SAND
A20	39%	24%	37%
A50	40%	23%	37%
B20	40%	21%	39%

B50	41%	20%	39%

The area of interest was chosen for specific reasons. The area is one of few agricultural areas of the island and is directly irrigated by a nearby dam. Almost all kinds of agricultural products that are produced in Cyprus are produced there, broadening the choice of the crops under scrutiny in this ing this study. The mildness of the weather was favorable in achieving usable satellite images, since remote sensing requires clear skies. In the area, there is a little cloud or it is cloud free during the year, especially in spring and summer time, due to its geographical position and the weather conditions prevelaing at the area. The homogenous flat terrain is also an advantage of the specific areas, since some of the algorithms estimating ETc have as prerequisite a flat terrain, while soil homogeneity is a prerequisite. Another advantage of the area of interest is that a national meteorological station is situated in the area. This fact facilitates the application of the ETc algorithms, since the needed meteorological inputs are taken directly from the specific station.

Since the study is about estimating ETc of crops during their whole life cycle, a consecutive time series of satellite images are needed while the existence of a Thermal band should be a prerequisite of the satellite for the needs of the specific study, as mentioned in Chapter 1 (1.5). Due to these limitations, the economic restrictions but also due to the rich literature regarding Landsat-5 TM and 7 ETM+, the specific satellites were chosen. Landsat-5 TM and Landsat-7 ETM+ pass over the area with a temporal resolution of 15 days each and 7 days between them. The time of overpass is 11:00am local time for Landsat-5 TM and 9:30am local time for Landsat-7 ETM+. As indicated by Alexandridis (2003), the spatial resolution of Landsat-5 and Landsat-7 (pixel size: 30mx30m for VI and IR bands and 60mx60m for thermal band for ETM+. 30mx30m for VI and IR bands and 120mx120m for thermal band for TM) is fine, especially when the work is related to hydrological applications.

2.2. Resources

A description of the resources used in the thesis is described below:

2.2.1. Field spectroradiometer

The GER (Geophysical Environmental Research) 1500 field spectroradiometer (Figure 2.3) is a light-weight, high performance, single-beam field spectroradiometer. It is a field portable spectroradiometer covering the ultraviolet, visible and near-infrared wavelengths from 350

nm to 1050 nm. It uses a diffraction grating with a silicon diode array which has 512 discrete detectors and provides the capability to read 512 spectral bands.

The instrument is very rapidly scanning, acquiring spectra in milliseconds. The spectroradiometer provides the option for stand alone operation (single beam hand-held operation) and the capability for computer assisted operation through its serial port, which offers near real-time spectrum display and hard disk data transfer. The maximum number of scans (512 readings), can be stored for subsequent analysis, using a personal computer and GER licensed operating software. The Lens barrel used for the specific spectroradiometer is the Standard 4° field of view. The data are stored in ASCII format for transfer to other software. GER 1500 specifications can be found at http://www.ger.com.

Figure 2.3. GER 1500 Field spectro-radiometer

McCloy (1995) describes the technique for measuring the reflectance factors using a control stable surface with known characteristics. This is the method that was followed in this research for the spectro-radiometric measurements. Many scientists (McCloy, 1995; Beisl, 2001; Anderson and Milton, 2006; Schaepman, 2007) highlight the advantages of using control surfaces in the measurement of reflectance factors (Bruegge et al., 2001). In this study, the control surface was a commercially available "Labsphere" compressed

"Spectralon" white panel (Figure 2.4). There is evidence that these types of panels are more consistent and retain their calibration better than painted panels (Jackson et al., 1992; Beisl, 2001).

Spectralon diffuse reflectance targets are ideal for laboratory and field applications such as field validation experiments, performed to collect remote sensing data due to their special features and properties which are summarised below:

- durable and washable
- high reflectance: have typical reflectance values of 95% to 99% and are spectrally flat over the UV-VIS-NIR spectrum
- impervious to harsh environmental conditions
- chemically inactive

Figure 2.4. Technique of using spectroradiometer and spectralon

2.2.2. SunScan canopy analyzer for LAI estimation

Leaf Area Index is commonly used for monitoring crop growth. Instead of the traditional, direct and labor-consuming method of physically measuring the plant with a ruler (direct method), an optical instrument, SunScan canopy analyser system (Delta-T Devices Ltd., UK)

is used (indirect method) (Figure 2.5). The instrument is indirectly measuring LAI by measuring the ratio of transmitted radiation through canopy to incident radiation. Indirect methods for LAI measurements based on the transmittance of radiation through the vegetation have been developed (Lang et al., 1991; Welles and Norman, 1991).

Figure 2.5. SunScan (Delta-T) canopy analyser for LAI and crop height measurements

The SunScan which concurrently measures the PAR (Photosynthetically Active Radiation) incident at the top and at the bottom of a crop canopy has been used to measure LAI (Lambert et al., 1999). The system is configured with SunScan probe and Data Collection Terminal. The SunScan probe has an array of 64 PAR sensors embedded in a 1m long probe, and may be connected via an RS-232 cable to the Data Collection Terminal or a PC. (The Data Collection Terminal is much more convenient to observe and store reading from the probe than portable PC for field work.) The portable and weatherproof instrument can be used in most light conditions. When a reading is taken, all sensors are scanned and the measurements transmitted to the Data Terminal. The average light level along the probe is calculated and

canopy leaf area index is estimated. All of the individual sensor readings are available, if required, for detailed PAR mapping.

In general, SunScan has shown good performance for homogenous canopies but important errors when there are large gaps within the vegetation (e.g. developing row crops, tree plantations) or when the leaves are not arranged randomly (Potter et al., 1996; Chiroro et al., 2006; Papadavid et al., 2011)

2.2.3. Satellite images

For studies dealing with crop water requirements, spatial, spectral and temporal resolution of satellite images is very important. Landsat-5 TM and 7 ETM+ have been widely used for hydrological studies due to their relatively good temporal resolution (16 days) which is important for providing regular snapshots during the crop growth season (Dadhwal et al., 1996; Okamoto et al., 1996; Barbosa et al., 1996; Oetter et al., 2000; Song et al., 2001). Alexandridis (2003) has indicated that Landsat images' resolution is appropriate for hydrological purposes. These sensors are suitable for agricultural areas with medium to big average fields due to their high spatial resolution (60m for thermal band, 15m for panchromatic and 30m for the rest).

However, the availability of images is highly dependant on weather conditions. An advantage of Landsat image for applications in Cyprus is that of the whole island coverage from a single image (Figure 2.1) which can be inferred on a regular basis since Landsat satellites overpass Cyprus on a systematic basis. In this perspective, users have the possibility to have remotely sensed data every 8 days which is very important in terms of phenological cycle monitoring.

The importance of image time series is also highlighted by D' Urso (1995) and Minacapilly et al. (2008), due to the high importance of water requirements in the different stages of the crops. The same crop in different stage has different water needs, hence the time series of satellite images is very important in studies regarding ETc and remote sensing. A time series of Landsat-5 TM and 7 ETM+ acquired in years 2008, 2009 and 2010 are used in this study, as listed in Table 2.2. The purpose is to have satellite images in all stages of the specific crops. The availability of images is important since these images will be transformed into ETc maps. Hence, the more images we have the better analysis we get. All images were pre-processed in order to remove atmospheric and radiometric effects, using the ERDAS Imagine software. The same software was used to transform the images into maps by applying the ETc

algorithms using the modeler module. The same satellite images were also used for evaluating the statistical models found, regarding Leaf Area Index (LAI) or Crop Height (CH) to one of the selected Vegetation Indices (VI).

2.2.4. Landsat Satellites

In this research, images from the Landsat-5 and Landsat-7 satellites have been used. Landsat is a series of satellites with its prime emphasis on remote sensing of land resources. The first of the series, Landsat-1, was launched in 1972 from the Earth Resources Technology Satellite (ERTS).

Table 2.2. Satellite Images used in the study

	Satellite	Sensor	Date	DOI	Cos Zenith Angle	Potatoes	Ground Nuts	Beans	Chickpeas
1	Landsat-7	ETM+	12/7/2008	193	0,76		x	x	
2	Landsat-7	ETM+	28/7/2008	209	0,81		x	x	
3	Landsat-7	ETM+	13/8/2008	225	0,86		x	x	
4	Landsat-7	ETM+	29/8/2008	241	0,91		x	x	
5	Landsat-7	ETM+	14/9/2008	257	0,92	x	x	x	x
6	Landsat-7	ETM+	30/9/2008	272	0,83	x			x
7	Landsat-7	ETM+	16/10/2008	289	0,76	x			x
8	Landsat-7	ETM+	1/11/2008	305	0,66	x			x
9	Landsat-7	ETM+	17/11/2008	321	0,59	x			x
10	Landsat-5	TM	2/1/2009	2	0,79	x			x
11	Landsat-7	ETM+	21/2/2009	52	0,62	x			x
12	Landsat-5	TM	29/6/2009	179	0,91		x	x	
13	Landsat-5	ETM+	7/7/2009	188	0,91		x	x	
14	Landsat-5	TM	15/7/2009	196	0,90		x	x	
15	Landsat-5	ETM+	23/7/2009	204	0,89		x	x	
16	Landsat-5	TM	16/8/2009	228	0,76		x	x	
17	Landsat-7	ETM+	13/4/2010	103	0,47	x			
18	Landsat-7	ETM+	31/5/2010	151	0,67	x	x		
19	Landsat-7	ETM+	16/6/2010	167	0,74	x	x		
20	Landsat-7	ETM+	24/6/2010	175	0,80	x	x		
21	Landsat-7	ETM+	10/7/2010	191	0,84		x	x	
22	Landsat-7	ETM+	27/8/2010	239	0,92			x	
23	Landsat-5	TM	7/11/2010	311	0,93			x	x
24	Landsat-7	ETM+	9/12/2010	343	0,65				x
25	Landsat-7	ETM+	2/5/2011	122	0,62	X		X	
26	Landsat-7	ETM+	19/6/2011	170	0,73	X	X	X	
27	Landsat-7	ETM+	5/7/2011	186	0,83		X		
28	Landsat-7	ETM+	21/7/2011	202	0,84		X		X
29	Landsat-5	TM	29/7/2011	210	0,86		X		X

30	Landsat-5	TM	30/8/2011	242	0,93	X	X

Landsats 1, 2, and 3 carried the multispectral scanner (MSS) sensor. Landsat 4 carried the MSS and Thematic Mapper (TM) sensors, the same as Landsat-5, which is still orbiting. Landsat-6 was launched unsuccessfully. On 15 April 1999 Landsat-7 was launched, carrying the Enhanced Thematic Mapper + (ETM+) sensor. Landsat-7 operates on a sun-synchronous orbit with a nominal altitude of 705 kilometres at an inclination of 98.2 degrees, imaging 185 km swaths of the Earth's surface every 16 days. Landsat-4, Landsat-5 and Landsat-7 have the same equatorial crossing times.

The TM and ETM+ sensor collects, filters and detects radiation from the Earth in a 185-km swath, as it passes overhead. Table 2.3 shows a comparison of bandwidths between the TM sensor carried by Landsat-4 and -5 and the ETM+ sensor carried by Landsat-7 satellite. Both sensors include a thermal band which, as it was mentioned, is a prerequisite for this study.

Table 2.3. Bandwidth comparison between TM and ETM+ sensors (internet: US Geological Survey)

Landsat TM and ETM+ spectral bandwidths (in μm)								
Landsat Sensor	Blue Band 1	Green Band 2	Red Band 3	Near infrared Band 4	Mid. infrared Band 5	Therm. infrared Band 6	Mid infrared Band 7	Panchr. Band 8
Landsat TM	0.45-0.52	0.52-0.60	0.63-0.69	0.76-0.90	1.55-1.75	10.4-12.5	2.08-2.35	N/A
Landsat ETM +	0.45-0.52	0.53-0.61	0.63-0.69	0.78-0.90	1.55-1.75	10.4-12.5	2.09-2.35	0.52-0.90

2.2.5. Meteorological records

Meteorological data for the period of the project were available from the National Meteorological Service (Paphos Airport Meteorological Station). These data were extracted by the author and used as input parameters in the ETc algorithms. The importance of detailed and accurate meteorological data for hydrological purposes is indicated by Papadavid (Papadavid et al., 2009; 2011).

2.2.6. ERDAS Imagine

ERDAS Imagine image processing software v.10 is used for the analysis and interpretation of multi-spectral digital satellite images. ERDAS IMAGINE is produced by the Engineering Department of ERDAS, Inc., Atlanta, Georgia, USA (http://www.erdas.com). The specific software was used to preprocess the satellite images but also for applying the algorithms on the images. Empirical equations, algorithms and the whole processing part were applied through the specific software. The Spatial Modeler is a programming tool available in the ERDAS IMAGINE which allows the user to define inputs, functions and outputs. This type of modeling is very similar to the drawing of computing flowcharts in which a logical flow of computational steps is required. The main advantage of using the Spatial Modeler is the ease of performing functions and mathematical calculations without being required to use a programming language.

2.3. Pre-processing of Satellite images

Prior to main analysis and manipulation of satellite data, a process defined as preprocessing is needed in order to bring the data or image to a more accurate and usable condition. Preprocessing is an operation which takes place for all raw satellite data and its purpose is to correct distorted or degraded image data for more accurate and more faithful representation of the real ground scene, by removing any undesirable image characteristics produced during the image acquisition process (Mather, 1999; Mather and Koch 2011). Preprocessing is essential and comprises a series of sequential operations such as atmospheric corrections, image rectification and masking (Hadjimitsis et al., 2008, Papadavid et al., 2011). Preprocessing includes geometric and radiometric corrections which are vital for the further use of the satellite images and are necessary for increasing the accuracy of the results (Richards and Jia, 2006). In order to bring the raw data to a usable condition, both geometric and radiometric corrections are needed. The correction of these errors has to be defined before the main analysis or processing of the images since the nature of the eliminated errors determines the use of the preprocessed data (Mather, 1999; Mather and Koch 2011). Pre-processing steps were applied using the ERDAS Imagine software. All Landsat images were radiometrically and geometrically corrected at this level. Also, all images were layer-merged into a single multilayer image of the first six bands: blue, green, red, near infrared, middle infrared and thermal infrared band (Table 2.3).

2.3.1. Radiometric corrections

Radiometric errors can be categorized into two groups, the atmospheric effects errors and the errors dealing with the construction of the satellite system. Hence, atmospheric corrections were applied to the satellite images in order to remove atmospheric effects. The Darkest Pixel algorithm (Hadjimitsis et al., 2008) was employed and applied to all images of Landsat 5 and 7. Radiometric corrections of remotely sensed data aim to remove effects sourcing from the sensor's building and effects from the atmosphere. The consideration of these effects is very important (Mather, 1999; Mather and Koch 2011).

2.3.1.1. Sensor calibration

All satellite images used for this study have undergone radiometric and geometric corrections. Regarding radiometric corrections (Figure 2.6.), the images were transposed from Digital Numbers (DN) into Radiance and then to Reflectance applying the necessary equations (Mather, 1999) using the ERDAS imagine software. Radiometric corrections refer, besides to satellite sensor system errors, to reflectance of the atmosphere, aerosol scattering and absorption, as well as their combined action (Kim and Elman, 1990). Calibration of sensors and specifically for Landsat images is well established in many studies (Mather, 1999; Hadjimitsis et al., 2008; Richards and Jia, 2006; Mather and Koch, 2011) as a preprocessing step. Sensor calibration is important when images from different sensors or time series images are used for pixel comparison and when specific parameters of the image such as reflectance and temperature, are to be extracted. Thus DN must be converted to radiances or reflectance, by using calibration offset and gain coefficient for each spectral band. The methodology followed for sensor calibration for Landsat images is described below.

Raw data are converted from digital numbers (DN) to units of radiance using the following equation:

$$\text{Radiance} = \left(\frac{(L\max - L\min)}{QCAL\max} * QCAL \right) + L\min$$

where:

- $L\min$ = spectral radiance at the minimum quantized and calibrated data digital number
- $L\max$ = spectral radiance at the maximum quantized and calibrated data digital number
- $QCAL\max$ = 255
- $QCAL$ = DN

A reduction in between-scene variability is achieved through normalization for solar irradiance by converting spectral radiance to reflectance using the following equation:

$$\rho_{ts} = \frac{(\pi * L_{ts})}{E_0 * \cos(\theta_0) * d}$$

Where:

- ρ_{ts} = reflectance at the top of the atmosphere
- L_{ts} = spectral radiance at the sensor's aperture
- d = correction coefficient accounting for variation in the sun-to earth distance
- E_0 = solar irradiance at the top of the atmosphere
- θ_0 = solar zenith angle

The thermal band of Landsat 7 ETM+ (band 6) is converted from spectral radiance to temperature of the viewed earth-atmosphere system by assuming unit emissivity. The conversion equation is:

$$T = \frac{K2}{\ln(\frac{K1}{L_\lambda} + 1)}$$

Where:

- T = effective at-satellite temperature in Kelvin
- $K1$ = calibration constant = 666.09 ($W * m^{-2} * ster^{-1} \mu m^{-1}$)
- $K2$ = calibration constant = 1282.71 (^{o}Kelvin)
- L_λ = spectral radiance ($W * m^{-2} * ster^{-1} \mu m^{-1}$)

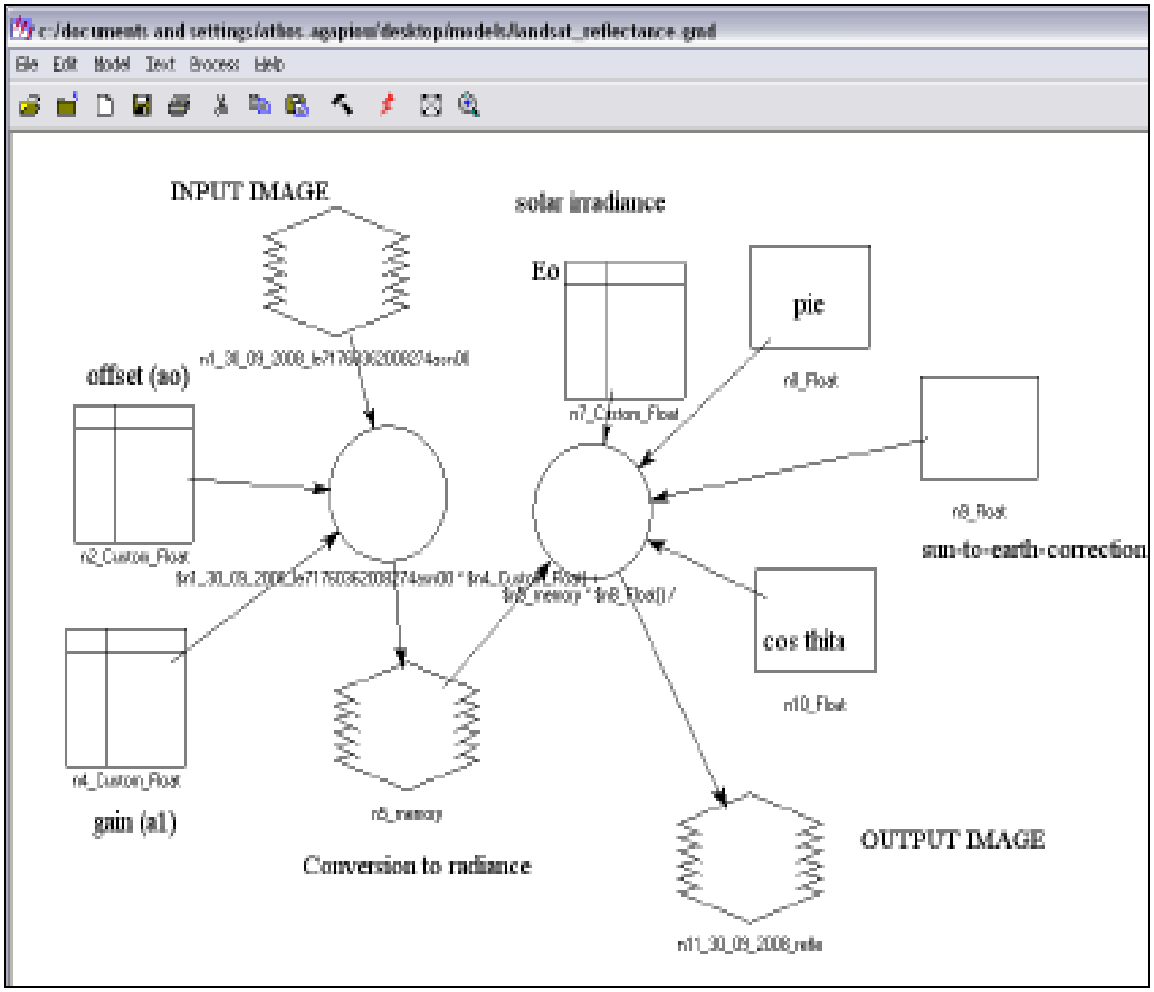

Figure 2.6. Radiometric calibration using ERDAS Imagine v.10

2.3.1.2. Atmospheric correction

The intervening atmosphere between the terrain of interest and the remote sensor can contribute significant noise and atmospheric attenuation. The objective of atmospheric correction is to retrieve the surface reflectance or target radiance from remotely sensed images by removing the atmospheric effects. It is useful to review how such errors may be removed from the remotely sensed data by considering the available approaches. The basic philosophy of atmospheric correction is to determine the optical characteristics of the atmosphere, and then to apply this information in a correction method (Hadjimitsis et al., 2000). Kaufman and Tanre (1992) presented a review of some of the atmospheric correction methods for every application. For the remote sensing of land surfaces, they mentioned the atmospheric correction is commonly applied using dark controllable objects such as dense dark vegetation or water. *Darkest pixel or histogram minimum method* was applied in order to compensate for atmospheric distortions on the satellite images. The specific method was applied from many researchers (Chavez et al., 1977; Crippen, 1987; Moran et al., 1992; Campbell, 1996; Jensen, 1996; Hadjimitsis et al., 2004) especially for satellite images of land cover, which is the case for this study.

The problem of atmospheric effects is especially significant when using multi-spectral satellite data for monitoring purposes such as agricultural or land use studies (Hadjimitsis et al., 2010; Papadavid et al., 2011). Papadavid et al. (2011) have shown that if atmospheric effects are not removed properly from satellite imagery intended for hydrological purposes, then there is always a reduction of irrigated water in the results. Hence, it is essential to consider the effect of the atmosphere by applying a reliable and efficient atmospheric correction during pre-processing of digital data. Atmospheric corrections interfere at the stage of pre-proccessing after Digital Numbers (DN) are converted to Radiance. At this stage, atmospheric correction algorithms are applied in order to remove the effects from the atmosphere. A considerable investigation on the effect of the atmosphere on dark targets has been already examined (Hadjimitsis et al., 2000; Hadjimitsis et al., 2009); the impact of atmospheric correction on vegetation indices as well on crops as separate targets has been raised (Hadjimitsis et al., 2009) and is investigated in this research. The main objective of this specific study is to examine the atmospheric effects on irrigation management using remote sensing, as opposed to conventional methods such as lysimeters and evaporation pan (Epan). Many atmospheric correction methods have been proposed for use with multi-spectral satellite imagery (Hadjimitsis et al., 2000). Such methods consist of image-based techniques, methods that use atmospheric modeling and finally methods that use ground data during the

satellite overpass. In the literature (Brown et al., 2000, 2009; Duanjun and Jie, 2004; Lawson et al., 2006;) it is often stressed the need for atmospheric correction on satellite images, especially when it comes to hydrological purposes. Hence, the rhetorical question raised in this study, is "what could happen if atmospheric corrections are not taken into account or if an atmospheric correction algorithm is not working properly". Darkest Pixel (DP) atmospheric correction algorithm was employed in this study for removing the atmospheric effects at the pre-processing level. Hadjimitsis et al. (2009) and Chrysoulakis et al. (2010) have found that DP is a very effective algorithm especially for the visible length. The principle of the DP approach states that most of the signal reaching a satellite sensor from a dark object is contributed by the atmosphere at Visible and Near Infra Red (NIR) wavelength. Therefore, the pixels from dark targets are indicators of the amount of upwelling path radiance in this band. The atmospheric path radiance is added to the surface radiance of the dark target, thus giving the target radiance at the sensor.

After the Digital Numbers (DN) of the selected dark target (Asprokremmos dam) near the area of interest are converted to units of radiance using calibration offset and gain parameters, the target reflectance at ground level is determined using the following simplified equation:

$$\rho_{tg} = \frac{\left(L_{ts} - L_{ds}\right)}{Eo.d.\cos(\theta)}$$

where

- ρ_{tg} is the target reflectance at the ground
- L_{ds} is the dark object radiance at the sensor
- L_{ts} is the target radiance at the sensor,
- $Eo.d$ is the solar irradiance at the top of the atmosphere corrected for earth-sun distance variation
- Θ is the solar zenith angle

It is important to mention that dark object radiance at the sensor corresponds to the atmospheric path radiance which is subtracted or added from each spectral band from the target radiance at the sensor.

2.3.2. Geometric Correction

Geometric corrections were made to the images following the indicated way. The most common method to register imagery to earth coordinates is to find the earth coordinates of known areas (of a geographical correct image or map) on the image and then warp the entire image by an interpolation so that these points have the true location (UTM coordinates, WGS, Zone 36 North).

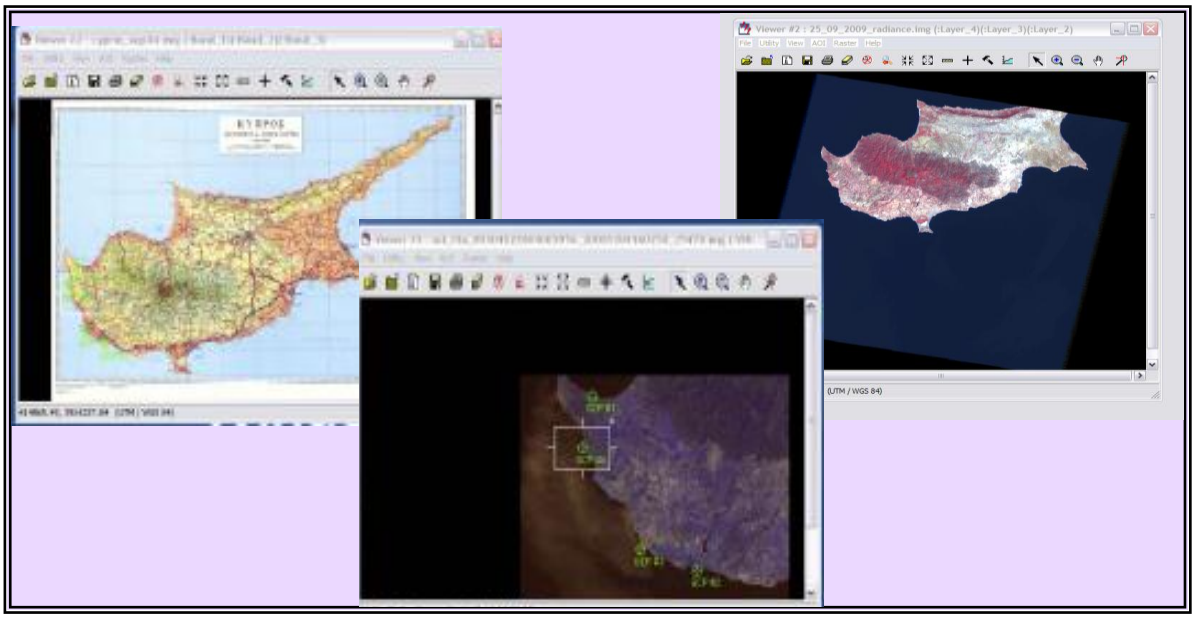

Figure 2.7. Geometric correction based on the GCP's

These locations, clearly identified both on the imagery and the map, have precise ground positions and are called Ground Control Points (GCPs) (Figure 2.7). GCPs can be road intersections, corners of woodlots, river bends, farm yields and other clear points and must be generally spatially small and well defined. Enough of GCPs must be chosen as pairs, so that the polynomial coefficients to be estimated by substitution into the mapping polynomials to yield sets of equations for the unknown parameters.

The numbers of GCPs are dependent on the degree of mapping polynomial that is chosen. If the mapping polynomial equation is first degree, then the required GCPs are three at least; if it is second degree then the number of GCPs is six and if third degree then ten GCPs are needed. In practice more GCPs than the required number are chosen and evaluated using the method of least squares estimation in order to avoid these points that may contain significant positional errors either on the map or the imagery. Since the grid of pixels in the source image rarely matches the grid for the reference map or image, the pixels are resampled so that new data file values for the output file can be calculated.

The nearest resampling method was used in order to finish geometric rectification. Hence, the choice, of these points on the Earth must carefully selected and the distribution of them must be around the edges of the image to be rectified with scattering of points over the body of the image. What is true during geometric correction is that the more GCPs are used the higher accuracy will occur for the image (Richards and Jia, 2006). After geometric correction was applied (Figure 2.8.) the time-series of satellite images were registered in the same earth coordinates and the plots with the needed cultivations were easily identified on the images. The images were geographically linked to each other using ERDAS Imagine commands.

.

(a)

(b)

Figure 2.8. Area of Interest before (a) and after geometric (b) correction

2.4. Methodology

An attempt hase been made to statistically describe the crop canopy factors, namely crop height (CH) and LAI, through the vegetation indices. Crop canopy factors are vital elements in the procedure of estimating ETc. These indices were produced from spectroradiometric measurements using a handheld field spectroradiometer (GER 1500) and after this data were filtered through the Relative Spectral Response (RSR) filters. At the same time LAI and CH

direct measurements were taken in situ. Hence, time series of LAI, CH and VI have been created and were used to model LAI and CH to VI. After applying the needed regression analysis and evaluating them, the best model for each crop, based on the determination factor (r^2), was used in specific ETc algorithms in a procedure to adapt and modify the algorithms in the geo-morphological and meteorological conditions of the island of Cyprus. Crop water requirements were inferred by applying the algorithms and it was tested to check if the specific modifications have assisted the algorithms to improve their precision when estimating ETc. The overall methodology is shown in Figure 2.9. The intended purpose is to estimate ETc of specific crops in the area of interest using remote sensing techniques.

- The area of interest was selected. The area is a flat area with mild climate, at sea level and with fertile soil.
- Spectroradiometric measurements were undertaken for two years (2009-10) in order to collect spectral signatures of each crop included in the study. For each crop (Potatoes, Groundnuts, Beans and Chickpeas) the average spectral signature in each phenological stage was created based on the two cultivating periods (2009-2010). The purpose is to have the reflectance of each crop during their phenological stages after the data was filtered through the Relative Spectral Response filters.
- Leaf Area Index (LAI) and Crop Height (CH) measurements were also taken simultaneously to spectroradiometric measurements and following the same phenological cycle of each crop for the corresponding cultivating periods. The purpose was to create time series of these two parameters to correlate them to Vegetation Indices (VI).
- Development of vegetation indices (VI). Time series of VI were created based on the reflectance of each crop, in each phenological stage.
- Modeling VI to LAI and CH. Different models were tested in order to identify the best possible model which better describes LAI and CH through VI.
- Preprocessing of satellite images was applied. Geometric rectification, radiometric correction including atmospheric correction of satellite data were applied before main processing of the data.
- Mapping LAI, CH and albedo was performed. The three crop canopy parameters were mapped using the ERDAS Imagine v.10 software. The satellite images were transformed into maps in order firstly to test in practice the models and secondly to be inserted as inputs in ETc algorithms.

- Models verification. After inferring the best model describing LAI or CH using VI, an evaluation of this procedure was taking place. A priori knowledge of satellite over passing over the area of interest has assisted the procedure of taking LAI and CH measurements in different plots and different cultivating period. These average measurements were compared to the predicted measurements arising from the models application found in the previous step.
- Application of ETc algorithms. Original and modified by previous equations, ETc algorithms have been applied to check, based on the reference method, if and how the models have boosted accuracy on estimating ETc for each crop.

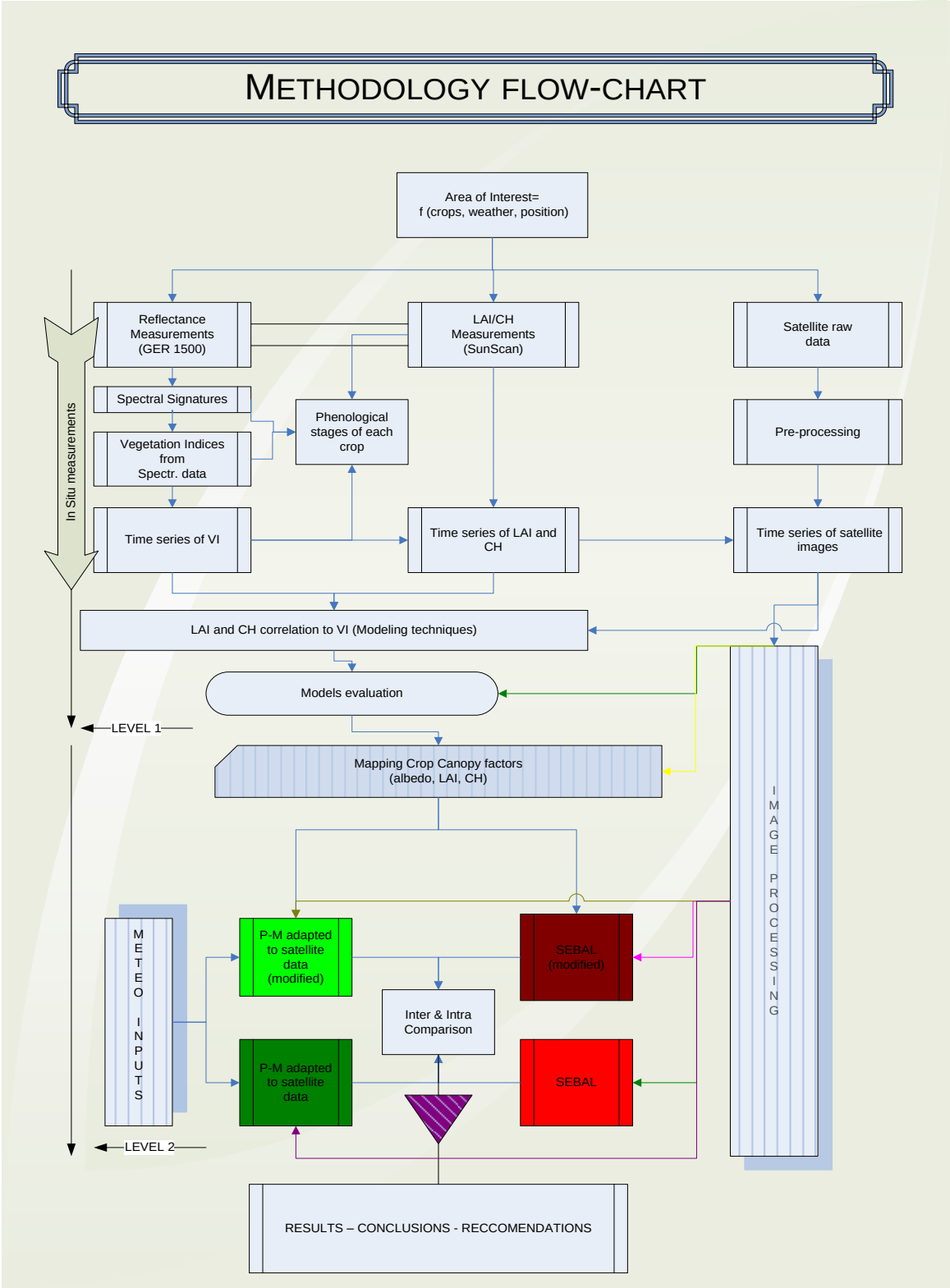

Figure 2.9. Overall methodology of the thesis

CHAPTER 3: GROUND DATA

In this Chapter, a brief background of field spectroscopy and optical properties of vegetation is described. Description of how ground measurements were conducted and how these measurements supported this study is explicated. The goal of this Chapter is to provide the techniques used to acquire essential ground data that are indispensable in the procedure for estimating ETc.

3.1. Field spectroscopy

Field spectroscopy is the quantitative measurement of radiance, irradiance, reflectance or transmission in the field (Milton, 1987; Hadjimitsis et al., 2009; Milton et al., 2009; Agapiou et al., 2010). It is used for a variety of studies including those that require the collection of field data for ground targets, for the more precise image analysis and investigation regarding irrigation water management (Dekker et al., 1995; Bojinski et al., 2003; Agapiou et al., 2010). The most widely used methodology in field spectroscopy concerns measurements of the reflectance of composite surfaces in situ (Milton et al., 2009). Increasingly, spectral data are being incorporated into process-based models of the Earth's surface and atmosphere, and it is therefore necessary to acquire data from terrain surfaces, both to provide the data for modeling specific parameters and for assisting in scaling-up data from the leaf scale to that of the pixel.

Over the last twenty years, a key role for field spectroscopy has emerged, as a means of scaling-up understanding of energy matter interactions from the fine scale of individual measurement elements (such as the leaf) to coarser canopy-scale studies (Gamon et al., 2006a; Milton et al., 2009). This has been reinforced by developments in airborne and satellite sensors which mean that spectral reflectance data from well-characterized areas of the Earth's surface are now essential to validate models. Field spectroradiometers were first used to study human colour vision, and in particular the color of the Earth's surface from the air (Penndorf, 1956). The development of airborne multispectral scanners in the 1960s spurred on the development of the first instruments capable of making accurate measurements of spectral reflectance in the field environment. One of the key challenges during the 1970s was to make accurate measurements in the short-wave infra-red region (1.1–

2.4 μm) which was known from laboratory measurements to be a very important part of the electromagnetic spectrum for geological applications (Kimes and Kirchner, 1982). Goetz (1975) described the first portable field spectroradiometer capable of measuring in this region as well as the visible and near infra-red. In most cases, the reflectance of a vegetation canopy or a soil surface is presented as a 'reflectance factor'. Nicodemus et al. (1977) introduced the concept of a reflectance factor, being the "ratio of the radiant flux actually reflected by a sample surface to that which would be reflected into the same reflected-beam geometry by a perfectly diffuse (Lambertian) standard surface irradiated in exactly the same way as the sample". This simplification of the measurement environment has proved a mixed blessing. It provided a practical method to make reflectance measurements in the field but it also introduced a second reflecting surface into the measurement procedure, the spectral and angular properties of which would affect the resulting reflectance. Despite considerable efforts by calibration panel manufacturers, reference panels are neither perfectly reflecting nor perfectly diffusive and because of the degree to which both these properties vary with wavelength, it has become necessary to pay close attention to the properties of the reference panel used (Gu and Guyot, 1993; Rollin et al., 2000). In particular, reference panels and spectroradiometer entrance optics must be carefully leveled, and care taken that the panel completely fills the field-of-view of the spectroradiometer, which is often difficult to check as very few spectroradiometers have provision for viewing the area measured (Bruegge et al., 2001). Using devices such as these, highly reproducible measurements can be made. The fixed sample/illumination geometry greatly reduces the uncertainty which is characteristic of ad hoc measurement configurations such as those used by Castro-Esau et al. (2006).

The use of a field spectroradiometer is essential and contributed significantly to this research by providing a number of direct comparisons between Landsat-5 TM / 7 ETM+ output and ground truth data. It provided the spectral signatures of indifferent crops following the phenological cycle of each crop so as to create vegetation indices from the red (R) and infra-red (IR) corresponding bands (3 and 4 respectively) of Landsat-5 TM and 7 ETM+, and correlate them to LAI and crop height.

3.1.1. Spectral signatures of crops

It is well established that the reflectance and transmission spectrum of leaves is a function of both the concentration of light absorbing compounds (chlorophylls, carotenoids, water, cellulose, lignin, starch, proteins, etc.) and the internal scattering of light that is not absorbed

or absorbed less efficiently (Newnham and Burt, 2001; Dangel et al., 2003). Each crop has a different spectral signature depending on the stage of its phenological cycle (Gouranga and Harsh, 2005; McCloy, 2010; Papadavid et al., 2011). A general view of the vegetation spectral signature is shown in Figure 3.1: there is strong absorption in blue and red part of the light spectrum while at green and infrared part there is light and strong reflectance, respectively.

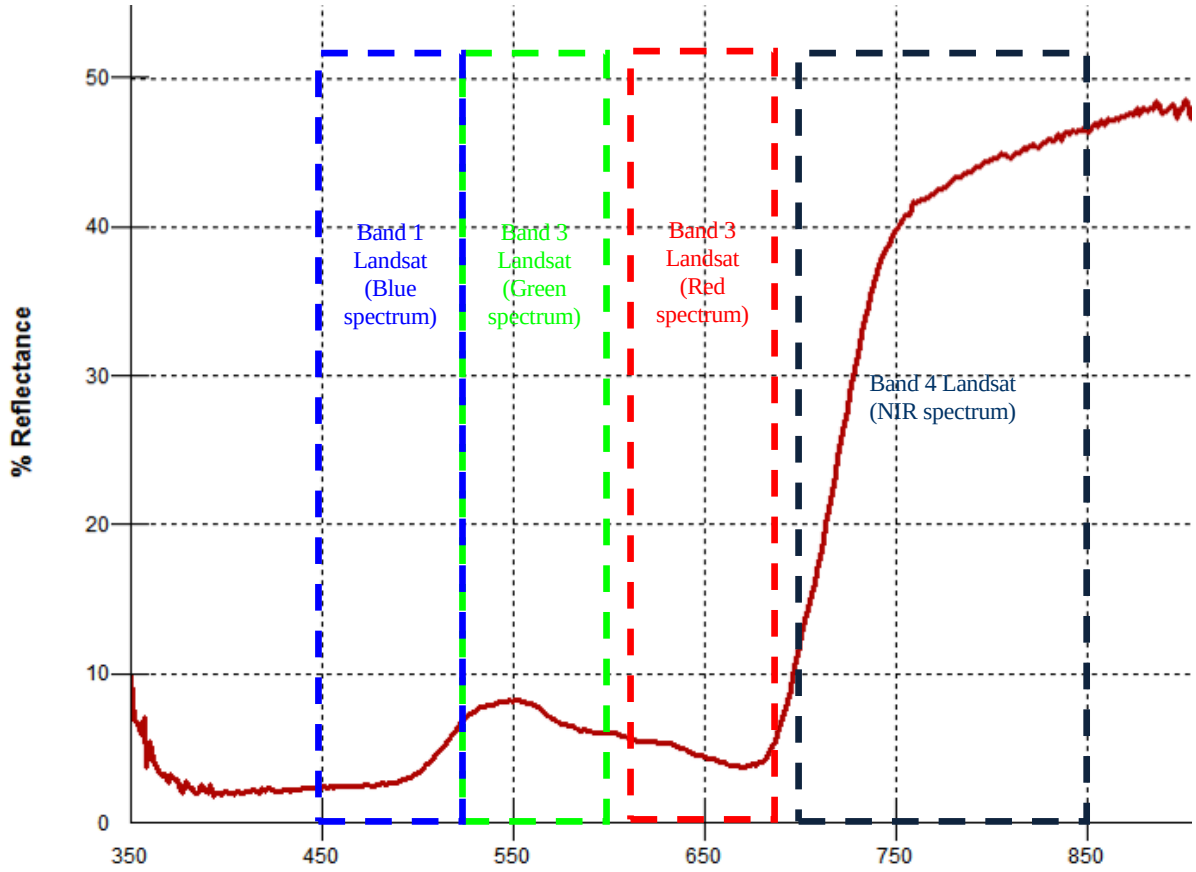

Figure 3.1. Vegetation spectral signature: Vegetation has low reflectance in the visible region and high reflectance in the near infrared (data analysis)

The domain of optical observations extends from 400 nm in the visible region of the electromagnetic spectrum to 2500 nm in the shortwave infrared region. The strong absorption of light by photosynthetic pigments dominates green leaf properties in the visible spectrum (400-700nm). Leaf chlorosis causes an increase in visible reflectance and transmission. The near-infrared region (NIR, 700-1100 nm) is a region where biochemical absorptions are limited to the compounds typically found in dry leaves, primarily cellulose, lignin and other structural carbohydrates (Wang et al., 2005). However, foliar reflection in this region is also affected by multiple scattering of photons within the leaf, related to the internal structure, fraction of air spaces, and air-water interfaces that refract light within leaves. The reflectance

and transmittance in the middle-infrared also termed the shortwave-infrared (SWIR, 1100 nm - 2500 nm) is also a region of strong absorption, primarily by water in green leaves (Maier, 2000).

More specifically, visible blue and red are absorbed by the two main leaf pigments, chlorophyll a and b in green-leaf chloroplasts. These strong absorption bands induce a reflectance peak in the visible green. Thus most vegetation has a green-leafy color. Chlorophyll pigments are also known as the green pigments.

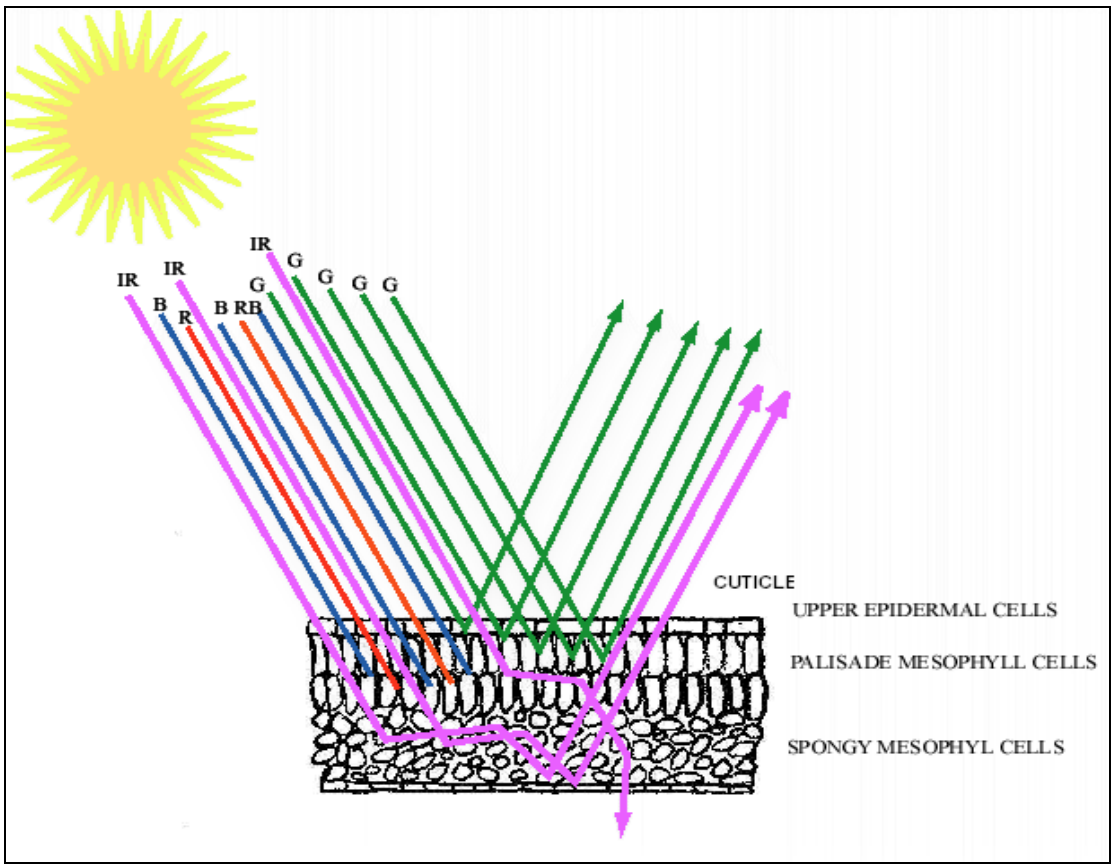

Figure 3.2. Leaf structure and light reflection (Source: www.photobiology.info)

Apart from chlorophyll, other leaf pigments have a significant effect on the visible spectrum. Carotene, a yellow to orange-red pigment strongly absorbs radiation in the 350-500 nm range and is responsible for the color of some flowers and leaves without chlorophyll. Xanthophyll, the red and blue pigment also strongly absorbs radiation in the 350-500 nm range, giving the distinctive color to the leaves in Autumn. In the near infrared range (700-1000 nm) of the electromagnetic spectrum, there is strong reflectance in the spongy mesophyll cells that occur at the back of leaves (Figure 3.2).

3.1.2. Phenology of the crops

Phenology can be defined as the study of the timing of biological events, the causes of their timing with regard to biotic and abiotic forces, and the interrelation among phases of the same or different species (Shaykewich 1994; Lieth 1974). As McCloy (2010) mentions the phenological cycle can be defined as the trace or record of the changes in a variable or attribute over the phenological period (usually one agricultural year) and a phenophase is defined as an observable stage or phase in the seasonal cycle of a plant that can be defined by start and end points. Obvious changes in each crop cycle can be identified in Figures 3.3-3.6 that show how crops grow during their life-cycle. In each figure, each photo represents a phenological stage of a crop, starting from the stage of 'closed lines' and ending at the stage of 'drying foliage', as it is shown in Table 3.1.

Figure 3.3. Phenological stages of beans

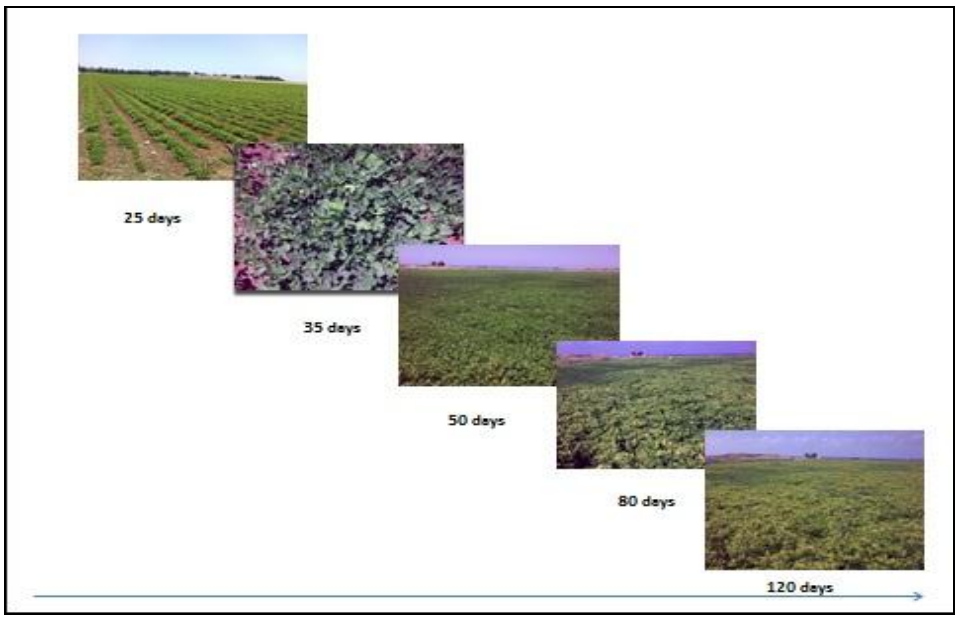

Figure 3.4. Phenological stages of groundnuts

Figure 3.5. Phenological stages of potatoes

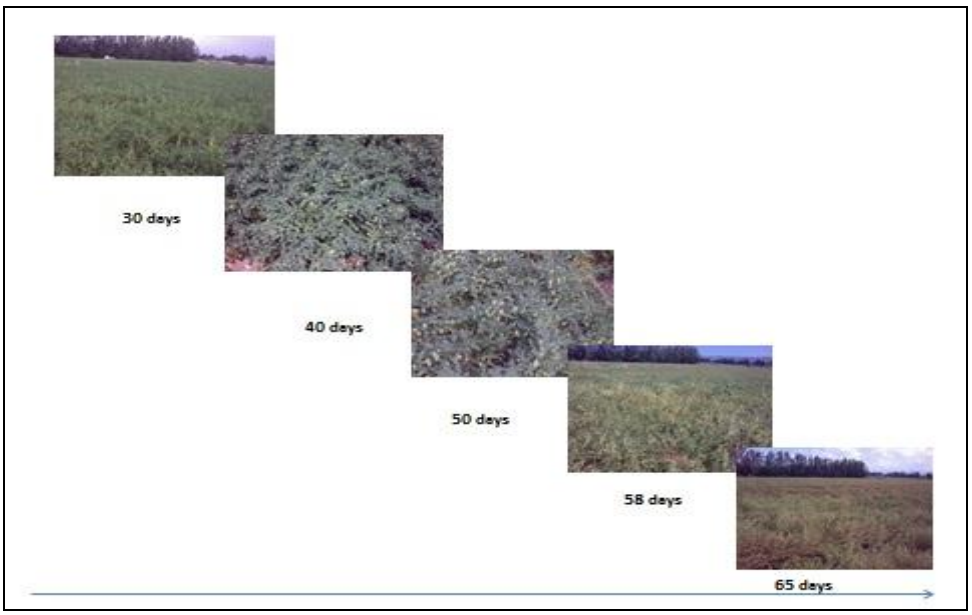

Figure 3.6. Phenological stages of chickpeas

Crop phenological stages are important indicators in agricultural production, management, planning, decision-making and irrigation scheduling (O' Leary et al. 1985; Gouranga and Harsh, 2005; Papadavid et al., 2011). Indeed, Food and Agriculture Organization (FAO) guidelines of estimating crop evapotranspiration for irrigation demands, take into account crop characteristics and the phenological stages of a crop; Crop coefficient (K_c)refers to crop growth stage and the length in time of this stage (Allen et al., 1998). Moreover crop phenology is difficult to be studied for large areas using traditional techniques and methods.

Traditionally, the monitoring of vegetation phenology has been based on human observers' reports (in situ observations) of the occurrence dates of easily-observed phenological stages. This need to understand crop phenology for large areas, has shifted scientific interest into satellite remote sensing data. The first attempts of remote sensing studies on phenological monitoring started in the mid 1980's (Justice et al., 1984). Satellite remote sensing has the potential to contribute to plant phenology monitoring at spatial and temporal scales relevant for regional and global scale studies. As opposed to field-based monitoring, remote sensing techniques can provide continuous information on phenology over time and space (Agapiou et al., 2009; Kross et al. 2011).

Recently, many studies have been performed in order to derive the crop phenological stages based on satellite images. These studies aim to validate vegetation indices for monitoring the development of the phenological cycle from times series data. For example, Sakamoto et al.

(2005), Minaccapili et al. (2008) and Papadavid et al. (2011) used times series of remotely sensed data in order to develop a new systematic method for detecting the phenological stages of different crops from satellite data while Bradley et al. (2007) in their study have introduced a curve fitting procedure in order to derive inter-annual phenologies from time series of noisy satellite NDVI data. Moreover, Funk and Budde (2009) have used an analogous metric of crop performance based on time series of NDVI satellite imagery. Moreover, ground spectro-radiometers have also been used in order to study the phenological cycle of potatoes. Papadavid et al. (2009; 2010; 2011) have shown that field spectroscopy and empirical modelling, when successfully integrated, can develop new models of Leaf Area Index (LAI) and Crop Height, during the phenological cycle of crops.

For this thesis, tables indicating the phenology of each crop were prepared with the help of the Agricultural Research Institute of Cyprus. Table 3.1 shows the phenological stages of each crop and the number of *in situ* measurements taken at each stage. The specific tables were prepared based on the crop calendar (Figure 3.7) for each crop.

Table 3.1. Tables with phenological stages of each crop. The number of spectroradiometric and LAI measurements are indicated for each stage

Phenological Stages of *Potatoes*	**GER1500 measurements**	**SunScan measurements**	**Phenological Stages of *Peas***	**GER1500 mean measurements**	**SunScan mean measurements**
Seed	0	0	Seed	0	0
Germ	0	0	Germ	0	0
Appearance	0	0	Appearance	0	0
Closed lines	3	3	Closed lines	1	1
Blossoming	5	5	Blossoming	2	2
Tube growth	5	5	Fruit growth	2	2
Foliage ageing	5	5	Fruit maturation	2	2
Tube maturation	5	5	Foliage ageing	2	2
Foliage drying	2	2	Foliage drying	1	1
Phenological stages of *Groundnuts*	**GER1500 measurements**	**SunScan measurements**	**Phenological stages of *Beans***	**GER1500 mean measurements**	**SunScan mean measurements**
Seed	0	0	Seed	0	0
Germ	0	0	Germ	0	0
Appearance	0	0	Appearance	0	0
Closed lines	3	3	Closed lines	2	2
Tube growth	5	5	Blossoming	4	4
Foliage ageing	5	5	Fruit growth	5	5

Tube maturation	4	4	Fruit maturation	5	5
Foliage drying	1	1	Foliage ageing	2	2
			Foliage drying	1	1

In each sub-table (Table 3.1), the phenological stages of each crop can be seen in the first column. In the 'GER 1500' column the number of spectroradiometric measurements taken at each stage are presented. For example, for Potatoes the measurements begun at the stage of 'closed lines' and there were 3 measurements during that stage (each measurement in the table is the average measurement from 25 measurements well spread in the plot, as it is mentioned in 3.2). In the third column labelled 'Sunscan measurements' the LAI measurements are presented for each phenological stage as for the second column which were taken simultaneously. The number of each spectroradiometric measurement is not random. There should be a change in the reflectance in the specific phenological stage to have another measurement meaning that the crop reflectance during two consecutive days could be the same so the measurement would not enter the table as different one.

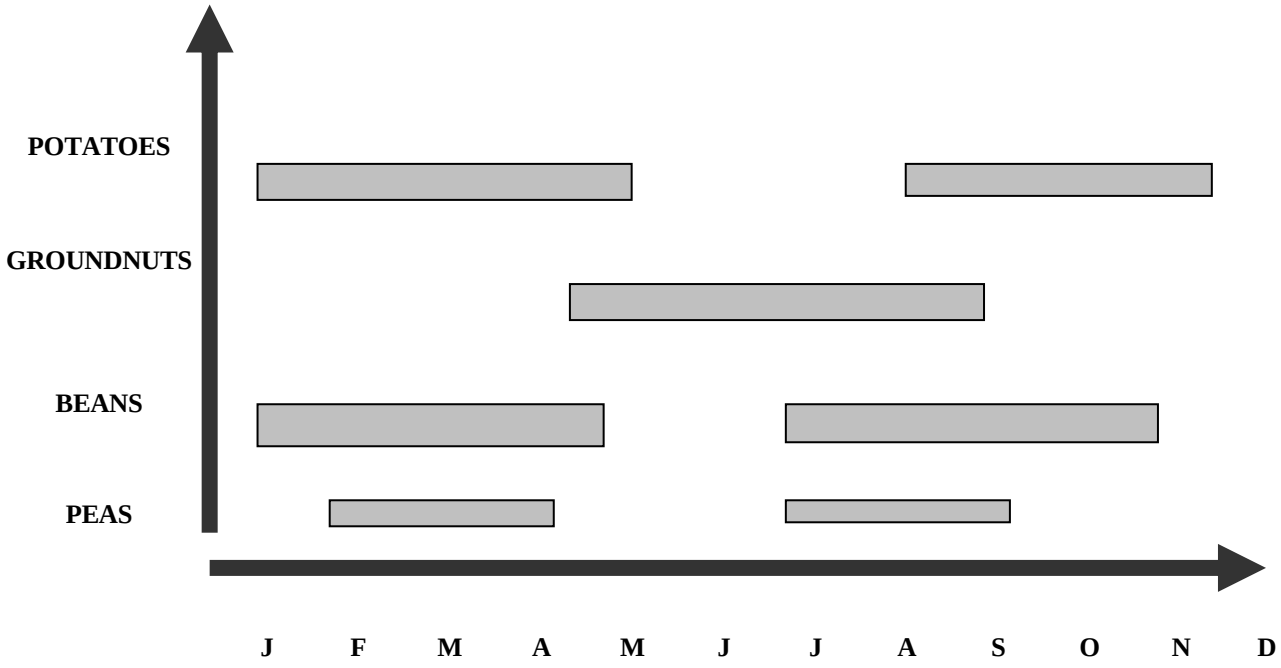

Figure 3.7. Crop calendar for Cyprus conditions (Agricultural Research Institute of Cyprus, 2008)

Changes in the phenological cycles of crops may occur from different parameters, such as weather conditions, soil and crop characteristics, and changes in the climate of an area (Minaccapili et al., 2008; Kross et al.,2011). Between years, phenological markers (such as length of growing season) may respond differently, a phenomenon which can be associated

with short-term climate fluctuations or anthropogenic forcing, such as groundwater extraction, urbanization (Bradley et al., 2007). However, the interpretation of phenological changes based on a large dataset volume for a period of many years can turn to be very complicated.

3.2. *In situ* field spectroradiometric sampling

Spectroradiometers are widely used to collect spectral data and are designed to match the wavebands of different satellites' sensors such as Landsat TM and ETM+ (McCloy, 1995; Hadjimitsis, 2000; Agapiou et al., 2010). For this research, a field spectroradiometer, GER 1500 was employed, with a range of spectrum from 350 nm to 1050 nm. The general and calibration characteristics of the GER 1500 are described by Milton et al. (1997).

The strategy for collecting the spectral reflectance of each crop had as a main axis the phenological stages of each crop, meaning any visible changes on the crop or any known expected changes of crops. The background of this strategy relies on the fact that any change in morphology or in color can cause change in the reflected radiance of the crop. Table 3.1 with the main phenological stages of each crop was used in order to take spectroradiometric measurements at each stage. Spectroradiometric and LAI measurements begun after the stage of closed lines for all crops, in order to avoid soil effects on spectroradiometric data and to have reliable data regarding LAI data (as referred in the SunScan manual).

For evaluation purpose, spectroradiometric measurements were also taken when there was a satellite over-pass. The aim is to have spectroradiometric data on these dates to compare them to the remotely sensed data for correction and atmospheric effects removal evaluation. The satellites' overpass is approximately at 9:30 and 11:00 am for Landsat-7 ETM+ and Landsat-5 TM respectively, so a suitable plan to cover as much as possible selected field points during an interval of ± 2 hours was made. When collecting field spectral measurements, it is necessary to be aware of the effects of various parameters during the acquisition of field data. Such parameters are solar illumination, target viewing, atmospheric characteristics, wind effects and target characteristics. Campbell (1996) and McCloy (1995) elaborate on the procedure for collecting spectral measurements and estimating the target reflectance, , while the main principles of field spectroscopy are presented by Milton (1987).

It is not easy to recommend a specific sampling strategy due to the limited availability of such studies. Campbell (1996) reviewed five sampling strategies, namely, simple random; sampling pattern; the stratified random pattern; systematic pattern; and the systematic stratified unaligned pattern; he found that the sampling procedure is depended on the nature of the problem. For the present work, simple random strategy was employed. Twenty five measurements well spread in each plot, were made randomly and collected in order to have a representative sample. However, the main concern for each spectroradiometric measurement carried out in the field is to ensure that these measurements are representative for the case study area. In order to overcome this critical consideration, Milton et al (2009) stated that the user has to ensure that reflectance measurements characterize variations in the inherent properties of the surface, and not the positional variations in the field. Indeed, the operator should be very careful to achieve a reproducible measurement position, such that the same point is measured on each visit. Such an approach was followed by the author (Figure 3.8). Spectroradiometric measurements were carried out using the GER 1500 field spectroradiometer. GER 1500 can record electromagnetic radiation between 350 nm up to 1050 nm. A reference calibrated spectralon panel was used to measure the incoming solar radiation. The spectralon panel (with reflectance ≈100%) measurement was used as a reference one, while the measurement over the crops as a target (Figure 3.9). Therefore, the reflectance for each measurement can be calculated using the following equation (1):

$$\text{Reflectance} = (\text{Target Radiance} / \text{Panel Radiance}) \times \text{Calibration of the panel} \quad (1)$$

In order to avoid any errors due to significant changes in the prevailing atmospheric conditions, the measurements over the panel and the target were taken with short time lag. In this case it was assumed that irradiance had not significant change which is true for non hazy days (Milton et al., 2009).

Figure 3.8. Field spectroradiometric measurements acquired over potatoes in Mandria village, Paphos, Cyprus

All the measurements have been taken from nadir view, from a height of 1.2 m using a 4^{o} Field of View (FOV) lens. The target area from that height is a circle with a 8 cm diameter. At latter stage the users could discard any unexpected spectral signatures sourcing from unexpected mistakes. For achieving the filtering and subsequent discarding of data, the authors used typical spectral signatures from spectral libraries of crops and from previous spectral measurements of crops acquired in other previous projects from the Remote Sensing Lab of the Cyprus University of Technology (Figure 3.6).

The direct comparison of reflectance measurements acquired from fine resolution sensors such as field spectroradiometers with other medium resolution sensors, such as the Landsat TM/ETM+, has been discussed by other researchers (Curran and Williamson, 1986; Milton and Rollin, 2006; Milton et al 2009). The question of how many samples are needed to characterize a surface has been addressed experimentally and statistically as mentioned by Milton and Rollin (2006). To ensure reliable data collection, the reflection of the white reference panel was recorded every three measurements (Figure 3.9).

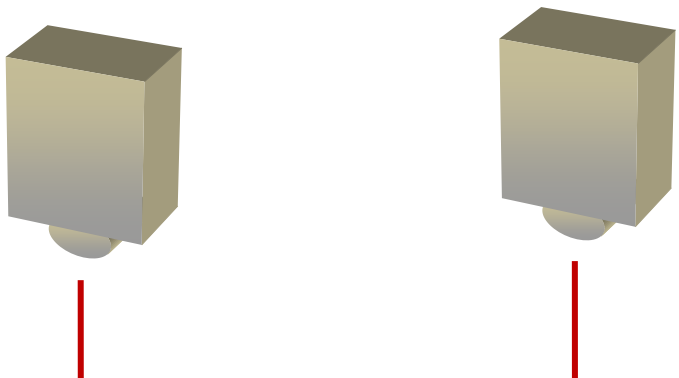

Figure 3.9. GER 1500 field spectro-radiometric measurements procedure

At the end of every set of measurements (in each plot), the reflectance of the white reference panel was recorded again. A typical diagram of a GER 1500 measurement can be seen in Figure 3.10. All spectra of a sampling point were averaged to produce a representative sample at each point. The same procedure was followed for the whole plot in order to have a representative sample of each plot in each stage of the crops. Figures 3.11-3.14 show the spectral signature of each crop during the main phenological stages. Each number corresponds to a phenological stage starting always from the 'closed lines' stage and ending with arithmetic sequence as it is explained in Table 3.1 in the stage of 'foliage drying'.

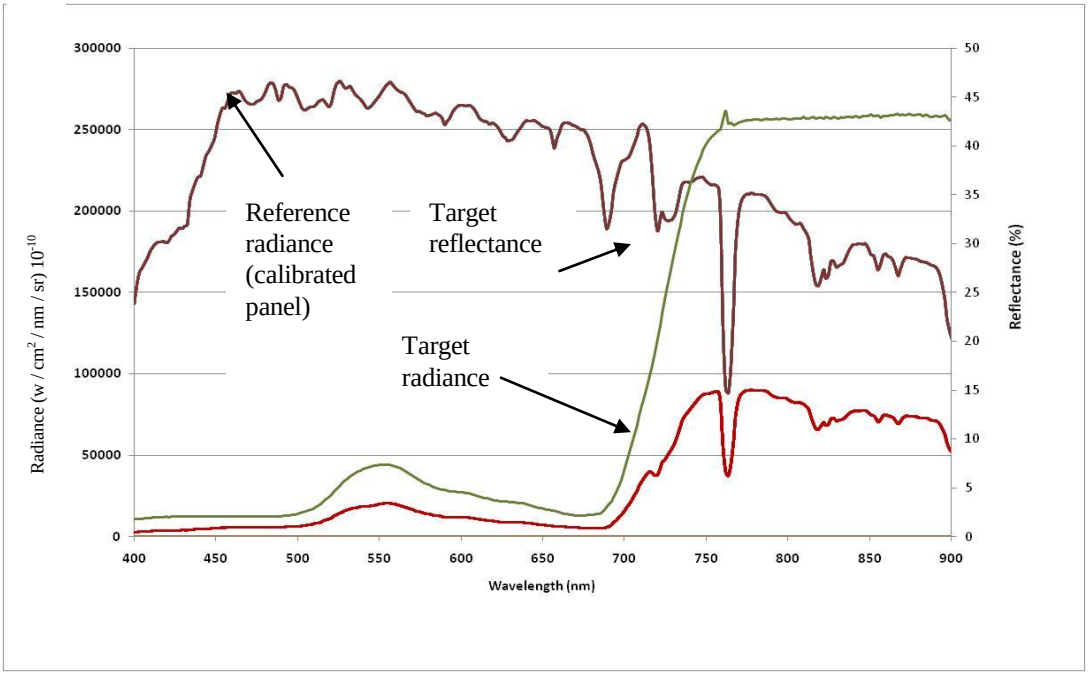

Figure 3.10. Typical diagram of in-situ measurements

For example, regarding Figure 3.13, number 1 refers to the stage of ‘closed lines, number 2 to the stage of ‘blossoming’, number 3 for the stage of ‘tube growth’, number 4 for the stage of ‘foliage ageing’, number 5 for the stage of ‘tube maturation’ and number 6 for the stage of ‘foliage drying’ for the potatoes.What is observed during the analysis of the reflectance from the spectroradiometer, is the cycle of the reflectance at the visible and infrared spectrum. The reflectance at the visible spectrum, as mentioned before, is reduced due to the chlorophyll’s and carotenoids absorption except a region in the green spectrum where there is a peek of green reflectance which explains why crop leaves are seen green.

In the NIR spectrum (wavelength > 0.7 micrometers), reflectance starts to differentiate for all the dates of acquisition for each crop. As it is observed, the reflectance increases as time passes, reaching a peak, at the stage of fruit or tube maturation and most generally the stage of carpophores. The maximum value is reached at the stage of fruit setting where the leaves are in the maximum turgor. When the crops are in this stage, they absorb the maximum of the potential soil nutrients and water (Sheeler and Bianchi, 1987). Thus, leaves are enabled to increase their volume due to water absorption and air that is stored among the mesophyll cells, which are responsible for the reflection of IR radiation. Then a reduction of reflectance starts, in the IR spectrum, until the crop gets dry, marking the end of the life cycle of the crop and the end of spectroradiometric measurements. This fact applies to all crops’ spectral signatures that were under investigation for this research, meaning that all crops followed the same reflectance stages (for IR spectrum), with low reflectance at the beginning of their life which is growing as crops grow-up. This development of reflectance comes to a peek and then starts to reduce until the crop is dried or ripened.

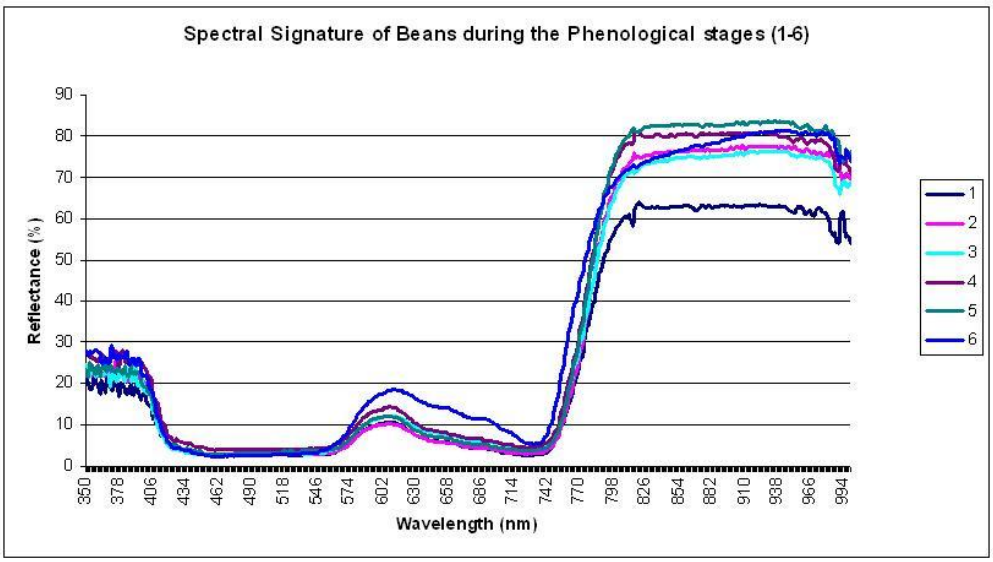

Figure 3.11. Spectral Signature of beans during its main phenological stages (1-6 as in Table 3.1)

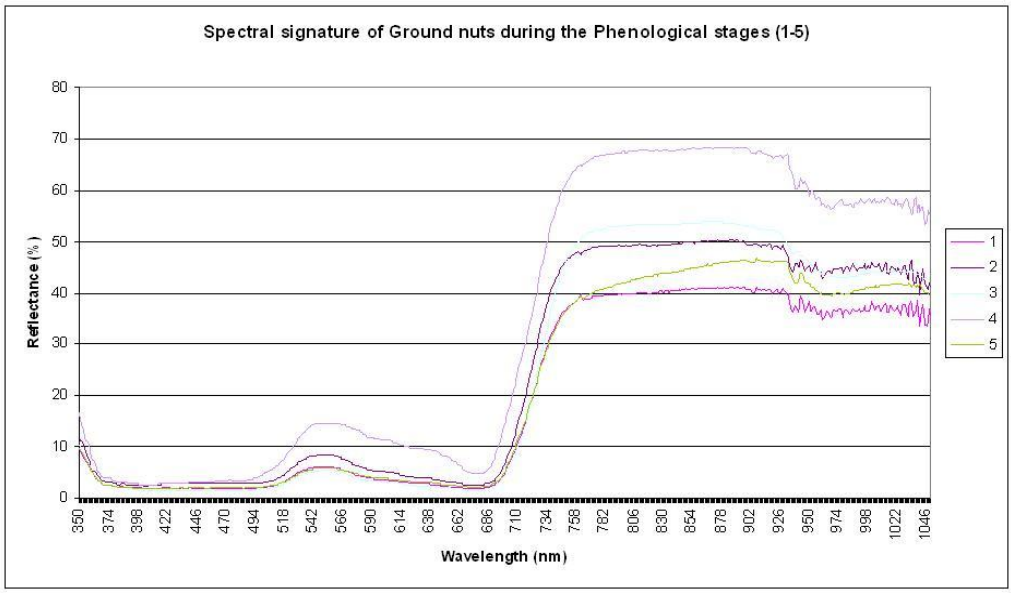

Figure 3.12. Spectral Signature of groundnuts during the main phenological stages (1-5 as in Table 3.1)

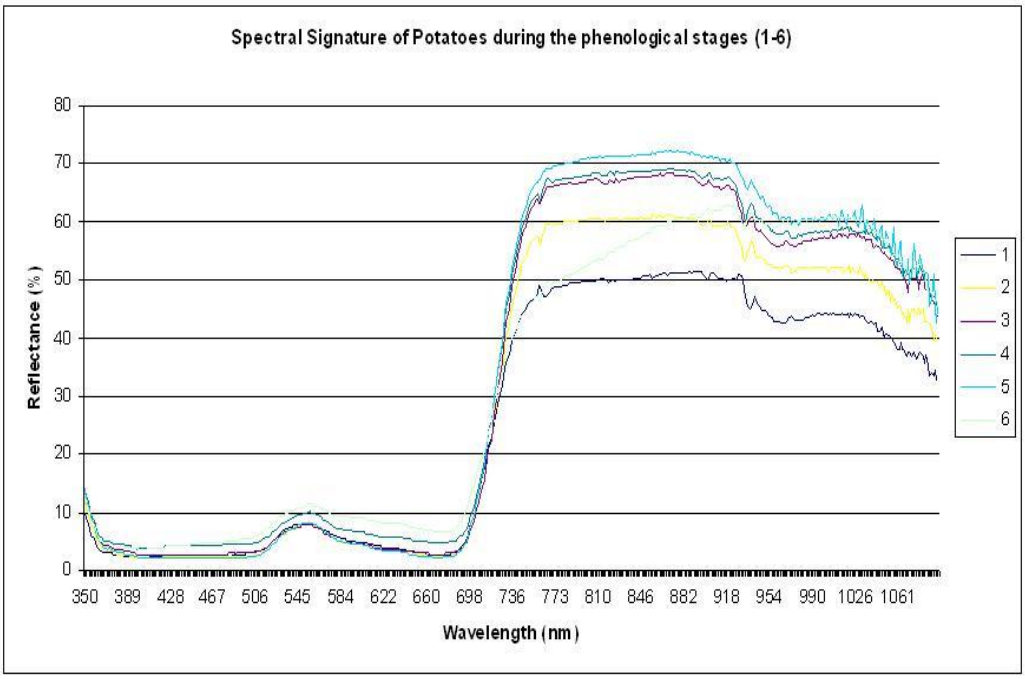

Figure 3.13. Spectral Signature of potatoes during the main phenological stages (1-6 as in Table 3.1)

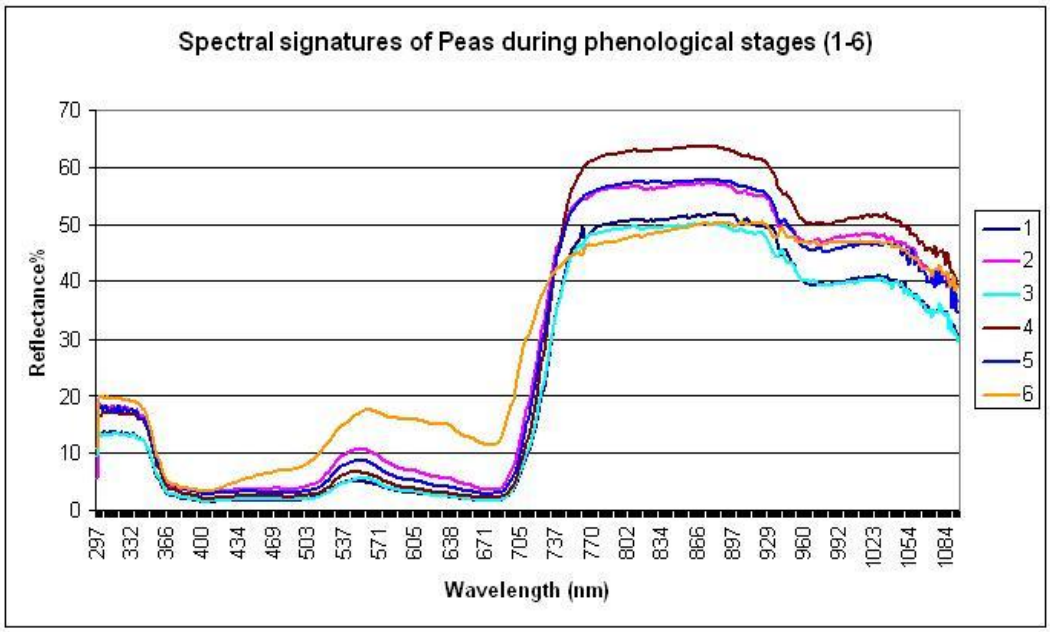

Figure 3.14. Spectral Signature of chickpeas during its main phenological stages (1-6 as in Table 3.1)

3.2.1. Converting GER 1500 spectroradiometric reflectance into 'Landsat 5TM / 7ETM+ in band reflectance'

After spectroradiometric data of each crop have been acquired, the task is to estimate the surface reflectance values equivalent to the Landsat-5 and 7 bands (1, 2, 3 and 4) using *in situ* the GER1500 spectroradiometer. To filter the data through the relative spectral response

(RSR) values of Landsat TM/ETM+ which are given from the satellite manufacturer, the GER1500 reflectance values were interpolated to obtain the reflectance values at the incremental wavelength of the RSR. This was done since the GER1500 reflectance values were given at a different incremental wavelength scale. In the case where a direct comparison of any ground data from any sensor or device with image data is performed, several authors reported that it is necessary to use the Relative Spectral Responses (RSR) of the sensor (Wilson, 1988; Tassan, 1992). This procedure is also called as "filtering" of ground data to match the satellite sensor bands (Tassan, 1992, Hadjimitsis et al., 2000; Agapiou et al., 2009). An example of this procedure can be seen in Figure 3.15.

The spectral resolution of the Landsat TM/ETM+ is indicated by the relative spectral response (RSR) of the various spectral bands. RSR describes the spectral integration of the received radiance (Schott, 1997; Schowengerdt, 1997). In order to match another spectral measurement with a TM/ETM+ band, it is necessary to use the TM/ETM+ relative spectral response functions (RSR) (Slater, 1980) and average within the limits of every TM/ETM+ bands to obtain the equivalent in-band reflectance values. This filtering procedure was used in this research to match the ground measurements obtained using a GER1500 field spectro-radiometer with those from TM/ETM+ bands 1, 2, 3 and 4. Details about the RSR of Landsat-5 TM can be found in Markham and Barker (1987), Schott (1997) and Schowengerdt (1997). For converting the at-satellite radiance into reflectance, a number of simplifying assumptions about the target, sensor and solar irradiance characteristics were made in the present study. These assumptions are listed below:

- Lambert's reflectance law (Campbell, 1996) was assumed to be valid for any point on the surface. That is, the reflecting surfaces were assumed to be perfectly diffuse, appearing equally bright from all viewing directions (Teillet 1986; Campbell, 1996). The incident energy is scattered more or less equally in all directions.
- The target surface was assumed to be illuminated by the sun with solar irradiance at the top of the atmosphere and the values found in the literature by several experiments were used (Neckel and Labs, 1984).
- Nadir viewing (i.e. vertical observation) was assumed for Landsat TM and ETM +) (considering the relatively small field of view of the Landsat TM ± 7.5°).

Then, the GER 1500 experimental data were filtered through the RSR functions and averaged within the limits of the first four TM/ETM+ bands, to yield the in-band reflectance values (average corresponding reflectance value).

	13-March 2009						
	GER wavelength (nm)	GER real spectrum ρ %	Interpolated real spectrum ρ %	wavelength (every 1nm) (nm)	Interpolated real spectrum ρ %	RSR (filter function)	GER*Filter
4	449,11	2,55		450	2,555053328	0,84	2,1436897
5	**450**		2,555053328	451	2,511447841	0,85	2,1221734
6	450,74	2,51		452	2,497955214	0,81	2,0233437
7	**451**		2,511447841	453	2,534461111	0,80	2,0326378
8	**452**		2,497955214	454	2,540055948	0,80	2,042205
9	452,37	2,5		455	2,536543611	0,78	1,9759675
10	**453**		2,534461111	456	2,542118432	0,80	2,0286105
11	453,99	2,54		457	2,52861673	0,82	2,0633513
12	**454**		2,540055948	458	2,534149809	0,88	2,2199152
13	**455**		2,536543611	459	2,550666841	0,89	2,2649922
14	455,62	2,54		460	2,567153808	0,90	2,3130056
15	**456**		2,542118432	461	2,572734577	0,92	2,3617703
16	**457**		2,52861673	462	2,569221448	0,90	2,3020224
17	457,25	2,53		463	2,585755563	0,90	2,3349373
18	**458**		2,534149809	464	2,591340348	0,89	2,3011102
19	458,88	2,55		465	2,627796042	0,89	2,3387385
20	**459**		2,550666841	466	2,633447216	0,86	2,2726649
21	**460**		2,567153808	467	2,639098391	0,86	2,2696246
22	460,51	2,57		468	2,65556079	0,84	2,2359822
23	**461**		2,572734577	469	2,671994025	0,87	2,3139468
24	**462**		2,569221448	470	2,668410309	0,88	2,334859
25	462,14	2,57		471	2,674087777	0,88	2,3558713
26	**463**		2,585755563	472	2,670565798	0,89	2,3714624
27	463,76	2,59		473	2,657022786	0,90	2,3860065
28	**464**		2,591340348	474	2,662640171	0,88	2,3404607
29	**465**		2,627796042	475	2,639111036	0,88	2,3329742
30	465,39	2,63		476	2,64466706	0,91	2,398713
31	**466**		2,633447216	477	2,621153967	0,93	2,4324309
32	**467**		2,639098391	478	2,577788926	0,93	2,4024993
33	467,02	2,65		479	2,58318179	0,96	2,4669386
34	**468**		2,65556079	480	2,549787518	0,96	2,4426964
35	468,65	2,67		481	2,555099575	0,95	2,4222344
36	**469**		2,671994025	482	2,541740196	0,95	2,4197367
37	**470**		2,668410309	483	2,528481864	0,96	2,4172287
38	470,28	2,67		484	2,533716816	0,98	2,4830425
39	**471**		2,674087777	485	2,550420688	0,98	2,4994123
40	471,9	2,67		486	2,647004419	0,98	2,5808293
41	**472**		2,670565798	487	2,65245093	0,97	2,5808348
42	**473**		2,657022786	488	2,657897441	0,98	2,5967658
43	473,53	2,66		489	2,674484821	0,96	2,5621565
44	**474**		2,662640171	490	2,731114741	0,97	2,6355257
45	**475**		2,639111036	491	2,787558757	0,96	2,6676937
46	475,16	2,64		492	2,793236066	0,95	2,6591607
47	**476**		2,64466706	493	2,849710983	0,97	2,7727688
48	476,79	2,62		494	2,915986092	0,97	2,8401705
49	**477**		2,621153967	495	2,921888898	1,00	2,9072795
50	**478**		2,577788926	496	2,988132417	0,99	2,9462986
51	478,41	2,58		497	2,994156878	0,99	2,9522387
52	**479**		2,58318179	498	3,060430181	0,99	3,0420676

Sheet1 | **Band 1 13-03** | Band 2 13-03 | Band3 1303 | Band 4 1303

Figure 3.15. Example of converting GER 1500 data into 'Landsat in-band reflectance'

From the field spectroradiometer measurements, directly by applying the ratio of the reflected radiance from the target to the reflected radiance from the panel, the reflectance of the target is obtained. Field spectroradiometric data was transposed into in-band reflectance, which means that it is comparable to the reflectance that one should find after applying atmospheric and radiometric corrections to the satellite images. The 'in-band reflectances' for each crop are shown in Tables 3.2-3.5 (for the first 4 bands of Landsat TM and ETM+) for each phenological stage and each crop. The new filtered GER 1500 spectroradiometric reflectance (see Appendix 1 in Appendices) match the Landsat reflectance as it is shown in Figure 3.1.

Table 3.2. Ground spectroradiometric data, NDVI, SAVI, WDVI, LAI and CH for beans

GER 1500 measurements	Band 1 (450-520 nm)	Band 2 (520-600nm)	Band 3 (630-669nm)	Band 4 (760-900 nm)	NDVI	SAVI	WDVI	LAI m^2/m^2	CROP HEIGHT m
1	0,04	0,09	0,07	0,53	0,77	0,67	0,43	1,10	0,16
2	0,03	0,11	0,08	0,58	0,76	0,69	0,47	1,10	0,17
3	0,04	0,11	0,08	0,55	0,75	0,67	0,44	1,40	0,17
4	0,04	0,11	0,09	0,59	0,74	0,68	0,47	1,60	0,18
5	0,03	0,12	0,09	0,58	0,73	0,67	0,46	1,80	0,19
6	0,03	0,12	0,09	0,64	0,75	0,72	0,52	1,90	0,23
7	0,04	0,13	0,08	0,66	0,78	0,75	0,55	2,00	0,26
8	0,05	0,13	0,10	0,67	0,74	0,72	0,53	2,00	0,26
9	0,04	0,13	0,10	0,68	0,74	0,73	0,54	2,10	0,27
10	0,03	0,14	0,08	0,68	0,79	0,76	0,57	2,10	0,28
11	0,05	0,13	0,09	0,71	0,78	0,76	0,59	2,20	0,28
12	0,03	0,14	0,08	0,72	0,80	0,79	0,61	2,30	0,29
13	0,04	0,14	0,08	0,74	0,80	0,79	0,63	2,40	0,29
14	0,05	0,13	0,08	0,75	0,81	0,81	0,64	2,40	0,30
15	0,05	0,13	0,07	0,77	0,83	0,84	0,67	2,60	0,31
16	0,04	0,14	0,07	0,79	0,84	0,85	0,69	2,60	0,30
17	0,03	0,13	0,07	0,76	0,83	0,83	0,66	2,60	0,29
18	0,03	0,12	0,06	0,72	0,85	0,82	0,63	2,20	0,26
19	0,05	0,14	0,06	0,61	0,82	0,75	0,53	1,60	0,24

Table 3.3. Ground spectroradiometric data, NDVI, SAVI, WDVI, LAI and CH for groundnuts

GER 1500 measurements	Band 1 (450-520 nm)	Band 2 (520-600 nm)	Band 3 (630-669 nm)	Band 4 (760-900 nm)	NDVI	SAVI	WDVI	LAI m^2/m^2	CROP HEIGHT m
1	0,03	0,14	0,08	0,42	0,68	0,54	0,31	0,90	0,19
2	0,02	0,14	0,08	0,40	0,66	0,52	0,29	0,90	0,20
3	0,03	0,13	0,09	0,48	0,69	0,59	0,36	0,90	0,21
4	0,03	0,15	0,10	0,50	0,66	0,58	0,36	1,00	0,22
5	0,03	0,14	0,10	0,50	0,67	0,58	0,36	1,10	0,25
6	0,02	0,12	0,11	0,51	0,65	0,57	0,36	1,40	0,27
7	0,02	0,13	0,10	0,52	0,68	0,60	0,38	1,40	0,28
8	0,02	0,13	0,09	0,53	0,71	0,63	0,41	1,60	0,29
9	0,02	0,12	0,08	0,53	0,74	0,65	0,42	2,00	0,35
10	0,05	0,15	0,09	0,56	0,72	0,65	0,44	2,40	0,37
11	0,05	0,16	0,08	0,57	0,75	0,68	0,46	2,50	0,41
12	0,03	0,13	0,07	0,66	0,81	0,77	0,57	2,70	0,43
13	0,03	0,13	0,08	0,69	0,79	0,77	0,58	2,90	0,44
14	0,04	0,13	0,08	0,68	0,79	0,76	0,57	2,80	0,44
15	0,03	0,09	0,07	0,63	0,80	0,74	0,53	2,70	0,43
16	0,03	0,09	0,05	0,62	0,86	0,78	0,55	2,50	0,43
17	0,01	0,08	0,05	0,53	0,81	0,70	0,45	2,50	0,42
18	0,02	0,05	0,06	0,43	0,76	0,60	0,35	2,20	0,41

Table 3.4. Ground spectroradiometric data, NDVI, SAVI, WDVI, LAI and CH for potatoes

GER 1500 measurements	Band 1 (450-520 nm)	Band 2 (520-600 nm)	Band 3 (630-670 nm)	Band 4 (760-900 nm)	NDVI	SAVI	WDVI	LAI m^2/m^2	CROP HEIGHT m
1	0,03	0,08	0,06	0,46	0,77	0,63	0,38	1,10	0,26
2	0,04	0,08	0,06	0,47	0,77	0,64	0,39	1,30	0,26
3	0,05	0,11	0,07	0,50	0,75	0,64	0,41	1,60	0,27
4	0,04	0,09	0,07	0,53	0,77	0,67	0,44	1,60	0,27
5	0,04	0,09	0,07	0,54	0,77	0,68	0,45	1,50	0,28
6	0,03	0,08	0,06	0,55	0,80	0,71	0,47	1,60	0,28
7	0,04	0,09	0,06	0,55	0,80	0,71	0,47	1,60	0,28
8	0,04	0,09	0,06	0,56	0,81	0,71	0,48	1,70	0,29
9	0,04	0,1	0,07	0,56	0,78	0,69	0,47	1,80	0,29
10	0,04	0,1	0,07	0,57	0,78	0,70	0,48	1,70	0,28
11	0,05	0,10	0,07	0,58	0,78	0,71	0,49	1,80	0,28
12	0,04	0,10	0,07	0,59	0,79	0,72	0,51	2,00	0,32
13	0,05	0,10	0,06	0,59	0,82	0,74	0,51	2,10	0,31
14	0,05	0,10	0,07	0,60	0,79	0,72	0,51	2,40	0,31
15	0,05	0,11	0,07	0,62	0,79	0,73	0,53	2,60	0,32
16	0,05	0,12	0,07	0,63	0,79	0,74	0,53	2,60	0,33
17	0,05	0,10	0,07	0,63	0,80	0,75	0,54	2,80	0,35
18	0,05	0,10	0,07	0,64	0,79	0,74	0,54	3,30	0,36
19	0,06	0,12	0,08	0,65	0,79	0,75	0,56	3,50	0,38
20	0,06	0,11	0,08	0,66	0,80	0,76	0,57	3,60	0,39
21	0,06	0,12	0,08	0,68	0,78	0,76	0,58	3,70	0,38
22	0,05	0,10	0,07	0,67	0,81	0,77	0,58	3,70	0,40
23	0,04	0,10	0,07	0,71	0,83	0,80	0,62	3,30	0,41
24	0,07	0,14	0,07	0,56	0,78	0,69	0,47	2,60	0,33
25	0,07	0,14	0,07	0,42	0,71	0,57	0,33	1,90	0,22

Table 3.5. Ground spectroradiometric data, NDVI, SAVI, WDVI, LAI and CH for chickpeas

GER 1500 measurements	Band 1 (450-520 nm)	Band 2 (520-600 nm)	Band 3 (630-669 nm)	Band 4 (760-900 nm)	NDVI	SAVI	WDVI	LAI m^2/m^2	CROP HEIGHT cm
1	0,02	0,04	0,03	0,51	0,89	0,74	0,47	0,90	0,17
2	0,04	0,07	0,02	0,50	0,92	0,75	0,47	1,40	0,19
3	0,02	0,05	0,02	0,54	0,93	0,78	0,51	1,70	0,2
4	0,02	0,04	0,02	0,54	0,93	0,78	0,51	1,90	0,21
5	0,03	0,06	0,02	0,55	0,93	0,79	0,53	1,90	0,21
6	0,03	0,05	0,03	0,61	0,92	0,83	0,58	2,10	0,22
7	0,04	0,08	0,02	0,57	0,93	0,81	0,54	2,20	0,22
8	0,03	0,07	0,02	0,52	0,92	0,76	0,49	1,90	0,21
9	0,03	0,06	0,03	0,46	0,89	0,70	0,42	1,60	0,17
10	0,03	0,07	0,04	0,48	0,85	0,69	0,43	0,90	0,17

It is very important that in addition to spectral measurements, other information was recorded concerning the *in situ* weather conditions, characteristics of the site and measurement method. Such details include (Milton, 1987):

- Geographical location of site (latitude and longitude)
- Time of measurement
- Cloud cover
- Details on reference panel
- Viewing geometry and instrument support (mast, tripod, hand-held)
- The height of measurements above target
- The delay between target and reference panel measurements

3.3. *In situ* LAI and Crop Height sampling (CH)

During the field campaign, and simultaneously to spectroradiometric measurements, LAI and crop height measurements were also taken (Tables 3.2-3.5). Using the SUN-SCAN canopy analyzer (Delta-T Devices Ltd., UK) (Figure 3.16), users can get the value of LAI directly by setting it up perpendicular to the crop rows (Stancalie et al., 2010) (all crops used in this study are annual crops having a "row" arrangement in the field). A calibration measurement above the canopy is needed for each time the user takes a measurement in the crops. The SunScan is calibrated under a standard light source against an accurate Photosynthetic Active Radiation (PAR) quantum sensor. The spectral and cosine responses of the sensors approximate to the ideal response, but fall off at the extremes of the range. Under most normal daylight conditions errors due to the deviation are small, but it is possible, for example under artificial light, to find larger errors in the absolute values measured. Because the Sunshine Sensor and Probe are closely matched, this has minimal affect on the canopy calculations which are based on ratios of incident and transmitted light (Lambert et al., 1999).

The specific instrument measures the LAI value of the crop under the current conditions. These values are used to subsequently create empirical models between them and vegetation indices. The same methodology, as for spectroradiometric measurements, was followed regarding the time of the measurements and the sample strategy. Hence, for every average spectroradiometric measurement there is a corresponding average LAI and CH measurement. CH measurements were conducted using a simple rule. Fifteen to twenty LAI and CH random measurements were conducted to proceed with an average value of each parameter (LAI and CH).

(a)

(b)

Figure 3.16. Use of SunScan canopy analyzer for LAI measurements (a and b)

3.4. Vegetation Indices from spectroradiometric data

Vegetation indices (VI) have been widely used for assessing vegetation condition, cover, phenology, and processes such as evapotranspiration (ET), climate and land-use-change detection and drought monitoring (Haboudane et al., 2004; Glenn et al., 2008; Toulios et al., 2010). VI are robust satellite data products computed the same way across all pixels in time and space, regardless of surface conditions. As ratios, they can be easily cross-calibrated across sensor systems, ensuring continuity of data sets for long-term monitoring of the land surface and climate-related processes (Glenn et al., 2008). More than fifty different remote sensing vegetation indices have been used in the literature so far (Bannari et al., 1995;

Hadjimitsis et al., 2009). For agricultural and land use applications, the most widely used vegetation indices are briefly reviewed for the purpose of this study:

NDVI, SAVI and WDVI are the spectral vegetation indices that were selected in order to be correlated to LAI and crop height. Such indices are found to be widely used in various evapotranspiration algorithms and models.

An overview of the basics of each of the above indices is shown below:

NDVI: The most known and widely used ratio-based index is the normalized difference vegetation index (NDVI) (Rouse et al., 1974). NDVI is very sensitive to soil background at low LAI, and the sensitivity of NDVI to LAI weakens when LAI exceeds a threshold value, which is typically around three (Huete, 1989).

$NDVI = (NIR - R)/(NIR + R)$

where, NIR is the reflectance of near infrared band, RED is the reflectance of visible red band. NDVI is ranging from –1 to +1.The negative value represents non-vegetated area while positive value represents vegetated area.

SAVI: Huete (1988) developed the soil-adjusted vegetation index (SAVI) by shifting the convergent point of iso-vegetation lines from the origin to a point in the quadrant of negative red and NIR values. Many studies have indicated that SAVI not only reduces the effect of soil variability for low LAI, but also increases the sensitivity to high LAI (Baret and Guyot, 1991; Elvidge and Chen, 1995; Barnes et al, 2003). However, in order to determine the optimal value of the soil background adjustment factor L, prior knowledge about vegetation density or LAI is required, which creates a loop problem since LAI is the unknown target variable. L varies with the reflectance characteristics of soil. The L factor chosen depends on the density of the vegetation. For very low vegetation L factor can be taken as 1.0 while for intermediate it can be taken as 0.5 and for high density 0.25. The best L value to select is where the difference between SAVI values for dark and light soil is minimal. As mentioned by Huete (1988), L is set to 0.5 for optimal results for a wide range of conditions. SAVI is mathematically expressed as:

$SAVI = (1 + L)(NIR - R)/(NIR + R + L)$

where, NIR is the reflectance of near infrared band, RED is the reflectance of visible red band and L is the soil adjustment factor.

WDVI: WDVI is a corrected near-infrared reflectance, known as Weighted Difference Vegetation Index. WDVI is calculated by subtracting the contribution of the soil from the measured reflectance.

As WDVI is a distance based index, relatively better atmospheric correction needs to be applied to the data, which is not necessary for ratio based indices like NDVI and SAVI. But using spectroradiometer, as mentioned before this limitation is bypassed. Weighted Difference Vegetation Index (WDVI) is defined as follows (Clevers, 1989):

$$WDVI=NIR-\gamma R$$

where, NIR is the reflectance of near infrared band, RED is the reflectance of visible red band, γ is the slope of the soil line (Baret et al., 1993). The WDVI index has the advantage to reduce to a great extent the influence of soil background on the surface reflectance values. Although simple, WDVI is as efficient as most of the slope based VI. The effect of weighting the red band with the slope of the soil line is the maximization of the vegetation signal in the near-infrared band and the minimization of the effect of soil brightness. After creating a set of data from bare soil of the area during the year, the slope of the line was set to 1.27. The slope line is created from the NIR and R spectrum which are the bands 4 and 3 of the Landsat 5TM and 7ETM+ correspondingly (Figure 3.17).

It has to be mentioned that WDVI is more sensible to atmospheric effects (Qi et al., 1994, Hadjimitsis et al., 2010) than SAVI and NDVI, but this effect was eliminated by using field spectroscopy. No atmospheric corrections need to be applied on the spectrum data since atmosphere is not interfering in spectroradiometric measurements.

This fact also means that the accuracy of the data is high (Curran and Williamson, 1985), while extra atmospheric correction work is avoided. It has to be mentioned that all three indices used in this study refer to the Landsat 5 TM and Landsat 7 ETM+ corresponding bands, and one should bear in mind that are not found from the satellite images but directly from the spectroradiometric measurements after resampling and transforming the data into ‘in

band' reflectance (Tables 3.2-3.5). The data were prepared so as to have the average values of the corresponding Landsat bands for each phenological stage and crop. Then by applying the mathematical formulations of each VI, time series of VI were created for each crop.

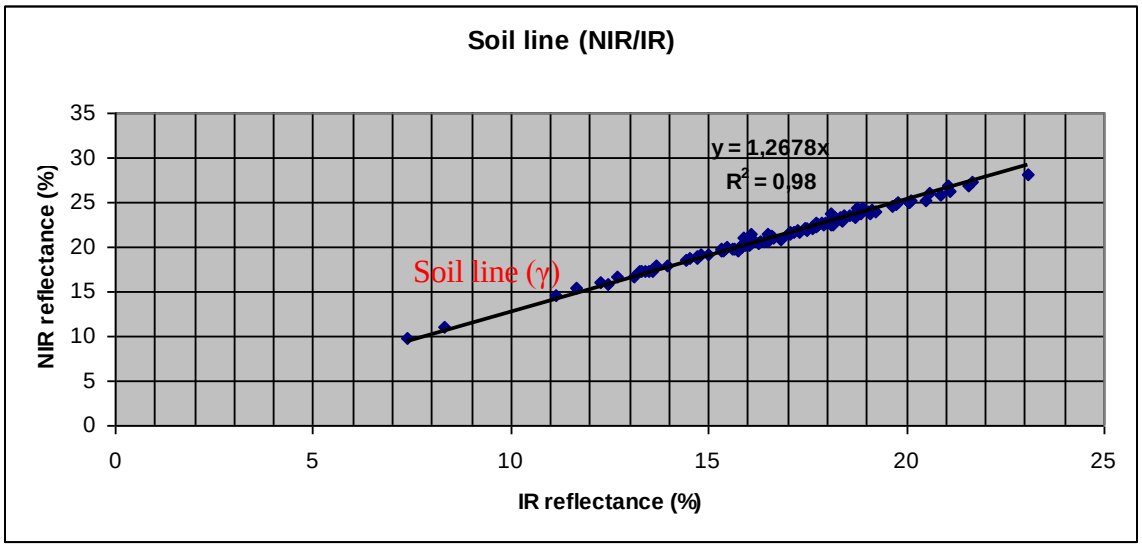

Figure 3.17. Slope line of the AOI from spectroradiometric measurements

An advantage of using field spectroscopy for acquiring the vegetation indices is the time of acquisition. Using the field spectroradiometer, one could take measurements any time contrary to satellite images where they have standard timing. Over and above, the limitation of cloud-free weather is outmatched. Field spectroradiometric data was transposed into in-band reflectance, which means that is comparable to the reflectance that one should find after applying atmospheric and radiometric corrections to the satellite images. Indeed, there is no need for applying atmospheric corrections to spectroradiometric data, since no significant height is projected between the lens of spectroradiometer and the crop canopy.

3.5. Time series of Spectroradiometric data, VI, LAI and CH

After *in situ* measurements are taken, time series of all parameters of each crop during their phenological stages, were created for proceeding with correlations, using statistical methods. Spectroradiometric data regarding the first four Landsat TM/ETM+ bands are represented in the first four columns of Tables 3.2-3.5, VI (NDVI, SAVI and WDVI) that were created from the specific data are shown in the next three columns while at the last two columns measured LAI and CH are shown. The specific tables are the raw data that were used in the next chapter (Chapter 4) for correlating LAI and CH to one of the three VI. The purpose is to find a semi-

empirical equation to describe statistically LAI and CH using remotely sensed data (in this case VI).

CHAPTER 4: MODELING VEGETATION INDICES (VI) TO LEAF AREA INDEX (LAI) AND CROP HEIGHT (CH)

In this Chapter, modeling techniques are used to correlate and evaluate measured crop canopy factors, such as Leaf Are Index (LAI) and Crop Height (CH), to remotely sensed data. The intention is to create semi-empirical models describing LAI and CH, which are indispensible parameters in almost all ETc algorithms, using remotely sensed data. Using these models, users can avoid direct measurements of these parameters every time there is an application of an ETc algorithm. Besides, the purpose of this study is to modify ETc algorithms to adapt to Cypriot conditions, thus introducing such models will support the stated purpose.

4.1. Theory: How LAI and CH can be related to VI

The commonly accepted equation for estimating evapotranspiration, according to the schematization of Monteith (Monteith and Unsworth, 1990), is a function of climate data such as temperature (T), humidity (RH%), solar radiation (R_s) and wind speed (U) and crop parameters, such as the surface albedo (*a*), the leaf area index (LAI) and the crop height (CH):

$$ETc = f(a, LAI, CH, T, RH\%, Rs, U)$$

Remote sensing techniques can be used for monitoring these vegetation characteristics. An analytical elaboration performed on Landsat reflectance values evidenced the possibility of retrieving the surface albedo (Brest and Goward, 1987), the leaf area index (Price, 1992) and the crop height (Moran and Jackson, 1991). Since these parameters directly affect the reflectance of cropped areas, it has been demonstrated that it is possible to establish a correlation between multispectral measurements of canopy reflectance and the corresponding canopy parameter's values (Bausch and Neale, 1987). In this study, the required crop parameters, *a*, LAI, CH have been derived from direct measurements and were correlated to reflectance measurements of the crops in each case.

The use of vegetation indices for statistically describing LAI and crop height is common in international literature and many empirical models are available depending on the conditions and the place (Running and Coughlan, 1988; Clevers, 1989; Tiktak and Van Grinsven, 1995; D'Urso et al., 2006). Time series of LAI, CH and VI (NDVI, SAVI, WDVI) were created, using the field spectro-radiometer (Chapter 3), in order to proceed to correlations. A very

close procedure was applied in two successful European projects regarding Mediterranean (Portugal, Spain, Italy, Greece) countries with close meteorological conditions. In these two projects, namely DEMETER (DEMonstration of Earth observation TEchnologies in Routine irrigation advisory services) and PLEIADeS (Participatory multi-Level EO-assisted tools for Irrigation water management and Agricultural Decision-Support), the ETc was estimated using remote sensing after CH and LAI maps were created using the SIMODIS (Simulation and Management of On-Demand Irrigation) procedure and the CLAIR (Clevers Leaf Area Index Relationship) model to specify LAI spatially (D'Urso et al., 2006). LAI and CH measurements were made in situ while VI are taken directly from satellite data instead from spectroradiometric data as in this case.

LAI, albedo and crop height are the canopy factors that affect spectral behavior of crop canopy (D'Urso and Menenti 1995; D'Urso et al., 2006). All of the three parameters are used in most models for estimating ETc from satellite images. Crop canopy is a basic element in almost all studies elaborating with crops, since it is the top layer or the surface where the incoming solar radiation is reflected along with the soil beneath the crop layer. As crop canopy cover increases, the process of transpiration increase while the soil evaporation gradually decreases due to leaf coverage of the ground soil (Minacapilli et al., 2008). The above implies that crop canopy factors are vital in the procedure of estimating evapotranspiration and have to be taken into account (D'Urso and Calera, 2006). In this Chapter, crop canopy measurements and vegetation indices (VI) sourcing from spectroradiometric measurements are elaborating in order to be statistically correlated. The purpose is to create empirical models for each crop describing the crop canopy factors with parameters that can be derived from remote sensing techniques, namely the vegetation indices (Figure 4.1). These empirical models were used from ETc algorithms in latter chapters to estimate the crop water requirements. A detailed analysis with the most known statistical models was carried out between the measured LAI and CH to vegetation indices. The model for each case was determined by the factor of determination, which was used in the procedure for estimating ETc. Specifically, these models assist to avoid direct measurements of the LAI and CH for all the dates for which satellite images are available and support future users or future studies regarding crop canopy. Albedo can be derived directly from satellite images using Liang's equation (Liang, 2000). For this reason, albedo modeling was not included in this study.

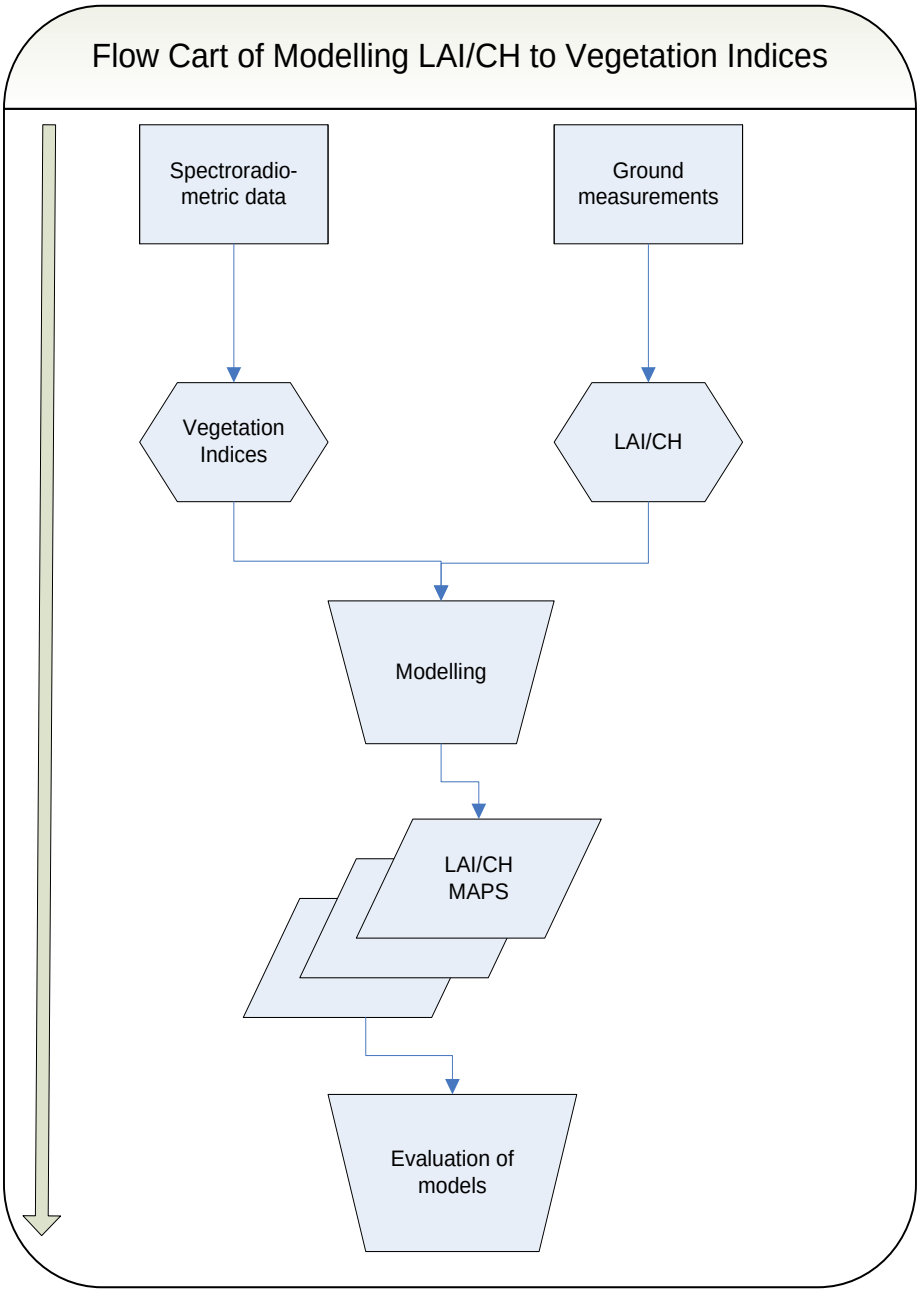

Figure 4.1. Proposed and applied method for modeling LAI/CH to VI

LAI is the projected leaf area per unit ground surface area. Since leaf area index was proposed by Watson (1947), many researchers have correlated it with vegetation productivity and evapotranspiration through models (Running and Coughlan, 1988; Tiktak and Van Grinsven, 1995; Clevers, 1989). Remote sensing data have been used to characterize plant canopy and several studies have been done to estimate LAI and correlated it to productivity and evapotranspiration (Moran et al., 1995; Franklin et al., 1997). It is possible to model the reflectance properties of different physiological types of vegetation canopy using a model which can be either stochastic, or deterministic or empirical (Curran, 1983). Empirical modeling is widely used by researchers thanks to their unconstraint application and

usefulness. Equations describing these relationships vary in both mathematical forms (linear, exponential, power, inverse of exponential, etc.) and empirical coefficients, depending on the experiments, the indices used and the vegetation type (Gilabert et al., 1996; Chen et al., 2002; Qi et al., 2000). The common procedure is to establish an empirical relationship between a given spectral index and LAI by statistically fitting measured LAI values and corresponding values of that spectral index (Gilabert et al., 1996).

Height is usually correlated to spectral indices or even LAI to avoid direct measurements *in situ* (Tucker, 1979; Wiegand et al., 1991; Thenkabail et al., 1999; Minacapilli et al., 2008). In this case, and using the same methodology as LAI, it is considered most appropriate to correlate crop height to one of the vegetation indices instead of LAI, since the latter will be indirectly measured through the VI.

In the past decades, a consistent effort has been made in the field of agricultural research to improve the understanding of physical processes involved in an irrigation system. Water transport phenomena can be accurately predicted by means of numerical simulation algorithms (Feddes et al., 1988; Santini, 1992). More recently, the spread of modeling techniques using distributed parameters has largely encouraged the use of input data from remote sensing (Azzali et al., 1991), with the support of Geographical Information Systems (GIS) for manipulating large data sets. Menenti et al. (1989) and D'Urso et al. (1992) have shown the potentiality of multispectral satellite images in the procedure for estimating ETc. By means of the appropriate interpretation methodologies and modeling techniques, digital images may be used to produce maps of crop canopy parameters and crop water requirements over agricultural areas.

Many studies have illustrated the need and the know-how for modeling or correlating LAI and Crop Height to remote sensing data and mainly to the vegetation indices inferred from handheld sensors. Leaf Area Index is an important structural property of crop canopy. High correlations were found between reflectance factor and LAI by Ahlrichs et al. (1983). Strong correlations between spectral data from crops and various characteristics of crops have been elucidated in numerous studies (Serrano et al, 2000; Goel et al., 2003; Lee et al., 2004). Darvishzadeh et al. (2008) examined the utility of hyper spectral remote sensing in predicting canopy characteristics by using a spectral radiometer. Among the various models investigated, they found that canopy chlorophyll content was estimated with the highest

accuracy. Some studies used multispectral image sensor system to measure crop canopy characteristics (Inoue et al., 2000)

4.2. Mapping LAI and Crop Height through Vegetation Indices

As mentioned above, the intended purpose of this Chapter is to use statistical techniques to test if there is a strong statistical relationship between LAI/CH and vegetation indices. From literature review, it is obvious that the canopy factors could be related to vegetation indices. The procedure followed to test and find out the strongest relationship is to create time series of the needed parameters and by using statistical methods to create empirical models to characterize LAI and CH. These produced models were then employed in the ERDAS Imagine software using the Modeler module (Figure 4.2), to create maps of LAI and Crop Height which are the needed inputs in the procedure for estimating ETc. These maps, that basically are the satellite images transposed into LAI and CH maps, contain quality information (meaning the values) regarding the LAI and the CH for the specific crop each time.

The relationships between LAI or CH and Vegetation Indices were studied through a series of statistical models in order to have the best possible correlation. Linear, exponential, logarithmic and polynomial models were used to infer the best relationship. The best correlation for each crop was identified from the determination factor (R^2). F-test was also employed to test the reliability of each model at a 0,95 level of confidence.

The models used in the study are mathematically expressed as:

$$\textbf{\textit{Linear}}: \quad LAI = a(VI) + b$$

$$\textbf{\textit{Exponential}}: \quad LAI = ae^{b(VI)}$$

Logarithmic: $LAI = a\ln(VI) + b$

***Polynomial*:** $LAI = a(VI)^2 + b(VI) + c$

and they were used for all 4 crops (potatoes, beans, chickpeas, groundnuts). In this modeling procedure, an attempt for modeling LAI and crop height (Y of the model) to one of the three vegetation indices (NDVI, SAVI, WDVI) (X of the model) found earlier, is made. Coefficients *a*, *b* and *c* were found from the statistical analysis and the strongest model depending on the determination factor (R^2) was used in the algorithms for estimating ETc.

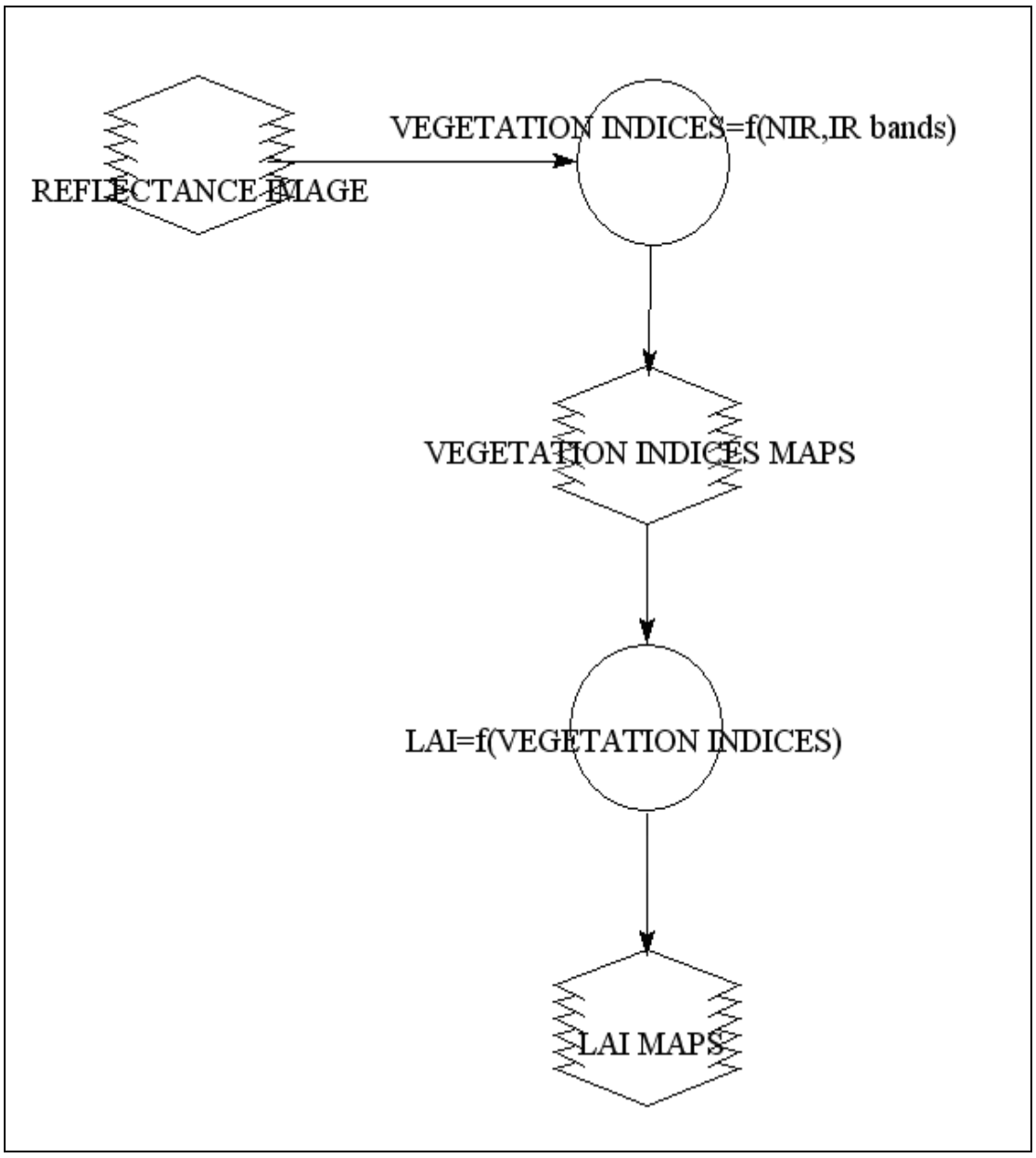

Figure 4.2. Steps for LAI maps creation using ERDAS Imagine software

A major limitation of this approach is the diversity of the LAI-VI equations, as well as the diversity of VI that exist in the literature. The fact that there is no universal equation of LAI-VI (Qi et al., 2000), obligates remote sensing users to create equations for each crop under the current conditions, using truth measurements of LAI/CH and remote sensing data, such as spectroradiometric measurements. As a result, each image must be transformed into LAI/CH map (Figure 4.3) for each crop, in order to retrieve the value of LAI and CH. Another limitation is the non-vegetated factors that affect the procedure negatively. Factors such as soil, atmospheric effects and topography which affect VI must be considered and minimized.

Improved VI were created for this purpose (Huete, 1988; Clevers, 1989; Kaufman and Tanre, 1992; Qi et al., 1994) and have to be used to avoid external effects.

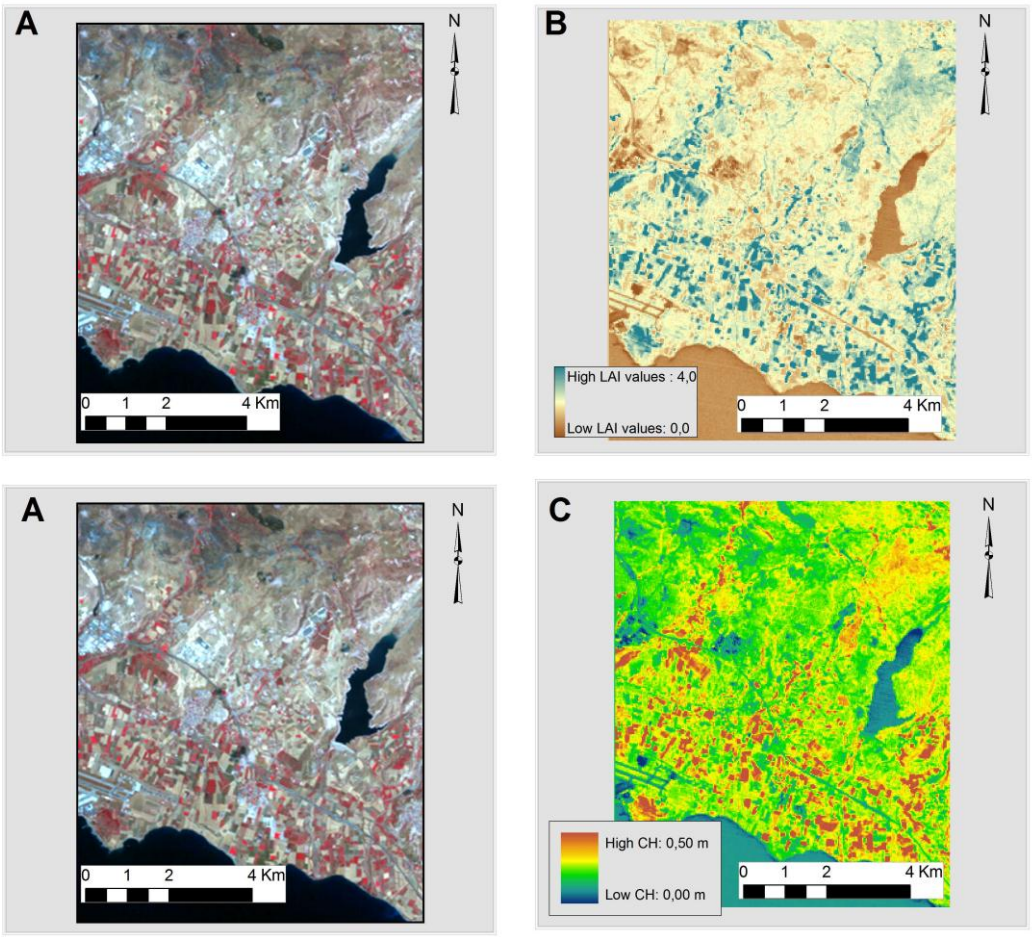

Figure 4.3. Production of LAI (B) and CH (C) maps (in pseudo color) using a Landsat image (A)

Figure 4.3 shows an example of how a satellite image, in reflectance form (A), can be transformed into LAI (B) and CH (C) maps, using semi-empirical models for retrieving the corresponding values for each image and each crop. Using pseudo color, it is possible to attribute color to the values in order to gradate or scale graphically the values of these two parameters.

4.3. The models

The common and widely used approach has been to develop relationships between ground-measured LAI and vegetation indices (Chen and Cihlar, 1996; Fassnacht et al., 1997).

Consequently, a large number of relationships have been established, and a wide range of determination factor ($0.05 < R^2 < 0.86$) between vegetation indices and LAI were found (Brown et al., 2000).

Time series of LAI, crop height measured directly in the field and all three vegetation indices, which were produced earlier from the spectroradiometric data which was acquired from the ground truth data campaign, were created and elaborated in order to test the level of correlation between LAI/VI and CH/VI. Coefficients for all four models were found and new models were created defining LAI and CH through the vegetation indices. This procedure was performed for all crops under investigation, while the best model in each case was chosen based on the determination coefficient.

4.3.1. Potatoes

Regarding potatoes, the results have indicated that the best relation between LAI and any of the three vegetation indices, namely NDVI, SAVI and WDVI, is the polynomial LAI/WDVI correlation with determination coefficient (R^2) R^2=0,78 while for Crop Height is the exponential model of CH-WDVI with determination coefficient (R^2) R^2=0,91. The determination coefficient is high for both cases, LAI and CH, since, as mentioned earlier the results of such regression analysis vary from $0,05 < R^2 < 0,86$.

Both models that have the strongest correlation at significance level of 5%**,**

$$\mathbf{y = 46,74x^2 - 34,82x + 7,89}$$

and

$$\mathbf{y = 0,10e^{2,23x}}$$

for LAI and CH respectively, were used in the algorithms for estimating ETc for potatoes (see Chapter 5).

The results of the statistical analysis for all the models regarding potatoes can be seen in Table 4.1. The worst relation was observed in the relation of LAI/NDVI with low fitted R^2 for the linear model. Probably, the poor fitting of the equation originates from the fact that NDVI does not take into account the soil effect. LAI/SAVI correlation has also lower fitted R^2 than LAI-WDVI but still is on high levels when an exponential model is used. As it was expected,

SAVI and WDVI have a higher determination coefficient since they were developed for the specific purpose, meaning the compensation of soil background and atmospheric effects (Bannari et al., 1996; Karnielli et al., 2001). Figures 4.4 and 4.5 illustrate the correlations for LAI and CH for the best fitted model respectively.

Table 4.1. Correlations of LAI/CH to vegetation Indices for potatoes

LAI	Linear		Exponential		Logarithmic		Polynomial	
to SVI's	Model	R^2	Model	R^2	Model	R^2	Model	R^2
LAI-NDVI	y = 14,89x - 9,41	0,16	y = 0,01e6,51x	0,17	y = 11,39Ln(x) + 5,04	0,16	y = 129,09x2 - 184,84x + 67,76	0,18
LAI-SAVI	y = 11,86x - 6,11	0,55	y = 0,05e5,22x	0,58	y = 7,84Ln(x) + 5,01	0,52	y = 88,39x2 - 109,81x + 35,48	0,72
LAI-WDVI	y = 10,03x - 2,65	0,68	y = 0,24e4,39x	0,69	y = 4,48Ln(x) + 5,50	0,61	y = 46,74x2 - 34,82x + 7,89	0,79

CH	Linear		Exponential		Logarithmic		Polynomial	
to SVI's	Model	R^2	Model	R^2	Model	R^2	Model	R^2
CH-NDVI	y = 1,46x - 0,83	0,42	y = 0,01e4,86x	0,46	y = 1,13Ln(x) + 0,58	0,42	y = 2,09x2 - 1,78x + 0,41	0,41
CH-SAVI	y = 0,86x - 0,30	0,79	y = 0,04e2,80x	0,86	y = 0,58Ln(x) + 0,51	0,76	y = 3,54x2 - 4,01x + 1,36	0,86
CH-WDVI	y = 0,69x - 0,03	0,86	y = 0,10e2,23x	0,89	y = 0,32Ln(x) + 0,54	0,82	y = 1,78x2 - 1,02x + 0,37	0,9

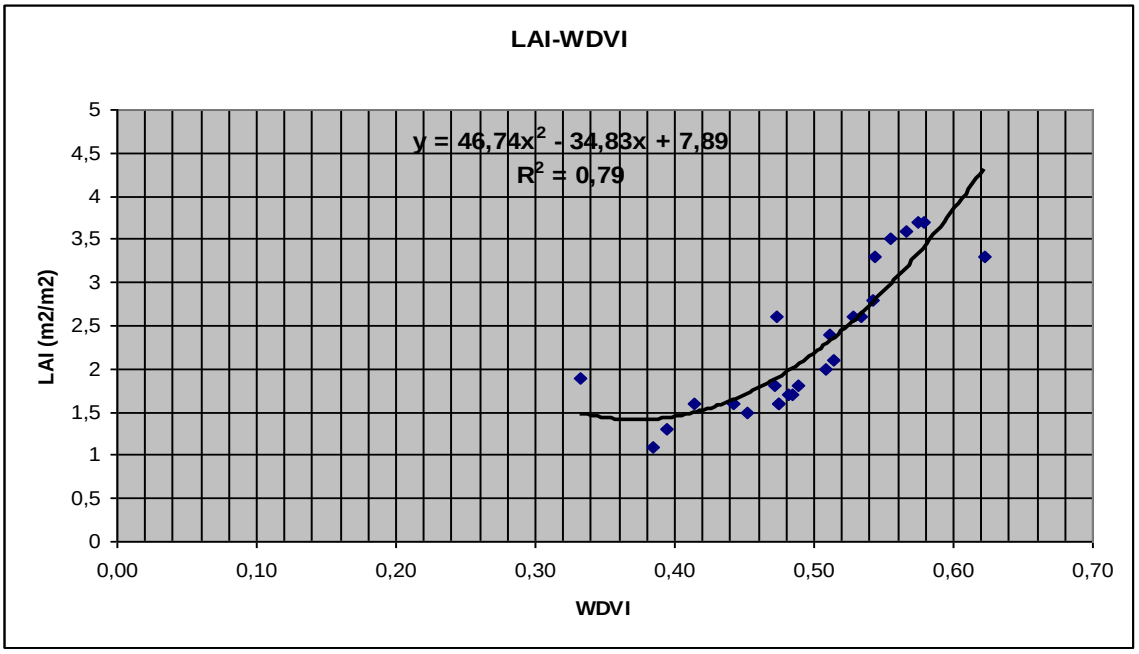

Figure 4.4. LAI to WDVI correlation for potatoes

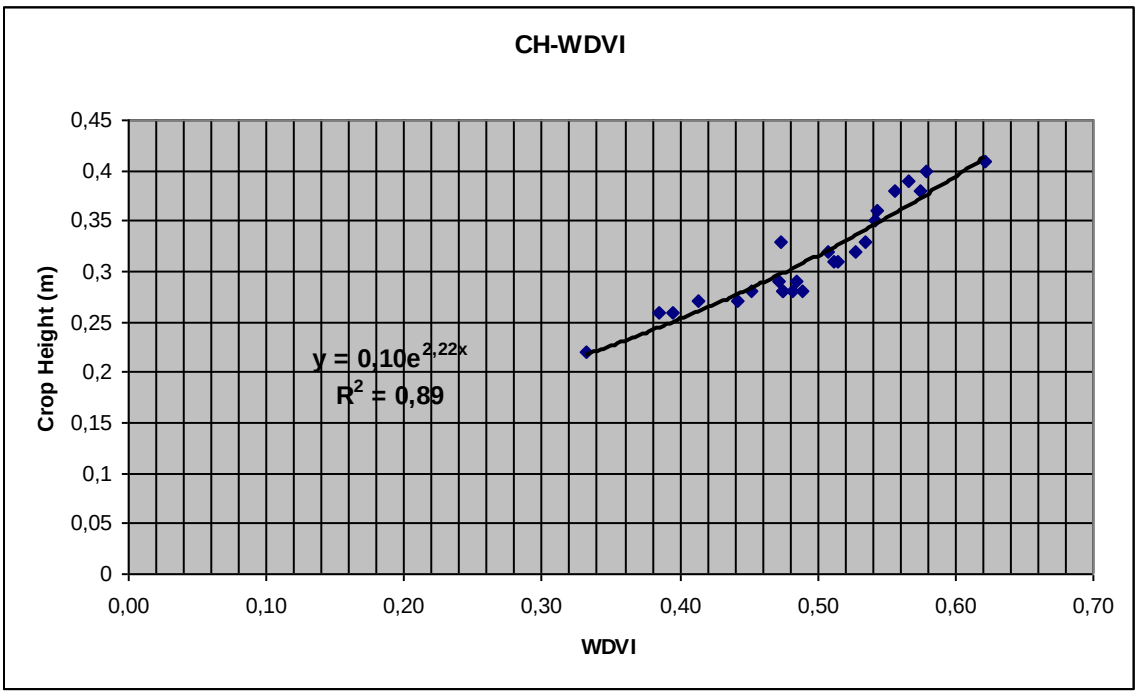

Figure 4.5. CH to WDVI correlation for potatoes

4.3.2. Beans

Regarding beans, the best relation between LAI and one of the VI is the logarithmic model of LAI-WDVI with determination coefficient (R^2) R^2=0,86 while for Crop Height is the logarithmic model of CH-WDVI with determination coefficient (R^2) R^2=0,93. The determination coefficient is also high for both cases, as for potatoes. Both models have a significance level of 5%.

y = 2,90Ln(x) + 3,71 for LAI

and

y = -236,32x^2 + 321,29x- 79,42 for CH,

were used in the algorithms for estimating ETc for beans.

The results of the statistical analysis regarding beans, for all the models used can be seen in Table 4.2. The worst correlation was observed in the relation of LAI/NDVI, with very low R^2 for the linear model, meaning that NDVI could not be used for such correlation. LAI-SAVI correlation had also lower R^2 than LAI/WDVI but still is on high levels when the polynomial model is used. Figures 4.6 and 4.7 illustrate the correlations for LAI and CH for the best fitted model, respectively, for beans.

Table 4.2. Correlations of LAI/CH to vegetation Indices for beans

LAI	Linear		Exponential		Logarithmic		Polynomial	
to SVI's	Model	R^2	Model	R^2	Model	R^2	Model	R^2
LAI-NDVI	y = 7,60x - 3,95	0,38	y = 0,09e3,89x	0,38	y = 5,95Ln(x) + 3,45	0,38	y = 27,36x2 - 35,47x + 12,95	0,38
LAI-SAVI	y = 6,71x - 3,04	0,76	y = 0,1295e3,62x	0,69	y = 5,03Ln(x) + 3,45	0,76	y = -8,43x2 + 19,40x - 7,78	0,76
LAI-WDVI	y = 5,25x - 0,94	0,85	y = 0,39e2,81x	0,78	y = 2,90Ln(x) + 3,71	0,86	y = -6,25x2 + 12,25x - 2,86	0,85

CH	Linear		Exponential		Logarithmic		Polynomial	
to SVI's	Model	R^2	Model	R^2	Model	R^2	Model	R^2
CH-NDVI	y = 87,72x - 43,85	0,43	y = 1,27e3,76x	0,41	y = 69,22Ln(x) + 41,82	0,44	y = -722,26x2 + 1224,5x - 490,17	0,46
CH-SAVI	y = 73,77x - 30,55	0,79	y = 2,19e3,20x	0,77	y = 55,84Ln(x) + 41,01	0,81	y = -493,13x2 + 815,42x - 307,68	0,88
CH-WDVI	y = 56,72x - 6,91	0,86	y = 6,12e2,46x	0,83	y = 31,82Ln(x) + 43,63	0,88	y = -236,32x2 + 321,29x - 79,44	0,93

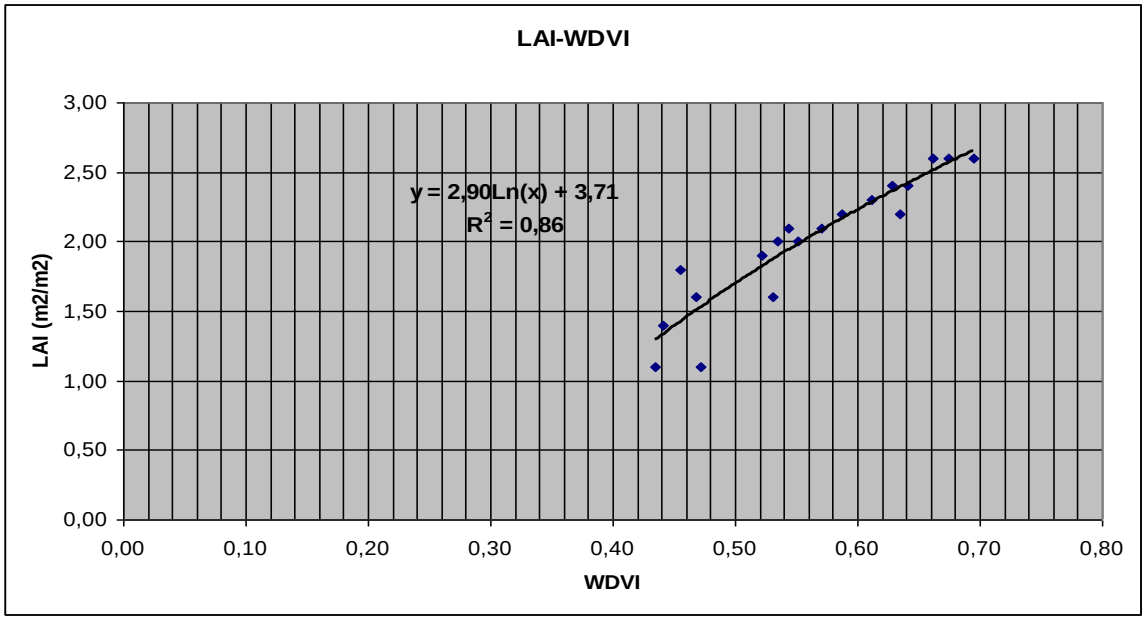

Figure 4.6. LAI to WDVI correlation for beans

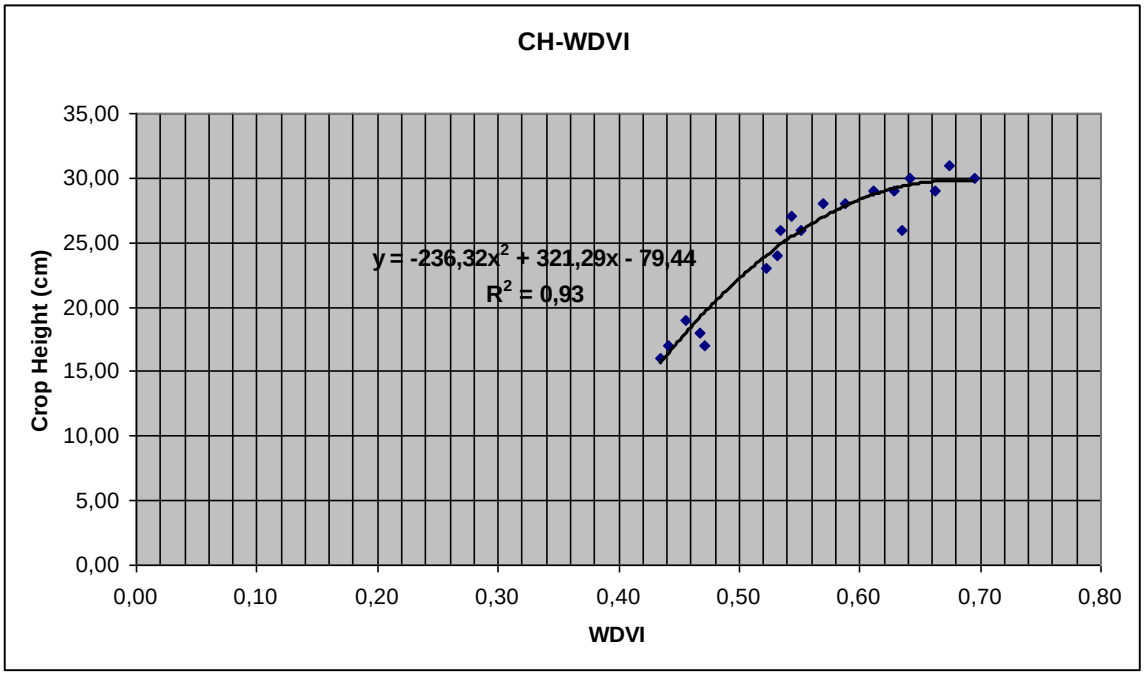

Figure 4.7. CH to WDVI correlation for beans

4.3.3. Groundnuts

Regarding groundnuts, the best relation between LAI and one of the VIs is the linear model of LAI/SAVI with determination coefficient (R^2) R^2=0,88. For Crop Height, the best fitted model is again the linear model of CH/SAVI with determination coefficient (R^2) R^2=0,87. It is obvious that NDVI has insignificant correlation to LAI or CH as for potatoes and beans.

Both models, that have the strongest correlation at significance level of 5%**,**

y = 7,14x – 3,02 for LAI

and

y = 0,61Ln(x) + 0,56 for CH,

were used in the algorithms for estimating ETc for groundnuts. The results of the statistical analysis regarding groundnuts, for all the models used can be seen in Table 4.3. Figures 4.8 and 4.9 show the correlations, respectively, for LAI and CH, for the best model for groundnuts.

Table 4.3. Correlations of LAI/CH to vegetation Indices for groundnuts

LAI	Linear		Exponential		Logarithmic		Polynomial	
to SVI's	Model	R^2	Model	R^2	Model	R^2	Model	R^2
LAI-NDVI	y = 0,07x + 0,58	0,78	y = 0,60e0,10x	0,79	y = 0,12Ln(x) + 0,66	0,74	y = 0,01x2 + 0,01x + 0,63	0,79
LAI-SAVI	y = 7,14x - 3,02	0,88	y = 0,09e4,19x	0,86	y = 4,81Ln(x) + 3,75	0,87	y = -2,36x2 + 10,39x - 4,10	0,87
LAI-WDVI	y = 6,56x - 1,08	0,81	y = 0,31e3,80x	0,78	y = 2,96Ln(x) + 4,31	0,82	y = -7,84x2 + 13,91x - 2,73	0,83

CH	Linear		Exponential		Logarithmic		Polynomial	
to SVI's	Model	R^2	Model	R^2	Model	R^2	Model	R^2
CH-NDVI	y = 1,32x - 0,64	0,81	y = 0,01e4,17x	0,76	y = 0,98Ln(x) + 0,64	0,83	y = -5,17x2 + 9,02x - 3,47	0,85
CH-SAVI	y = 0,89x - 0,28	0,86	y = 0,04e2,90x	0,85	y = 0,61Ln(x) + 0,56	0,87	y = -1,02x2 + 2,30x - 0,75	0,86
CH-WDVI	y = 0,81x - 0,03	0,77	y = 0,09e2,6x	0,76	y = 0,37Ln(x) + 0,633	0,79	y = -1,62x2 + 2,32x - 0,37	0,8

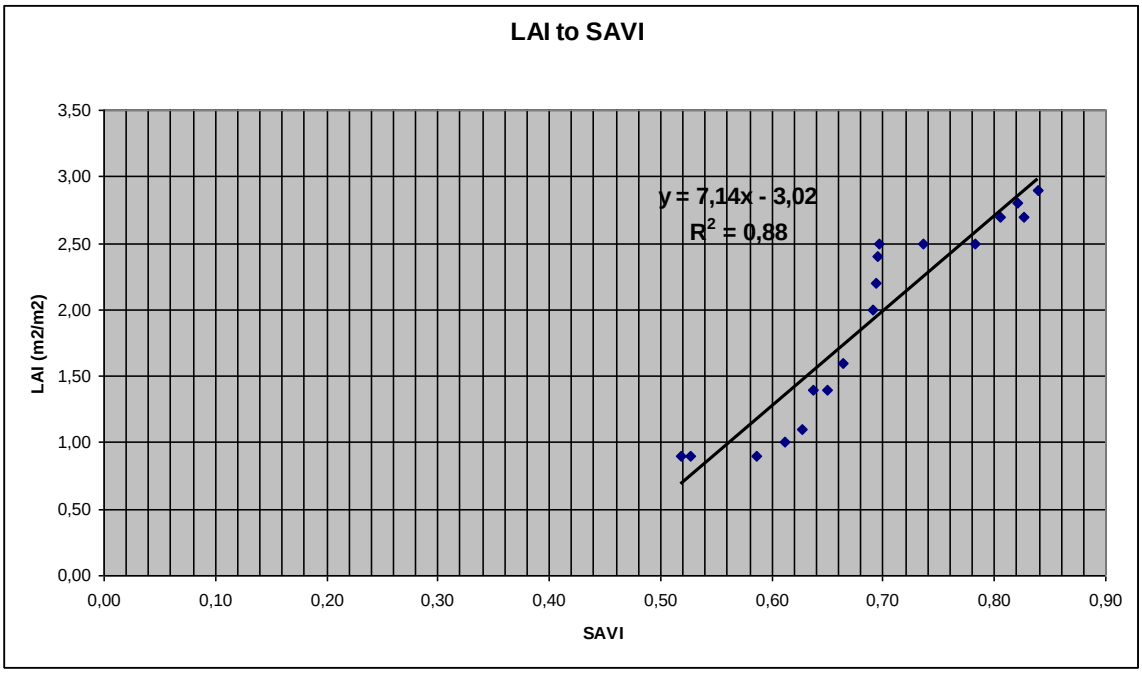

Figure 4.8. LAI to SAVI correlation for groundnuts

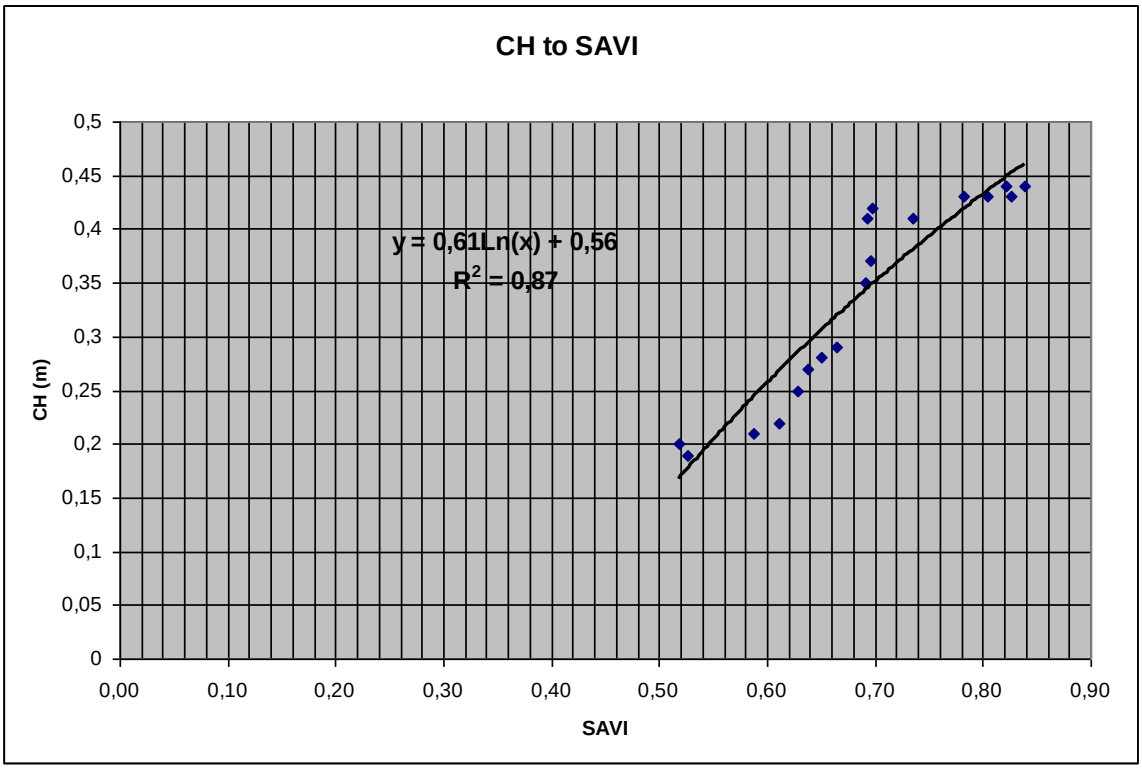

Figure 4.9. CH to SAVI correlation for groundnuts

4.3.4. Chickpeas

Regarding chickpeas, it has to mentioned that the measurements were obviously fewer than other crops due to crop short phenological cycle, compared to other crops. This may have an impact on the correlations and afterwards in the estimation of ETc in terms of statistical validity. The best relation between LAI and one of the VI is the logarithmic model of LAI/NDVI with determination coefficient (R^2) R^2=0,73 while for Crop Height is the logarithmic model of CH/SAVI with determination coefficient (R^2) R^2=0,85. Both models that have the strongest correlation at significance level of 5%

y = 0,06Ln(x) + 0,88 for LAI

and

y = 42,67x - 12,86 for CH

were used in the algorithms for estimating ETc for chickpeas. The results of the statistical analysis regarding chickpeas, for all the models used can be seen in Table 4.4. Figures 4.10 and 4.11 show the correlations for LAI and CH, for the best model, for chickpeas.

Table 4.4. Correlations of LAI/CH to vegetation Indices for chickpeas

LAI	Linear		Exponential		Logarithmic		Polynomial	
to SVI's	Model	R^2	Model	R^2	Model	R^2	Model	R^2
LAI-NDVI	y = 0,04x + 0,83	0,7	y = 0,83e0,05x	0,69	y = 0,06Ln(x) + 0,8789	0,73	y = -0,02x2 + 0,12x + 0,78	0,72
LAI-SAVI	y = 0,08x + 0,63	0,62	y = 0,64e0,10x	0,62	y = 0,10Ln(x) + 0,7155	0,57	y = 0,06x2 - 0,11x + 0,76	0,68
LAI-WDVI	y = 6,86x - 1,75	0,56	y = 0,16e4,56x	0,49	y = 3,36Ln(x) + 4,0209	0,55	y = 8,14x2 - 1,21x + 0,23	0,56

CH	Linear		Exponential		Logarithmic		Polynomial	
to SVI's	Model	R^2	Model	R^2	Model	R^2	Model	R^2
CH-NDVI	y = 69,07x - 43,13	0,74	y = 0,72e3,63x	0,76	y = 61,48Ln(x) + 25,54	0,74	y = 1103,9x2 - 1906,4x + 839,8	0,84
CH-SAVI	y = 42,67x - 12,86	0,85	y = 3,61e2,22x	0,85	y = 32,13Ln(x) + 28,44	0,85	y = 10,3x2 + 27,11x - 7,00	0,85
CH-WDVI	y = 36,91x + 1,38	0,8	y = 7,59e1,91x	0,79	y = 18,28Ln(x) + 32,59	0,81	y = -99,4x2 + 135,69x - 22,91	0,81

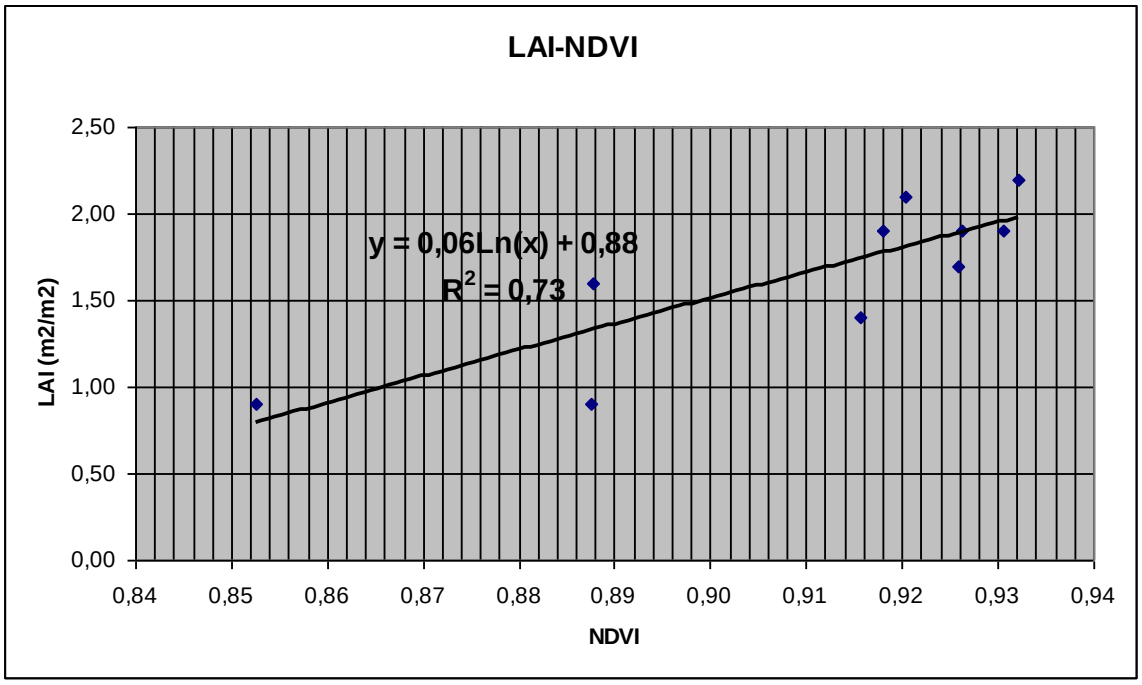

Figure 4.10. LAI to NDVI correlation for chickpeas

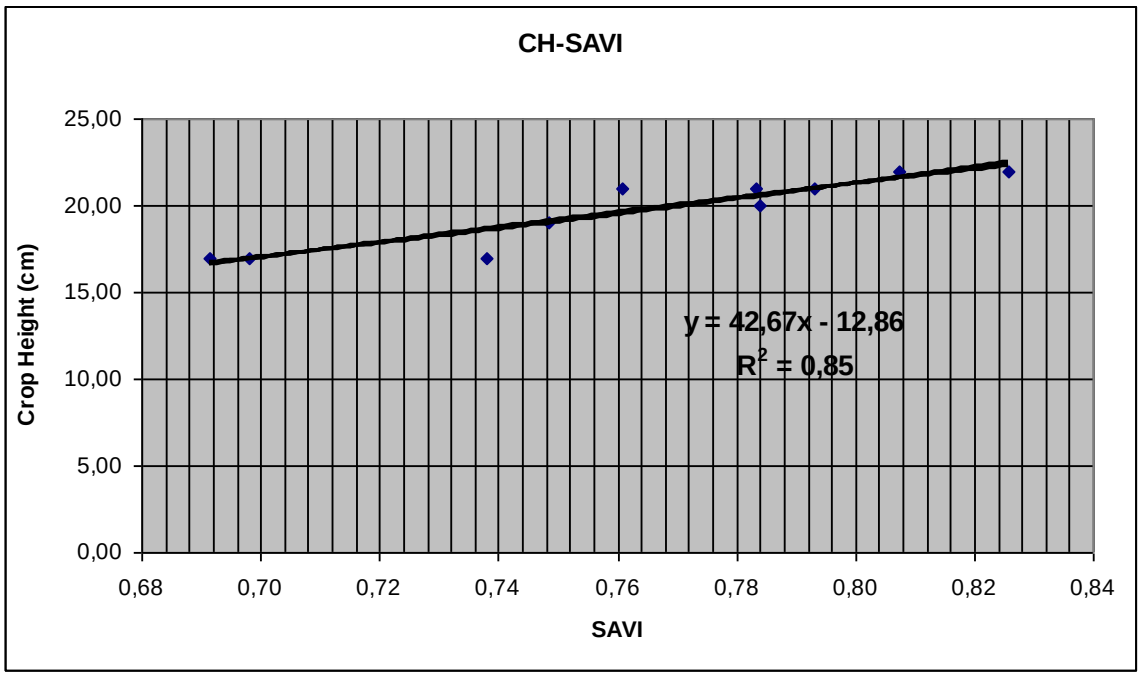

Figure 4.11. CH to SAVI correlation for chickpeas

4.4. Field evaluation of the models

Though correlation analysis of LAI and CH to VI has indicated that the relationships are of high determination factor, at 95% confidence level, the approval of these relations, at field scale with ground truth data, was considered to be imperative so as to enhance the method followed. The purpose was to verify in a statistical way the results of the correlations by using them directly on satellite images. For this purpose, 2011 Landsat images were used. Prior to main analysis, the images were preprocessed. Then the images were transposed into LAI and CH maps using the models ($LAI / CH = f(VI)$) found earlier. During the satellite overpass direct LAI and CH measurements were undertaken. These values were compared to the values given from the empirical models produced earlier. Then a Student's t-test was used to test if the difference between the paired values is significant. SPSS statistical software was used to infer the value of t for each case.

Table 4.5 shows the number of satellite images used for evaluation in the study and the number of plots used in the area for each crop. Student's t-test was employed to test how reliable are the results found and if there is a significant statistical difference between the measured (directly) and estimated (models) parameters. It was consider rational to use 2011 Landsat satellite images since this year was not included in the field campaign and is considered as a new cultivating period for the crops.

Table 4.5. Number of plots and satellite images used for the evaluation of the models

Crop	Plots	Sat. images	Sample
Potatoes	4	2	8
Beans	3	2	6
Chickpeas	3	3	9
Groundnuts	3	5	15

4.4.1. LAI models evaluation

Table 4.6 illustrates that all the models developed earlier (section 3 of this Chapter), can predict successfully the value of LAI in the field under the current meteorological, soil and morphological conditions of the area. $t_{observed}$ for all crops was smaller than $t_{statistical}$, which implies that, for n-1 degrees of freedom and at a confidence level of 95%, the predicted LAI has no significant statistical difference from the measured LAI (if $t_{observed} < t_{statistical}$ then *Ho:* $\sigma_1^2 = \sigma_2^2$ where σ_1^2 is the variation of LAI measured sample and σ_2^2 is the variation of LAI predicted sample).

Table 4.6. T-test results (obs.) compared to the statistical values (T stat.) of the test, for LAI

Crop	$t_{observed}$	R^2	$t_{statistical}$	N(sample)	Stand. Error mean
Potatoes	-1,93	0,97	2,365	8	0,03
Beans	0,59	0,74	2,571	6	0,08
Chickpeas	1,49	0,95	2,306	9	0,05
Groundnuts	1,65	0,93	2,145	15	0,05

Tables 4.7-4.10 show the pair of values for each satellite image and each crop for LAI measured and predicted. The values refer to the mean value of LAI measurements using the SunScan canopy analyser for *measured LAI* and the mean value of *estimated or predicted LAI* in the specific fields (mean value of pixels) (see Appendix 4 in Appendices).

Determination coefficients also show the high correlation between the pair of values (LAI measured and predicted) for all crops, though sometimes it doesn't imply that there is no significant difference among the parameters.

Table 4.7. LAI measured against LAI predicted for potatoes

Plot	Date of sat. image	LAI measured	LAI predicted
plot 1	2/5/2011	2,6	2,5
	19/6/2011	1,8	2
plot 2	2/5/2011	2,4	2,5
	19/6/2011	1,8	1,9
plot 3	2/5/2011	2,3	2,5
	19/6/2011	1,6	1,6
plot 4	2/5/2011	2,6	2,7
	19/6/2011	1,8	1,9

Table 4.8. LAI measured against LAI predicted for beans

Plot	Date of sat. image	LAI measured	LAI predicted
plot 1	2/5/2011	2,2	1,9
	19/6/2011	1,9	1,8
plot 2	2/5/2011	2	2,2
	19/6/2011	1,8	2
plot 3	2/5/2011	1,4	1,3
	19/6/2011	2	1,8

Table 4.9. LAI measured against LAI predicted for chickpeas

Plot	Date of sat. image	LAI measured	LAI predicted
plot 1	21/7/2011	0,6	0,3
	29/7/2011	0,8	0,6
	30/8/2011	1,7	1,6
plot 2	21/7/2011	0,9	1
	29/7/2011	1,1	1
	30/8/2011	1,8	1,6
plot 3	21/7/2011	0,6	0,6
	29/7/2011	0,9	1,1
	30/8/2011	1,8	1,7

Table 4.10. LAI measured against LAI predicted for groundnuts

Plot	Date of sat. image	LAI measured	LAI predicted
plot 1	19/6/2011	0,5	0,8
	5/7/2011	0,7	0,9
	21/7/2011	1,5	1,8
	29/7/2011	1,7	1,8
	30/8/2011	2,1	2
plot 2	19/6/2011	0,9	0,8
	5/7/2011	1,3	1,1
	21/7/2011	1,7	1,5
	29/7/2011	2	1,8
	30/8/2011	2,2	1,9
plot 3	19/6/2011	0,8	0,7
	5/7/2011	1	0,8
	21/7/2011	1,4	1,1
	29/7/2011	1,8	1,6
	30/8/2011	2,3	1,9

4.4.2. CH models evaluation

The same procedure and for the same dates was followed to evaluate CH models. Table 4.11 shows the results found from the t-test application. For all the cases, $t_{observed}$ was smaller than $t_{statistical}$ meaning that there is no important statistical difference between them.

Table 4.11. T-test results (obs.) compared to the statistical values (T stat.) of the test, for CH

Crop	**$t_{observed}$**	**R^2**	**$t_{statistical}$**	**n(sample)**	**Stand. Error mean**
Potatoes	0,23	0,8	2,365	8	0,55
Beans	-0,67	0,95	2,571	6	0,49
Chickpeas	-2,17	0,94	2,306	9	0,51
Groundnuts	1,58	0,85	2,145	15	0,97

Tables 4.12-4.15 show the pair of values for each satellite image and each crop regarding the measured and predicted crop height. The values refer to the mean value for measured CH and the mean value of CH (predicted) found from the images after models application. T-test application has shown as for LAI, that the models can be used for estimating CH in the area of interest.

Table 4.12. CH measured against CH predicted for potatoes

Plot	Date of sat. image	CH measured	CH predicted
plot 1	2/5/2011	33	31
	19/6/2011	28	26
plot 2	2/5/2011	29	28
	19/6/2011	25	24
plot 3	2/5/2011	31	30
	19/6/2011	28	26
plot 4	2/5/2011	30	30
	19/6/2011	28	27

Table 4.13. CH measured against CH predicted for beans

Plot	Date of sat. image	CH measured	CH predicted
plot 1	2/5/2011	27	29
	19/6/2011	26	29
plot 2	2/5/2011	22	22
	19/6/2011	22	23
plot 3	2/5/2011	23	26
	19/6/2011	25	26

Table 4.14. CH measured against CH predicted for chickpeas

Plot	Date of sat. image	CH measured	CH predicted
plot 1	21/7/2011	14	16
	29/7/2011	15	18
	30/8/2011	21	22
plot 2	21/7/2011	20	22
	29/7/2011	21	24
	30/8/2011	27	26
plot 3	21/7/2011	18	19
	29/7/2011	20	20
	30/8/2011	25	24

Table 4.15. CH measured against CH predicted for groundnuts

Plot	Date of sat. image	CH measured	CH predicted
plot 1	19/6/2011	15	17
	5/7/2011	17	18
	21/7/2011	21	19
	29/7/2011	28	22
	30/8/2011	32	28
plot 2	19/6/2011	19	23
	5/7/2011	23	25
	21/7/2011	24	28
	29/7/2011	27	29
	30/8/2011	34	32
plot 3	19/6/2011	23	20
	5/7/2011	26	21
	21/7/2011	32	26
	29/7/2011	36	29
	30/8/2011	38	35

4.5. Conclusions

Study results demonstrated that spectral information can provide acceptable estimates of LAI and CH of the specific area under the current geo-morphological and meteorological conditions. Quantification of the canopy leaf area index (LAI) and its spatial distribution provides an avenue to improve the interpretation of remotely sensed data over vegetated areas. The research in this Chapter was carried out in order to test the existing relation between vegetation indices with LAI and crop height and their prediction from remotely sensed data. It allowed us to compare, on a consistent basis, the performance of a set of indices found in international literature, in the prediction of LAI and CH which are basic parameters in the algorithms of estimating ETc.

Analysis based on remotely sensed data showed significant problems in the relationships between LAI and NDVI. Other indices, such as SAVI and WDVI, exhibited better performances, with high determination factor. Evaluation of the models produced, by employing the t-test, has shown that the models can predict the two parameters, LAI and CH, with accuracy.

Correlation coefficients and prediction accuracy should be interpreted with caution, as well as with regards to the specific variable the indices were designed to measure. Nevertheless, one of the main conclusions of this study is the important role of modeling of canopy. Moreover, these models are essential to the development of predictive algorithms that can not be efficiently designed from measurements and observations in the field and/or laboratory. Such an approach of algorithm development from purely simulated data, together with its successful application to real remotely sensed data holds a strong potential for operational quantification of canopy parameters. Models produced from the modeling procedure for LAI and CH cover the whole crop cycle and can serve as a basis for developing satellite-based monitoring systems for the specific area and crops.

CHAPTER 5: RESULTS OF "ET_C" ALGORITHMS APPLICATION AND MODIFICATION WITH GROUND MODELS AND DISCUSSION

"SEBAL" and "Penman-Monteith adapted to satellite data" algorithms are employed in this Chapter to estimate ETc. An analytical description is provided for the algorithms and their application. Then a modification based on the semi-empirical models of LAI and CH is applied in an attempt to test if the algorithms' accuracy can be improved and if ground data support the application procedure.

5.1. SEBAL algorithm

ETc in the study area was firstly estimated by applying the Surface Energy Balance Algorithm for Land (SEBAL) on the satellite images which included a thermal band (Landsat 5TM / 7ETM+) as shown in Figure 1.

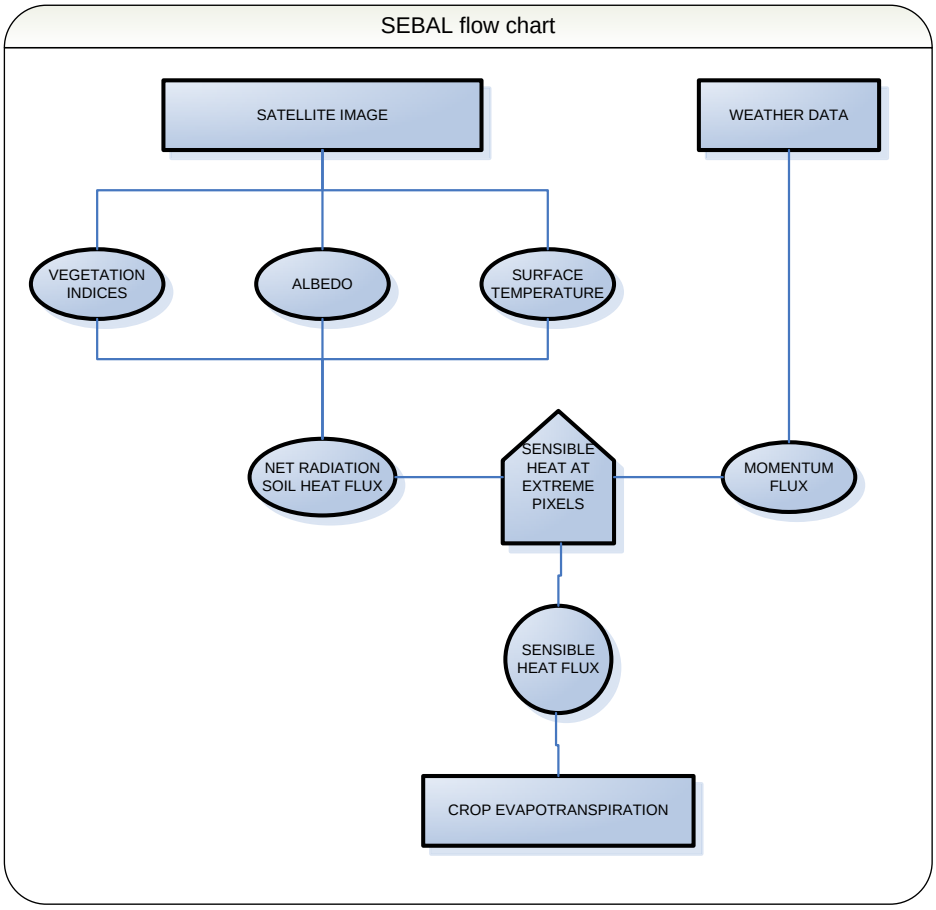

Figure 5.1. SEBAL flow chart for estimating ET_c

SEBAL is a thermodynamically based model, using the partitioning of sensible heat flux and latent heat of vaporization flux as described by Bastiaanssen et al., (1998) who developed the

algorithm. In the SEBAL model, ETc is computed from satellite images and weather data using the surface energy balance as illustrated in Figure 5.1. Remotely sensed data in the visible, near-infrared and thermal infrared bands are used to derive the energy balance components along with ground measured solar radiation, if available. The other ground measurements that are required as model input are air temperature, relative humidity and wind speed at a point within the image.

SEBAL has an internal calibration for removing atmospheric effects using a series of iteration on Sensible Heat Flux (H) (Baastianssen et al., 2000; 2008). Since the satellite image provides information for the overpass time only, SEBAL computes an instantaneous ET flux for the image time. The ET flux is calculated for each pixel of the image as a "residual" of the surface energy budget equation:

$$\lambda ET = R_n - G - H$$

(Equation 5.1)

where:

- R_n is the instantaneous net radiation ($W.m^{-2}$)
- G is the instantaneous soil heat flux ($W.m^{-2}$),
- H is the instantaneous sensible heat flux ($W.m^{-2}$)
- λET is the instantaneous latent heat flux ($W.m^{-2}$)

In Equation (5.1), the soil heat flux *(G)* and sensible heat flux *(H)* are subtracted from the net radiation flux at the surface *(R_n)* to compute the "residual" energy available for evapotranspiration *(λET)* (Figure 5.2). Soil heat flux is empirically calculated using vegetation indices, surface temperature and surface albedo. Sensible heat flux is computed using wind speed observations, estimated surface roughness and surface to air temperature differences. SEBAL uses an iterative process to correct for atmospheric instability due to the buoyancy effects of surface heating. Once the latent heat flux *(λET)* is computed for each pixel, an equivalent amount of instantaneous ET (mm/hr) is readily calculated by dividing by the latent heat of vaporization *(λ).* Then, daily ETc is inferred.

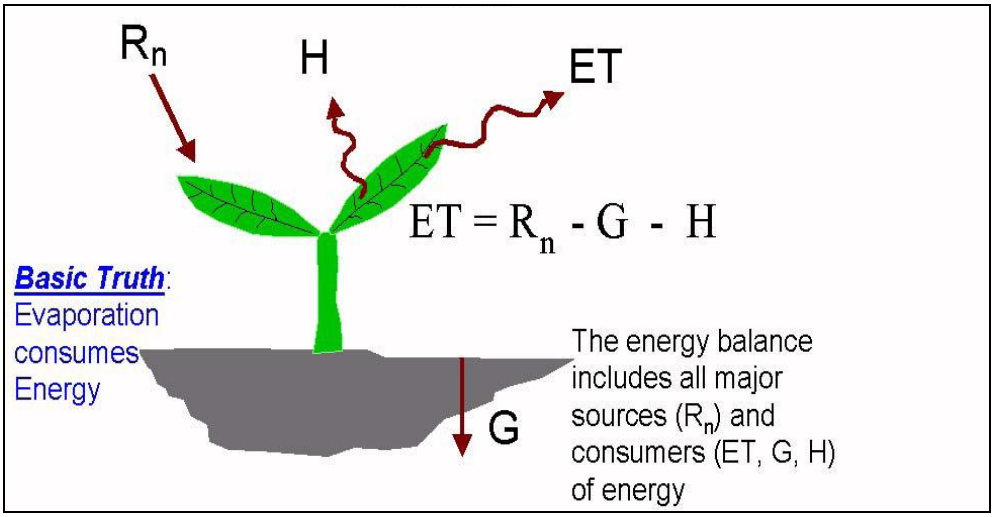

Figure 5.2. Energy Balance equilibrium (Source: Waters et al. 2002)

The net radiation flux at the surface *(R_n)* represents the actual radiant energy available at the surface. It is computed by subtracting all outgoing radiant fluxes from all incoming radiant fluxes. Basically, it is the amount of energy that remains to earth's surface when subtracting the outgoing short and long wave radiation from the corresponding incoming ones. This is given in the surface radiation balance equation 5.2:

$$R_n = R_s - aR_{s\downarrow} + R_{L\downarrow} - R_{L\uparrow} - (1-\varepsilon_0)R_{L\downarrow}$$

(Equation 5.2)

where:

- $R_{S\downarrow}$ is the incoming shortwave radiation (W/m^2)
- α is the surface albedo (dimensionless)
- $R_{L\downarrow}$ is the incoming longwave radiation (W/m^2)
- $R_{L\uparrow}$ is the outgoing longwave radiation (W/m^2)
- ε_o is the surface thermal emissivity (dimensionless)

In Equation (5.2), the amount of shortwave radiation *($R_{S\downarrow}$)* that remains available at the surface is a function of the surface albedo *(α)*. Surface albedo is a reflection coefficient defined as the ratio of the reflected radiant flux to the incident radiant flux over the solar spectrum. The radiation balance equation is explained in detail by Monteith and Unsworth

(1990). Estimation of albedo using Landsat 5 TM / 7 ETM+ satellite images is described by Liang (2000).

The surface emissivity is the ratio of the actual radiation emitted by a surface to that emitted by a black body at the same surface temperature. In SEBAL, emissivity is computed as a function of *LAI*. The final term in Equation (5.2), $(1-\varepsilon_o)RL_{\downarrow}$, represents the fraction of incoming long wave radiation that is lost from the surface due to reflection. Emissivity, expressed as ε_o, represents the surface behavior for thermal emission in the broad thermal spectrum (600 to 1400 nm), and is used to calculate total long wave radiation emission from the surface.

The surface emissivity is computed in SEBAL using the following empirical equation:

$$\varepsilon_0 = 0.95 + 0.01\,LAI \qquad \text{(Equation 5.3)}$$

where:

- *LAI* is the Leaf Area Index of the specific crop and is expressed in SEBAL using the semi-empirical equation (Waters et al. 2002):

$$LAI = \frac{\ln\left(\frac{0.69 - SAVI}{0.59}\right)}{0.91}$$

(Equation 5.4)

where:

- SAVI is the soil adjusted vegetation index (see chapter 4)

Soil heat flux *(G)* is the rate of heat storage into the soil and crops' canopies due to conduction. SEBAL first computes the ratio G/R_n using the following empirical equation developed by Bastiaanssen (2000) representing values near midday:

$$G/R_n = T_s/\alpha\,(0.0038\alpha + 0.0074\alpha^2).(1 - 0.98NDVI^4)$$

(Equation 5.5)

where:

- T_s is the surface temperature (^oC)
- α is the surface albedo
- NDVI is the Normalized Difference Vegetation Index (see Chapter 4)

G is then readily calculated by multiplying G/R_n by the value for R_n. Soil heat flux is a term that is sourcing from an empirical equation and usually is evaluated with ground measurements. If there are no ground measurements, then tables with *G* values exist for evaluation (Baastianssen et al., 1998). G/R_n is dimensionless and vary from 0.04 to 0.15 for crops (low values indicate full crop coverage), 0.2-0.4 for bare soils and 0.5 for clear waters and snow (Waters et al., 2002). These values were used as indicators in the procedure for estimating *G* in this thesis.

Sensible heat flux *(H)* is the rate of heat loss to the air by convection and conduction, due to a temperature difference. It is computed using Equation (5.6) for heat transport. The sensible heat flux (H) is a function of the temperature gradient, surface roughness and wind speed. The sensible heat flux, *H*, can be estimated with a bulk transfer equation written in the form (Monteith and Unsworth, 1990):

$$H = (\rho.c_p.dT) / r_{ah} \qquad \text{(Equation 5.6)}$$

where:

- ρ is air density (kg/m^3),
- c_p is air specific heat (1004 J/kg/K),
- dT (K) is the temperature difference ($T_a - T_s$) where a is for the air and *s* is for the surface of foliage
- r_{ah} is the aerodynamic resistance to heat transport (s/m)

The aerodynamic resistance to heat transport (r_{ah}) is computed for neutral stability as:

$$r_{ah} = \frac{\ln(\frac{z_2}{z_1})}{u_*.\kappa}$$ (Equation 5.7)

where:

- z_1 and z_2 are heights in meters above the zero plane displacement (d) of the vegetation,
- u_* is the friction velocity (m/s) which quantifies the turbulent velocity fluctuations in the air,
- *K* is von Karman's constant (0.41).

A series of iterations is required to determine the value for r_{ah} for each period that consider the impacts of instability (buoyancy) on r_{ah} and *H*. Assuming neutral atmospheric conditions, an initial r_{ah} is computed using Equation (5.7). z_1 is the height just above the zero plane displacement (d ≅ 0.67 × Crop Height) for the crop canopy and z_2 is some distance above the zero plane displacement but below the height of the surface boundary layer. Values of 0.1 meter for z_1 and 2.0 meters for z_2 are assigned based on field experience (Waters et al., 2002; Baastianssen et al., 2000; 2008).

The friction velocity (u_*) is computed using the logarithmic wind law for neutral atmospheric conditions:

$$u_* = \frac{u_x.\kappa}{\ln(\frac{z_x}{z_{om}})}$$ (Equation 5.8)

where:

- *K* is von Karman's constant,
- u_x is the wind speed (m/s) at height z_x, and

- z_{om} is the momentum roughness length (m).

The z_{om} is a measure of the skin friction for the layer of air that interacts with the surface of crops. The momentum roughness length (z_{om}) is empirically estimated from the average crop height using the following equation (Brutsaert, 1982):

$z_{om} = 0.12$. Crop Height

(Equation 5.9)

In the procedure for applying SEBAL algorithm, a crucial point is the selection of the two 'anchor' pixels, the 'hot' and the 'cold' pixel, in the area of interest. These two pixels are used to find the difference (dT) of the temperature between the surface temperature (Ts) and the air temperature (near the surface) which is a basic assumption that SEBAL relies on. It is assumed that a linear relationship connects the Ts and the dT in the form of:

$dT = aTs + b$ (Equation 5.10)

The linear equation above is developed by using the dT values for the cold and hot pixels and the surface temperature (Baastianssen et al., 1998; Alexandridis 2003; Papadavid et al., 2011). The cold pixel in SEBAL is used to define the amount of ETc, through H, occurring from the most vegetated and well-watered areas of the image. Usually, an alfa-alfa cultivation or water body is used to identify cold pixels in the area of interest. Surface Temperature (Ts) (cold temperature), albedo values (0.22-0.24) and LAI (LAI>3) values are the combination that was used to identify the 'cold' pixel in the area of interest from vegetated areas in the image (see Appendix 3 in Appendices). The 'hot' pixel is a pixel where ETc should be zero. This pixel is usually located in dry bare agricultural fields. Both of these "anchor" pixels should be located in large and homogeneous areas that contain more than one pixel of Landsat band 6(60m×60m for Landsat 7ETM+ and 120m×120m for Landsat 5TM). The anchor cold and hot pixels in this thesis were selected in the area of interest where the cold

pixel was planted to Lucerne under center pivot irrigation systems. The hot pixels were always found on bare soil surfaces.

The sensible heat flux (H) for each pixel is computed in SEBAL using Equation (5.6). This is the first estimation of H assuming neutral atmospheric conditions. In order to account for the buoyancy effects generated by surface heating, SEBAL applies the Monin-Obukhov theory (Foken, 2006) in an iterative process. Atmospheric conditions of stability have a large effect on the aerodynamic resistance (r_{ah}) and must be considered in the computation of sensible heat flux (H), especially for dry conditions (Waters et al., 2002). SEBAL repeats the computation of H through a number of iterations, each one correcting for buoyancy effects, until the value for r_{ah} stabilizes. The dT artifice is expected to compensate for errors due to lack of proper atmospheric effects correction in the process of obtaining radiometric surface temperature estimates (Kramber et al., 2002).

The Monin-Obukhov length (L) is used to define the stability conditions of the atmosphere in the iterative process. Monin-Obukhov length is then used to correct friction velocity (u_*) and *a posteriori* aerodynamic resistance to heat transport (r_{ah}), in an iterative procedure until r_{ah} stabilizes (Bastiaanseen et al., 1998).

When all parameters in Equation (5.1) are known, an instantaneous estimation of ETc can be conducted**.** Latent heat flux (λET) in Equation (5.1) is the rate of latent heat loss from the surface due to evapotranspiration, at the time of the satellite overpass. An instantaneous value of ETc_{inst} in equivalent evaporation depth is computed as:

$$ETc_{inst.} = 3600\frac{\lambda ET}{\lambda}$$

(Equation 5.11)

where:

- ETc_{inst} is the instantaneous evapotranspiration (mm/hr)
- 3600 is the time conversion from seconds to hours

- λ is the latent heat of vaporization or the heat absorbed when a kilogram of water evaporates (J/kg)

The Reference ET Fraction (ET_rF) is defined as the ratio of the computed instantaneous ET (ET_{inst}) for each pixel to the reference ET (ET_r) computed only from weather data:

$$ET_rF = \frac{ET_{inst}}{ET_r} \quad \text{(Equation 5.12)}$$

where:

- ET_r is the reference ET at the time of the image from the REF-ET software (mm/hr). ETrF is also known as crop coefficient, Kc. ETrF is used to extrapolate ET from the image time to 24-hour or longer periods. ET_rF values usually range from 0 to 1.

Finally, to get the daily values of ETc which are more useful than the instantaneous ones, SEBAL computes the ET_{daily} by assuming that the instantaneous ET_rF is the same as the 24-hour average. The daily ET_c (mm/day) is computed as:

$$ET_c = ET_rF \times ET_r(24h) \quad \text{(Equation 5.13)}$$

where:

- ET_r (24h) is the total reference evapotranspiration of the day in mm/day.

Daily ET_c is the final 'product' of SEBAL algorithm, meaning that satellite images are transformed into ET_c maps where one could retrieve ET_c for each pixel (see Appendix 2 in Appendices). Of course, each time ET_c is referred to the semi-empirical model used each time. For example, if LAI and CH for Potatoes models (found in Chapter 4) are used then ET_c values are correct only for the plots that are cultivated with potatoes.

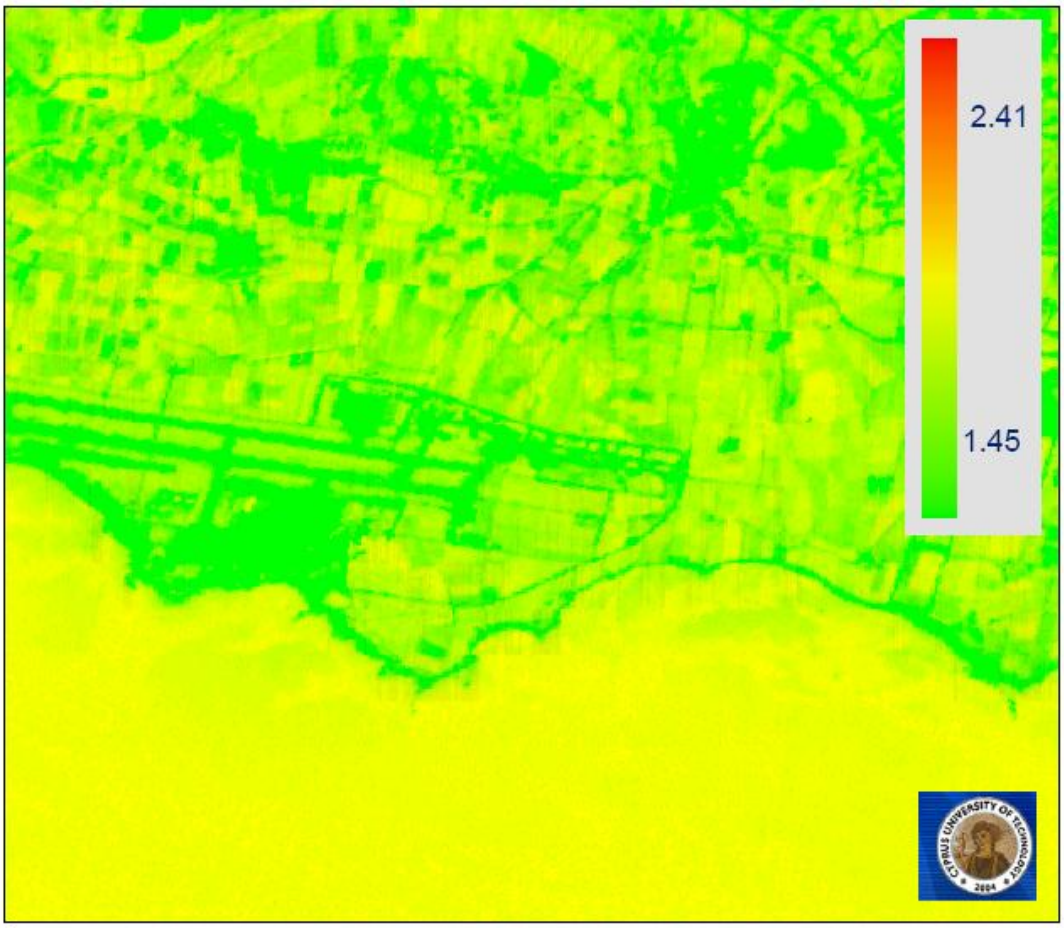

Figure 5.3. ETc map of the area of interest (Landsat 5 TM image 2/1/2009)

5.2. Penman-Monteith adapted to satellite data algorithm

Penman-Monteith method adapted to satellite data was used to estimate ET_c in mm/day. The specific equation needs both meteorological and remotely sensed data to be applied (Figure 5.3).

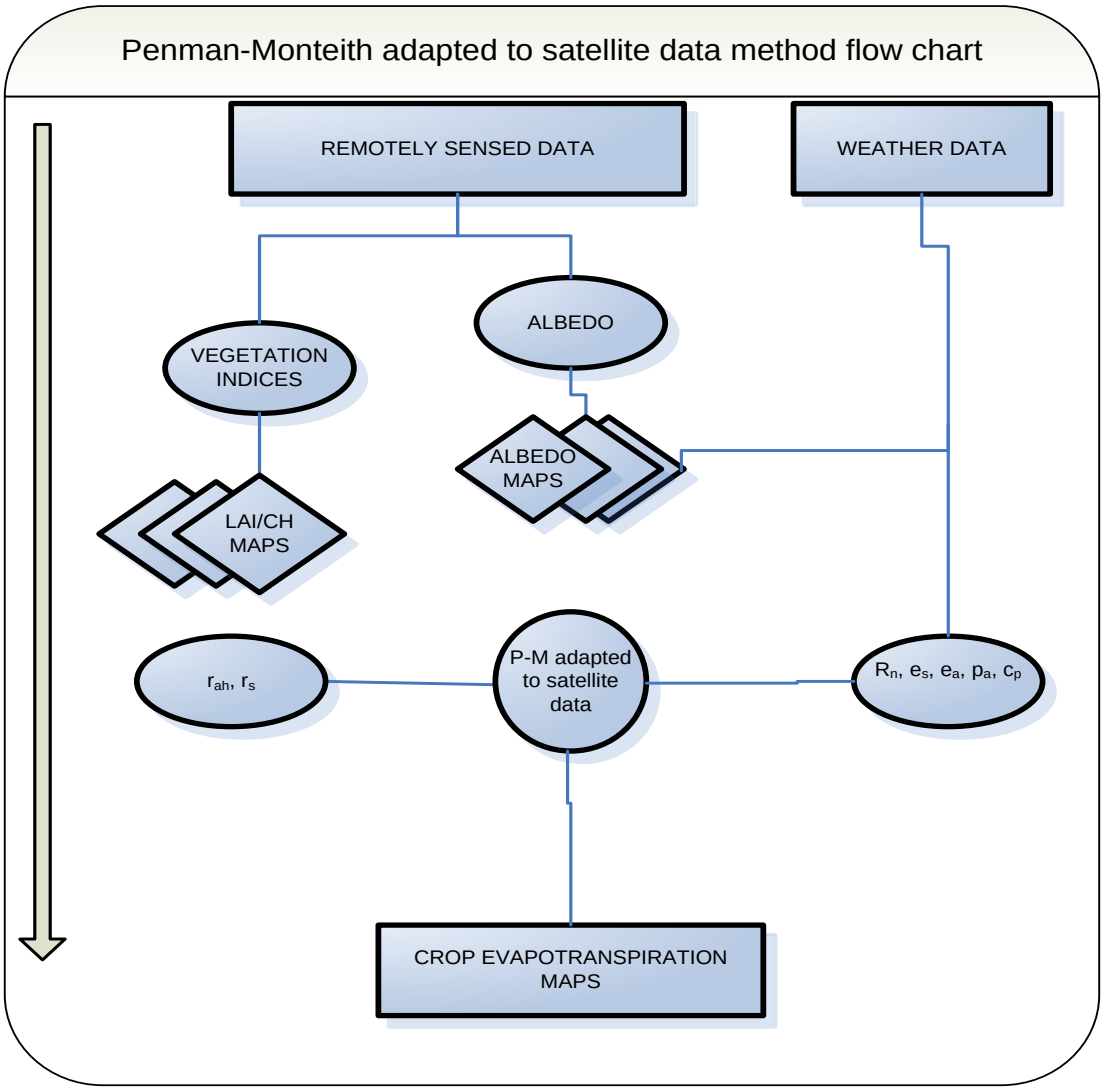

Figure 5.4. Penman-Monteith adapted to satellite data algorithm flow chart for estimating ET_c

The equation is used to estimate ET_c under some assumptions and depends on the direct application of the Penman-Monteith equation (Monteith, 1965; Rijtema, 1965; Smith, 1992; Allen et al., 1998) also based on EB theory, with canopy parameters estimated from satellite imagery (D' Urso, 2001; D'Urso et al., 2006; Minaccapili et al., 2008; Agapiou et al., 2009; Papadavid et al., 2010; 2011). Air temperature, atmospheric pressure, wind speed and other necessary meteorological data were collected from a weather station, located at the Paphos International Airport, very close to our study area. The method also needs empirical equations for describing the crop canopy factors (similar to SEBAL), namely albedo, crop height and LAI. It is a method with strong likelihood of correctly predicting the crop evapotranspiration in a wide range of locations and climates and has provision for application in data-sparse situations. The equation has a strong theoretical basis, combining an energy balance to account for radiation and sensible heat transfer with an aerodynamic transport function to

account for transfer of vapor away from the evaporating surface. The method is described as follows:

$$\lambda ETc = \left[\frac{\Delta(R_n - G) + c_p p_a (e_s - e_a)/r_{ah}}{\Delta + \gamma(1 + r_s / r_{ah})} \right] \qquad \text{(Equation 5.14)}$$

or

$$ETc = \frac{86400}{\lambda} \left[\frac{\Delta(R_n - G) + c_p p_a (e_s - e_a)/r_a}{\Delta + \gamma(1 + r_s / r_a)} \right] \qquad \text{(Equation 5.15)}$$

where

- ETc is the crop evapotranspiration (mm/day)
- Δ represents the slope of the saturated vapor pressure temperature relationship (kPa / K1)
- R_n is the net solar radiation (W/m^2)
- G Soil Heat flux (W/m^2)
- c_p is the air specific heat (J/kg K)
- ρ_a is the air density (kg / m^3)
- e_s is the saturated vapor pressure (kPa)
- e_a is the actual vapor pressure (kPa)
- r_a is the aerodynamic resistance (s/m)
- r_s is the surface resistance (s/m)
- λ is the latent heat of vaporization of water (J / kg)
- γ is the thermodynamic psychrometric constant (kPa / K)

This equation is valid under conditions of intense solar irradiance (typical summer condition in Mediterranean climate) and for $0{,}5 < LAI < 3$, which is the case for Cyprus annual crops. What is important in the specific model is that of its use without the need of the thermal band of any satellite, contrary to the other Energy Balanced based models which thermal band is a prerequisite (Papadavid et al. 2011). Another difference that is rising in this model compared to SEBAL, is the need of atmospheric corrections where SEBAL and other models have an internal calibration for compensating atmospheric effects. The parameters G, u_2, e_s–e_a, R_n and Δ are calculated according to the formulae of the method by the conventional data of the

meteorological station situated in the area of interested. The formulae for calculating each parameter can be found extensively in 'FAO Irrigation and Drainage paper No. 56' by FAO (1998).

$$R_n = (1-a)R_s - R_{nl} \qquad \text{(Equation 5.16)}$$

where

- α is the albedo (dimensionless)
- R_s is the incoming solar radiation (MJ/m^2/day)
- R_{nl} is the net outgoing longwave radiation (MJ/m^2/day)

Aerodynamic resistance (r_{ah})

The transfer of heat and water vapor from the evaporating surface into the air above the canopy is determined by the aerodynamic resistance r_{ah} . In most practical applications, the aerodynamic resistance r_{ah} is calculated as a function of crop height *CH* (m) and wind speed (m/s) *uz* (Allen et al., 1990, 1996, 1998; Brutsaert, 1982; D'Urso, 2001):

$$r_{ah} = \frac{\ln\left(\frac{z_u - d}{z_{om}}\right) x \ln\left(\frac{z_t - d}{z_{oh}}\right)}{k^2 u} \qquad \text{(Equation 5.17)}$$

where

- r_{ah} aerodynamic resistance (s/m)
- z_u height of wind measurements (m)
- z_t height of humidity measurements (m)
- d zero plane displacement height (m)
- z_{om} roughness length governing momentum transfer (m)
- z_h roughness length governing transfer of heat and vapour (m)
- k von Karman's constant, 0,41 (dimensionless)
- u wind speed (m/s)

Many studies have explored the nature of the wind regime in plant canopies (Kustas and Norman 2004; Baastianssen et al., 2005; Allen, 2007b). Zero displacement heights and roughness lengths have to be considered when the surface is covered by vegetation. The factors depend upon the crop height and architecture of the canopy. Several empirical equations for the estimate of d, z_{om} and z_{oh} have been developed. For a wide range of crops,

the zero plane displacement height, d, and the roughness length governing momentum transfer, z_{om}, can be estimated from the crop height (CH) by the following equations:

$$d = 2/3(CH) \qquad \text{(Equation 5.18)}$$

and

$$z_{om} = 0{,}123(CH) \qquad \text{(Equation 5.19)}$$

The roughness length governing transfer of heat and vapour, z_{oh}, can be approximated by:

$$z_{oh} = 0{,}1\ z_{om} \qquad \text{(Equation 5.20)}$$

Finally, Equation 5.17 becomes

$$r_{ah} = \frac{\ln\left(\frac{z_u - 0.67CH}{0.123(CH)}\right) x \ln\left(\frac{z_t - 0.67}{0.0123(CH)}\right)}{0.168u} \qquad \text{(Equation 5.21)}$$

where (CH) is found from remotely sensed data for each crop and each date.

(Bulk) surface resistance (r_s)

An acceptable approximation to a much more complex relation of the surface resistance of dense full cover vegetation is:

$$r_s = \frac{r_l}{LAI_{active}} \qquad \text{(Equation 5.22)}$$

where

- r_s is (bulk) surface resistance (s/m)
- r_l is bulk stomatal resistance of the well-illuminated leaf (s/m)
- LAI_{active} is active (sunlit) leaf area index (m^2 (leaf area) / m^2 (soil surface))

The Leaf Area Index (LAI), is the leaf area per unit area of soil below it. The active LAI is the index of the leaf area that actively contributes to the surface heat and vapor transfer. It is generally the upper, sunlit portion of a dense canopy. The bulk stomatal resistance, r_l, is the average resistance of an individual leaf. This resistance is crop specific and differs among crop varieties and crop management. It usually increases as the crop ages and begins to ripen and is affected both by climatic conditions and water availability. The resistance increases when the crop is water stressed and the soil water availability limits ETc. The stomatal resistance of a single leaf has a value of about 100 s/m under well-watered conditions.

A general equation for LAI_{active} is:

$$LAI_{active} = 0.5\ LAI \qquad \text{(Equation 5.23)}$$

Employing the above simplification Equation 5.21 becomes:

$$r_s = \frac{200}{LAI} \qquad \text{(Equation 5.24)}$$

where LAI is estimated from remotely sensed data for each crop.

The ETc is estimated using remote sensing after CH and LAI maps are created using the SIMODIS procedure and the CLAIR model to specify these parameters spatially through Vegetation Indices (D'Urso et al., 1995; D'Urso et al., 2006; Minaccapily et al., 2008; Papadavid et al., 2011). The algorithm provides at the end of the procedure, direct values of daily ETc through maps of evapotranspiration. As for SEBAL, the method provides the opportunity to have ETc estimations for all the crops that appear in the map (transformed satellite image) in different plots in the area of interest.

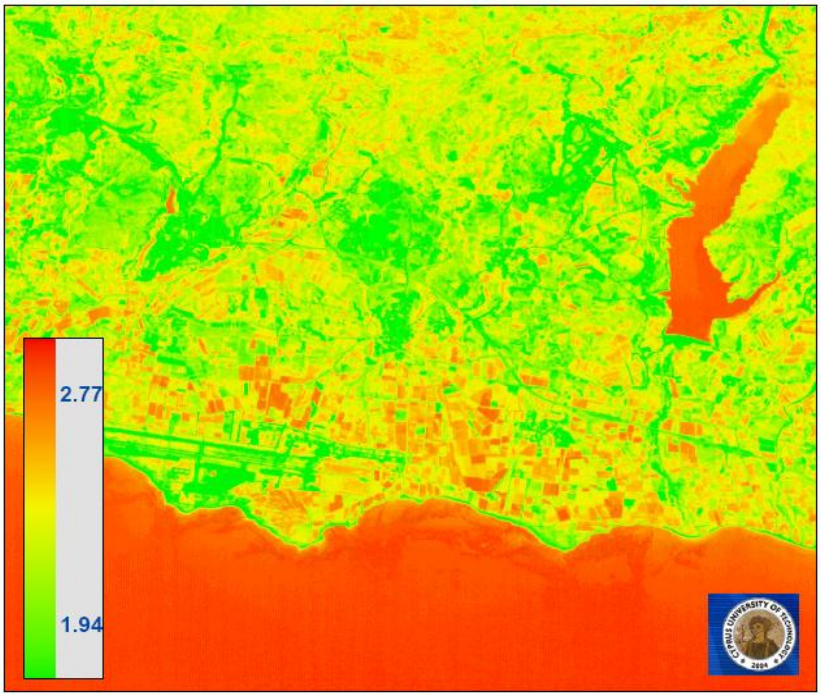

Figure 5.5. ETc map of the area of interest (Landsat 7 TM image 2/1/2009)

5.3. Results of SEBAL and Penman-Monteith adapted to satellite data direct applications

The results of the direct application of the two algorithms are shown in Tables 5.1 and 5.2. ETc per crop is illustrated along with the crop coefficient (Kc) which is simply the ratio of ETc/ETref and allow users to identify the stage of crop life cycle. The maximum value that Kc should take is 1 but in some cases, when the density of the crops is high and well watered then it can reach the value of 1.1 (Waters et al., 2002).

Table 5.1. Results of SEBAL and P-M adapted to satellite data for 2008

2008	POTATOES				GROUNDNUTS				BEANS				CHICKPEAS				
	P-M		SEBAL		P-M		SEBAL		P-M		SEBAL		P-M		SEBAL		
	Kc	ETc	Kc	ETc	Kc	ETc	Kc	ETc	Kc	ETc	Kc	ETc	Kc	ETc	Kc	ETc	ETref
12/07					0,83	4,90	0,94	5,56	0,66	3,90	0,68	4,01					5,90
28/07					1,06	6,30	0,99	5,91	0,75	4,50	0,78	4,68					5,97
13/08					0,93	5,67	1,09	6,62	0,76	4,62	0,79	4,83					6,10
29/08					0,67	4,59	0,73	5,00	0,76	5,25	0,82	5,65					6,88
14/09	0,36	2,01	0,39	2,21									0,43	2,44	0,47	2,67	5,66
30/09	0,60	2,20	0,82	3,02									0,75	2,75	0,76	2,79	3,68
16/10	0,78	3,20	0,86	3,53									0,80	3,26	0,90	3,69	4,08
1/11	0,99	4,90	1,01	5,00									0,72	3,56	0,69	3,44	4,95
17/11	0,68	3,13	0,77	3,50									0,70	3,21	0,68	3,11	4,57

Table 5.2. Results of SEBAL and P-M adapted to satellite data for 2009

2009	POTATOES				GROUNDNUTS				BEANS				
	P-M		SEBAL		P-M		SEBAL		P-M		SEBAL		
	Kc	ETc	Kc	ETc	Kc	ETc	Kc	ETc	Kc	ETc	Kc	ETc	ETref
2/1	0,45	2,38	0,47	2,49									5,34
21/2	0,58	3,57	0,49	3,00									6,12
29/6					0,49	4,38	0,47	4,22	0,66	5,89	0,65	5,79	8,89
7/7					0,69	6,19	0,69	6,22	0,71	6,37	0,73	6,52	8,99
15/7					0,83	7,59	0,86	7,83	0,46	4,15	0,48	4,41	9,12
23/7					0,96	7,67	0,93	7,47	0,38	3,02	0,49	3,95	8,03
16/08					0,61	5,54	0,77	6,98					9,06

Table 5.3. Results of SEBAL and P-M adapted to satellite data for 2010

2010	POTATOES				GROUNDNUTS				BEANS				CHICKPEAS				
	P-M		SEBAL		P-M		SEBAL		P-M		SEBAL		P-M		SEBAL		
	Kc	ETc	Kc	ETc	Kc	ETc	Kc	ETc	Kc	ETc	Kc	ETc	Kc	ETc	Kc	ETc	ETref
13/4	0,66	2,79	0,75	3,19													4,23
31/5	0,79	4,43	0,93	5,22	0,40	2,23	0,60	3,34					0,32	1,79	0,40	2,22	5,60
16/6	0,92	6,10	0,92	6,12	0,57	3,78	0,59	3,94					0,45	3,00	0,40	2,67	6,63
24/6	0,68	4,83	0,80	5,71	0,83	5,91	0,88	6,25					0,61	4,37	0,72	5,12	7,10
10/7					0,98	6,94	1,02	7,22					0,56	3,99	0,46	3,23	7,07
27/8					0,76	5,79	0,86	6,59									7,66
7/11									0,67	2,49	0,68	2,56					3,74
9/12									0,90	3,21	0,98	3,50					3,58

Tables 5.1-5.3 show the results of the direct application of the two algorithms. In each table, the ETc and Kc values are shown for all the crops and all the dates of satellite images for the years 2008, 2009 and 2010. The last column shows the reference evapotranspiration (ETref) for each date. It has to be mentioned that all plots used in this study are greater than 120 meters x 120 meters (4 Landsat pixels x 4 Landsat pixels) so as to have the opportunity to exclude all the pixels which are the edges of each plot. This procedure allows for avoiding any mixed pixels (non-vegetated - vegetated) that could provide any misleading results regarding ETc.

A general rule that arise from the results is that when the crop coefficient factor is high, ETc is high and when is low then respectively ETc is low. One should bear in mind that ETc is affected not only from crop factors but also from meteorological parameters. Thus, in some cases even though Kc is increasing (meaning that crops are growing up) ETc has not the proportional increase or even has a decrease in its value. Another noticeable phenomenon

indicated from the above results, similarly to spectroradiometric results, is that ETc is increasing as crops are growing up (see Kc) until it reaches a peek, at the stage of carpophore-fruit set and then the value decreases gradually until the ripening-harvesting.

Statistical techniques were used to find out if the results of the two methods employed have a statistical significant difference. Student's t-test was applied based on the results (paired values of ETc with criterion the different model-algorithm used to obtain the results) of the crop for the three years. The results of the test are shown in Tables 5.7-5.10.

SPSS statistical software was used to proceed with the statistical analysis and obtain the values of T-test to be compared with those of existing Statistical Tables for T-test. The analysis has illustrated that the values of $T_{observed}$ for all crops was greater than the $T_{statistical}$, which implies that for (n-1) degrees of freedom and at a confidence level of 95%, the two methods provide results which have a significant statistical difference between them. The coupled values of the results have shown that when using the two algorithms as they referred to in the literature provide close results but with a statistical significant difference. The null hypothesis for this case should be that of providing identical results for the ETc. Thus, the null hypothesis is rejected since the results have a significant statistical difference. The next step is to provide the algorithms with ground data results (semi-empirical models) to test if the null hypothesis can stand.

5.4. Modification of algorithms

Modifications, simplifications and improvements of ETc algorithms are quite common in the procedure for estimating ETc (Nagler et al., 2005; Yang et al., 2006; Groweneveld and Baugh 2007; Scott et al., 2008, Edward et al., 2010; Papadavid et al., 2011). SEBAL and Penman-Montheith are algorithms which take into account the crop canopy and meteorological factors in order to estimate the actual ETc. This fact provides the opportunity to feed the model with local crop and meteorological data in an attempt to increase its accuracy. Empirical equations (using Vegetation Indices, VI)) describing LAI and Crop Height (CH) could be used in the algorithm sourcing from the local geomorphological conditions of the area of interest. The methodology of the thesis as described in Chapter 2 is based on the hypothesis that if the algorithm is supported with ground data, regarding the crop canopy factors and the meteorological conditions of the area, could increase its accuracy.

Data requirements for forming the necessary equations are retrieved from ground measurements (Chapter 3) which are used to improve the reliability (Kite and Droogers, 2000). It is noticeable that in the two algorithms empirical equations are used to describe parameters that need to be directly measured. The intended purpose is to supply the algorithm with the needed local empirical equations in order to check if the accuracy can be boosted. In this perspective, empirical equations adapted to the Cypriot conditions have been created and integrated in the algorithm. In Chapter 4 models regarding LAI and CH were formed using VI for each crop. In this Chapter, the specific models are employed to be used in the algorithms to estimate crop canopy factors (LAI and CH) which are used in the algorithms. For each satellite image, all four models (one for each crop) were used separately to retrieve the value of ETc for each crop included in the image. The same procedure as for the classic algorithms, was followed but now using the specific models. For discrimination reasons, when using the specific models in the algorithms, SEBAL and P-M algorithms will be called CYSEBAL and CYP-M.

Tables 5.4-5.6 show the results of the modified algorithms for the years 2008, 2009 and 2010 in mm/day for each date that there is a satellite image available (see Appendix 5 in Appendices). It is obvious that the results are different from the results of the classic algorithms. Kc is also different since it is affected from the ETc. The difference seems to be small in terms of mm/day but when employing statistical techniques to check if the difference is significant the results have indicated that the difference when using the semi-empirical models (modified algorithms) is significant at 95% confidence level.

For all the crops, there is a significant difference between the results of PM-SEBAL, PM-CYPM and SEBAL-CYSEBAL (Tables 5.7-5.10) with an exception regarding SEBAL-CYSEBAL for the Chickpeas. For all the other cases, modified algorithms provide significantly different results from the classic algorithms for all the crops. The important outcome of this statistical analysis though focuses on the fact that the results of the two modified algorithms (CYPM and CYSEBAL) is found to have no significant difference for all the cases which is actually the null hypothesis ‘The two algorithms should provide the same results using different ways’. Thus, the procedure of adapting the algorithms to the local conditions is very important to “guide” the ETc algorithms to provide users with most accurate results.

Table 5.4. Results of CY-SEBAL and CYP-M adapted to satellite data for 2008

2008	POTATOES				GROUNDNUTS				BEANS				CHICKPEAS				
	CYP-M		CYSEBAL		CYP-M		CYSEBAL		CYP-M		CYSEBAL		CYP-M		CYSEBAL		
	Kc	ETc	Kc	ETc	Kc	ETc	Kc	ETc	Kc	ETc	Kc	ETc	Kc	ETc	Kc	ETc	ETref
12/07					0,81	4,79	0,84	4,96	0,64	3,79	0,66	3,91					5,90
28/07					1,01	6,06	1,02	6,10	0,75	4,45	0,76	4,56					5,97
13/08					0,89	5,46	0,91	5,54	0,75	4,55	0,76	4,66					6,10
29/08					0,61	4,22	0,63	4,30	0,72	4,98	0,75	5,16					6,88
14/09	0,36	2,00	0,36	2,05									0,43	2,41	0,45	2,56	5,66
30/09	0,60	2,19	0,60	2,22									0,73	2,69	0,73	2,69	3,68
16/10	0,78	2,98	0,74	3,03									0,74	3,03	0,76	3,10	4,08
1/11	0,99	4,33	0,88	4,34									0,69	3,41	0,71	3,54	4,95
17/11	0,68	2,90	0,65	2,99									0,65	3,00	0,68	3,10	4,57

Table 5.5. Results of CY-SEBAL and CYP-M adapted to satellite data for 2009

2009	POTATOES				GROUNDNUTS				BEANS				
	CYP-M		CYSEBAL		CYP-M		CYSEBAL		CYP-M		CYSEBAL		
	Kc	ETc	Kc	ETc	Kc	ETc	Kc	ETc	Kc	ETc	Kc	ETc	ETref
2/1	0,43	2,31	0,44	2,33									5,34
21/2	0,57	3,51	0,54	3,32									6,12
29/6					0,45	4,00	0,46	4,12	0,65	5,79	0,66	5,88	8,89
7/7					0,65	5,86	0,67	5,99	0,69	6,23	0,72	6,43	8,99
15/7					0,81	7,37	0,82	7,47	0,44	4,00	0,45	4,11	9,12
23/7					0,93	7,45	0,90	7,20	0,37	2,99	0,38	3,03	8,03
16/08					0,66	6,01	0,70	6,34					9,06

Table 5.6. Results of CY-SEBAL and CYP-M adapted to satellite data for 2010

2010	POTATOES				GROUNDNUTS				BEANS				CHICKPEAS				
	CYP-M		CYSEBAL		CYP-M		CYSEBAL		CYP-M		CYSEBAL		CYP-M		CYSEBAL		
	Kc	ETc	Kc	ETc	Kc	ETc	Kc	ETc	Kc	ETc	Kc	ETc	Kc	ETc	Kc	ETc	ETref
13/4	0,63	2,67	0,71	3,00													4,23
31/5	0,70	3,90	0,73	4,10	0,39	2,20	0,42	2,33					0,27	1,52	0,38	2,13	5,60
16/6	0,90	5,99	0,85	5,62	0,55	3,64	0,57	3,78					0,37	2,45	0,38	2,54	6,63
24/6	0,65	4,61	0,64	4,52	0,67	4,79	0,84	6,00					0,60	4,27	0,59	4,16	7,10
10/7					0,97	6,89	0,97	6,86					0,43	3,05	0,42	2,98	7,07
27/8					0,71	5,44	0,70	5,34									7,66
7/11									0,68	2,53	0,62	2,33					3,74
9/12									0,74	2,66	0,83	2,95					3,58

Tables 5.7-5.10 show a statistical comparison among all the algorithms. Using the Student's T-test, P-M to SEBAL, P-M to CYP-M, SEBAL to CYSEBAL and CYP-M to CYSEBAL are tested to find out if there is a statistically significant difference between the coupled values (results). The value of T found from the t-test application is given in the second row while at the third row T from the statistical tables is provided. R^2 is also provided along with the mean standard error for each case in the fourth and fifth rows.

Table 5.7. Results of Student's T-test for potatoes

POTATOES	P-M-SEBAL	P-M-CYP-M	SEBAL-CYSEBAL	CYP-M-CYSEBAL
Tobs.	-2,45	3,42	3,68	-0,27
Tstat.	2,23	2,23	2,23	2,23
R^2	0,95	0,99	0,95	0,99
Mean st. error	0,12	0,19	0,45	0,18

Table 5.8. Results of Student's T-test for beans

BEANS	P-M-SEBAL	P-M-CYP-M	SEBAL-CYSEBAL	CYP-M-CYSEBAL
Tobs.	-2,85	2,74	4,45	-0,55
Tstat.	2,26	2,26	2,26	2,26
R^2	0,97	0,99	0,98	0,99
Mean st. error	0,27	0,17	0,25	0,19

Table 5.9. Results of Student's T-test for groundnuts

GROUNDNUTS	P-M-SEBAL	P-M-CYP-M	SEBAL-CYSEBAL	CYP-M-CYSEBAL
Tobs.	-2,85	2,67	4,43	-1,74
Tstat.	2,16	2,16	2,16	2,16
R^2	0,93	0,98	0,96	0,98
Mean st. error	0,53	0,33	0,41	0,33

Table 5.10. Results of Student's T-test for chickpeas

CHICKPEAS	P-M-SEBAL	P-M-CYP-M	SEBAL-CYSEBAL	CYP-M-CYSEBAL
Tstat.	-0,41	2,92	2,13	-1,58
Tobs.	2,31	2,31	2,31	2,31
R^2	0,84	0,92	0,95	0,98
Mean st. error	0,46	0,29	0,33	0,20

Figures 5.6-5.9 illustrate graphically the results of the direct application of the two ETc algorithms (SEBAL and P-M) and the results of the two modified algorithms (CYSEBAL and CYP-M) for each crop. Y-axis represents the ETc in mm/day and X-axis the dates for which there were satellite images available for each crop in the years 2008, 2009 and 2010. It is obvious that the results are very close but it is more obvious that when the algorithms are modified, the results come even closer. SEBAL, for all the cases, is the algorithm which has the highest deviation, but when modified with the semi-empirical equations, it is calibrated to provide results identical to those of the modified Penman-Monteith adapted to satellite data.

The whole procedure of modifying the two algorithms has proved that when using auxiliary ground truth data can boost algorithms' accuracy and avoid any discrepancies of the results. This is the rule for the three (potatoes, groundnuts and beans) crops but for the chickpeas, the rule is not valid since no statistical difference is observed for the classic algorithms too. This fact may be random since as mentioned in Chapter 4 (4.3.4) the regression analysis was based on few spectroradiometric measurements and though it had a strong R^2 the results could be misleading. Thus the 'rule braking' is attributed to the short phenological cycle of the specific crop which prohibits the opportunity for high volume of spectroradiometric measurements and as a result the dependence of effects on that case is expected to be minimal, compared to the other cases.

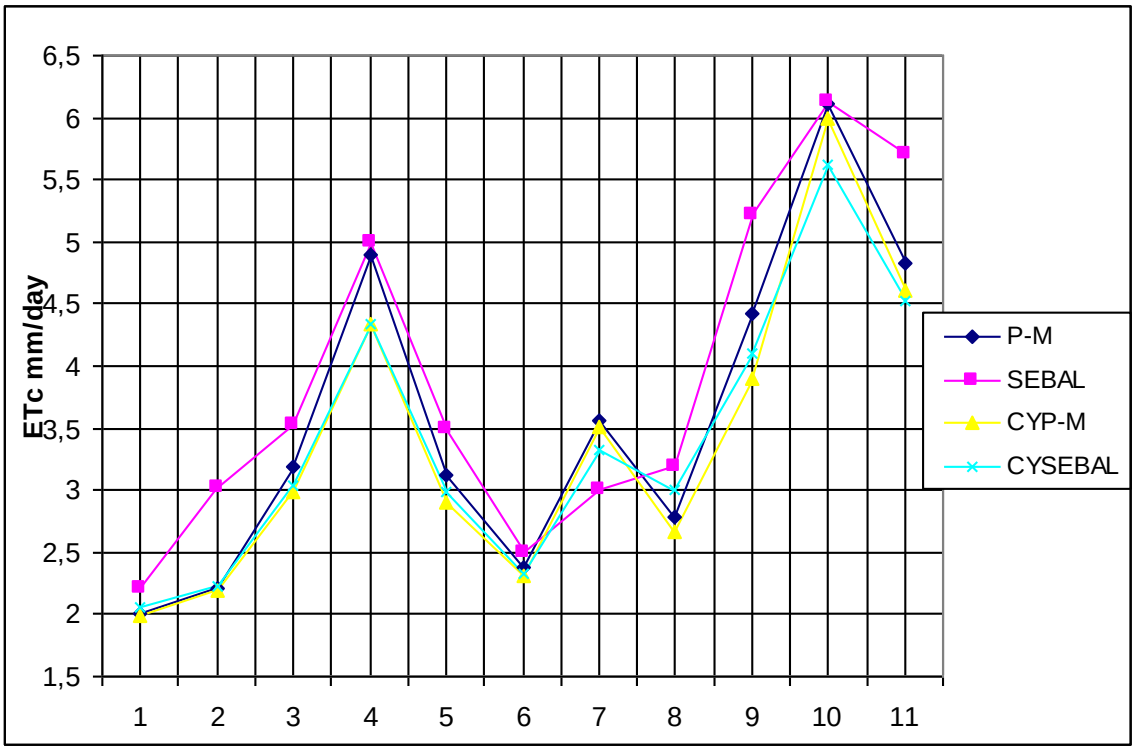

Figure 5.6. Results of the application of classic and modified SEBAL and P-M ETc algorithms for potatoes

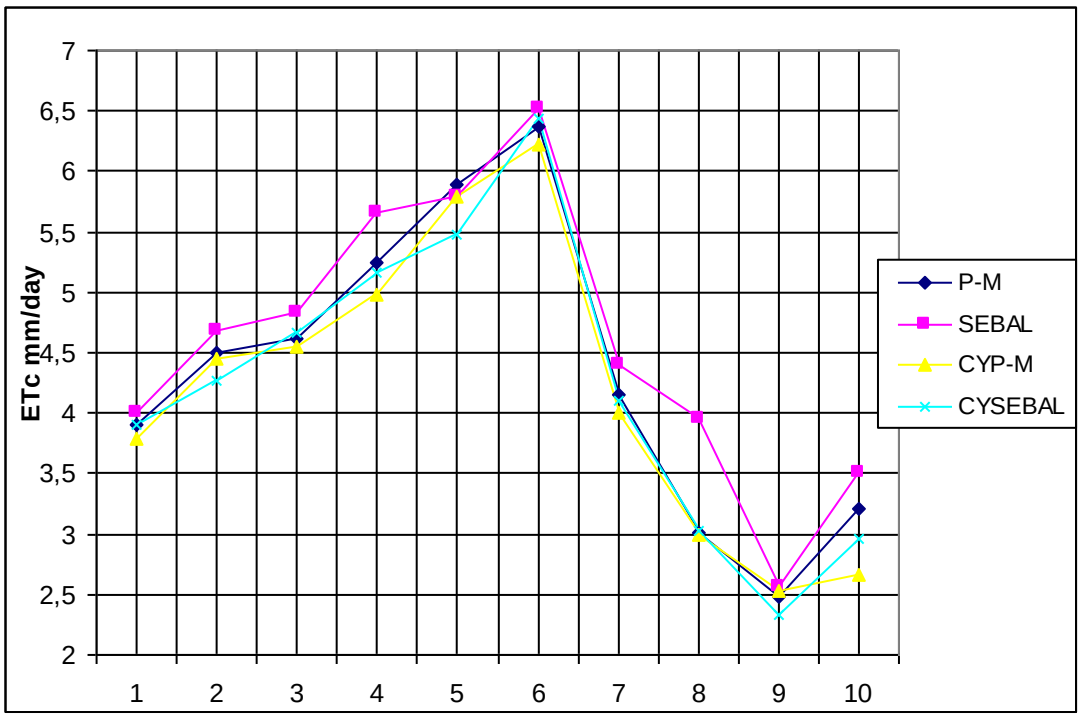

Figure 5.7. Results of the application of classic and modified SEBAL and P-M ETc algorithms for beans

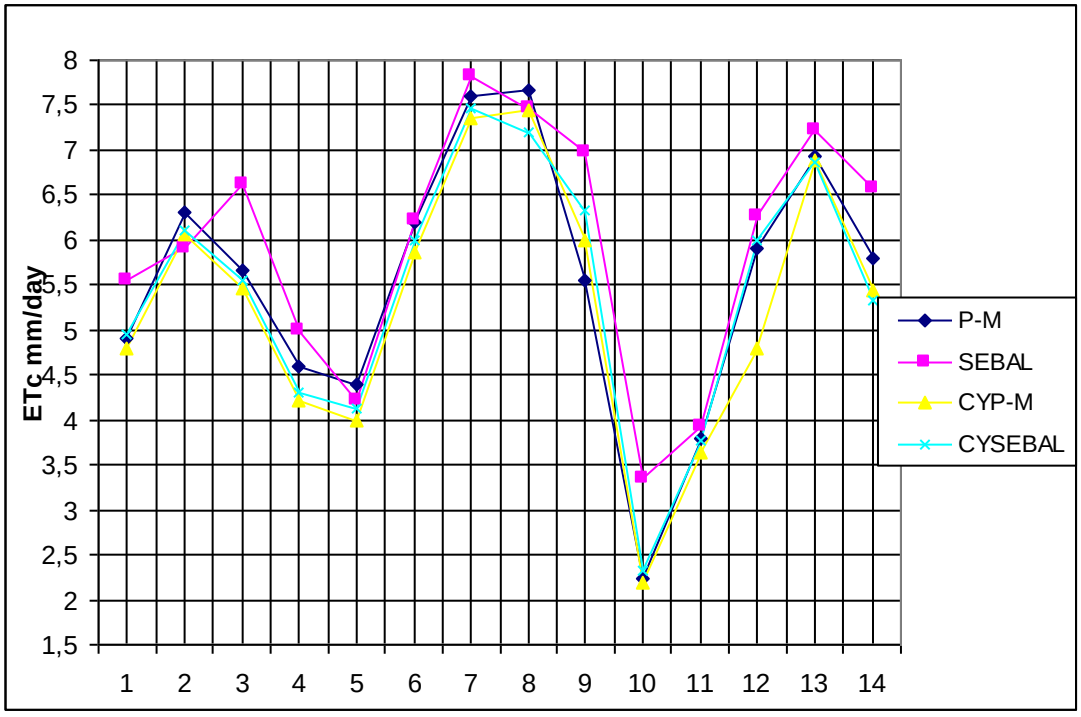

Figure 5.8. Results of the application of classic and modified SEBAL and P-M ETc algorithms for groundnuts

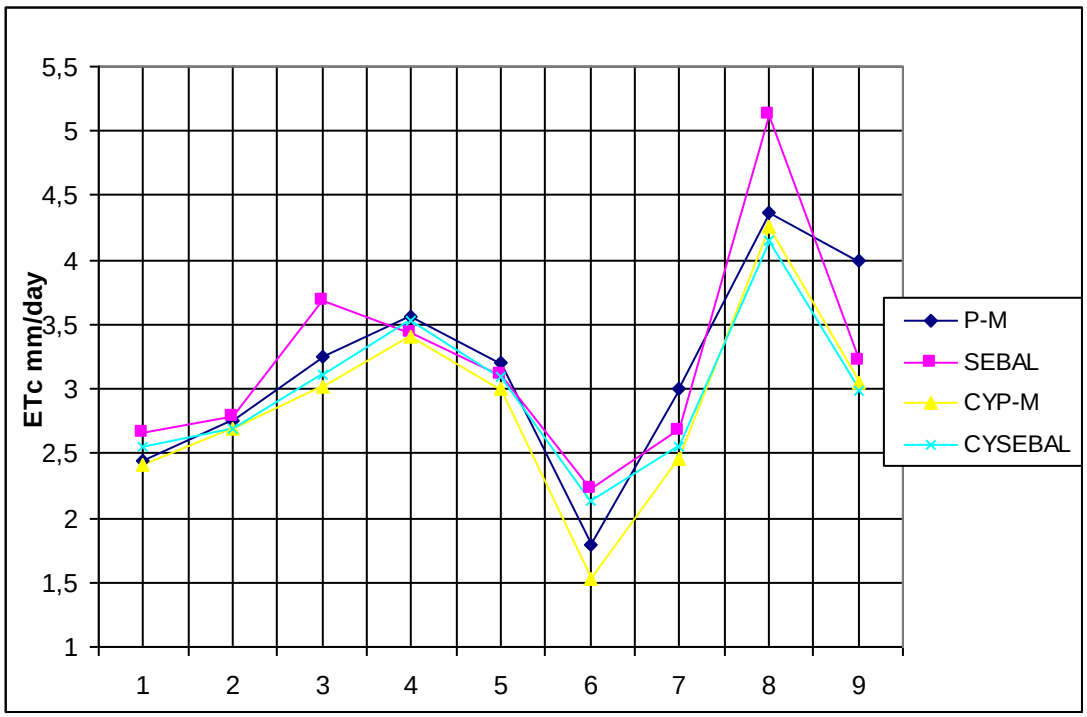

Figure 5.9. Results of the application of classic and modified SEBAL and P-M ETc algorithms for chickpeas

CHAPTER 6: DISCUSSION AND CONCLUSIONS

In this chapter, discussion regarding results and the most important conclusions which have resulted from the research for estimating crop evapotranspiration for annual crops in Cyprus using remote sensing are described.

6.1. Discussion

Evapotranspiration is the sum of the water used by plants in a given area through transpiration and water evaporated from the soil at any specified time period. As a key component in water resources management, it is essential to estimate evapotranspiration accurately for water resources evaluation, drought monitoring and crop production simulation. Accurate estimates of ETc are needed for numerous agricultural and natural resource management procedures. However, this is difficult to achieve in practice because actual evapotranspiration cannot be measured directly and varies considerably in time and space. Remote sensing can assist in improving the estimation of ETc, and consequently water demand in cultivated areas for irrigation purposes and sustainable water resources management. In this Thesis, a novel approach for ETc estimation has been applied and tested. In this approach, remotely sensed data along with meteorological data, modeling techniques and surface energy balance algorithms were combined. All these procedures combined can provide the spatial distribution of ETc in maps where users can derive the value of ETc for each crop in mm/day. The parameters that are required in the empirical equations can be easily evaluated using remote sensing techniques and field spectroscopy. Using fine resolution instruments – spectroradiometers - it is possible to model crop canopy parameters to Vegetation Indices for the development of semi-empirical models which describe these parameters during the entire phenological cycle of each crop.

The literature review has indicated that many algorithms have been developed for estimating ETc based on remote sensing techniques and there is a possibility for improving these algorithms' results if they are fed with ground truth data regarding the area of interest. The improvement of the ETc results is very important especially in a region where drought is a common phenomenon and for the sustainable use of irrigation water. Especially in eastern Mediterranean countries there is a need for improving irrigation management, since as shown it will be one of the regions that will face water scarcity in the future. The implementation of

the innovative approach from the author for estimating ETc combining remotely sensed data, meteorological parameters, modeling techniques and ETc algorithms aims at filling the gap in the literature regarding modifications of ETc algorithms for improving results. The combination of ground and remotely sensed data is extremely important in areas with insufficient *in situ* networks for monitoring ETc. Satellite data provide spatially distributed estimates of albedo, normalized difference vegetation index and surface temperature, enabling the water managers to estimate the water evaporating per day. The accuracy of the methods estimating the regional evapotranspiration is expected to increase even more if ground truth data are somehow integrated in the algorithms for adapting algorithm in the current conditions.

A two year campaign for collecting *in situ* data was conducted. A field spectroradiometer was used for acquiring the spectral signature of each crop during their phenological stages. A standard procedure for collecting these measurements was followed. Then, the spectroradiometric data were transformed into Landsat's first four bands (Blue, Green, Red and Infrared spectrum) reflectance which is the reflectance that Landsat satellites should provide after the necessary pre-processing steps (or otherwise 'in band' reflectance). These data were finally used to retrieve the Vegetation Indices which were used in the modeling procedure.

Simultaneously to spectroradiometric data, LAI and crop height measurements were conducted. Using a Sunscan canopy analyzer and a simple ruler, the two canopy parameters were recorded during each crop's phenological cycle. The *in situ* data collected for the crop canopy factors along with the remotely sensed data for Vegetation Indices have been used to create time series of each crop. Based on the theory and using regression analysis, semi-empirical models have been developed. The regressions had very high coefficient of determination (R^2) which is interpreted into very efficient models, describing crop canopy factors. The most known Vegetation Indices – such as NDVI, SAVI and WDVI - were used in these models. These models were integrated into the algorithms to describe canopy factors wherever they appear in the algorithm sequence. For each crop, a model was developed and employed in the procedure for estimating ETc. Thus each satellite image had to be transformed into an ETc map for each crop. Therefore,, in a specific ETc map only values of a specific crop can be derived in terms of ETc in mm/day. This has to be borne in mind, since in the classic approach of algorithms one single and common model is used for estimating

each crop canopy factor (crop height and LAI). This difference implies additional effort for the user but it can provide more accurate results. It is obvious from the results that when using the novel approach, the results are more accurate than the results from the classic approach.

The specific semi-empirical models developed for each crop were merged and used in the two algorithms that are presented and applied for the estimation of ETc. SEBAL and Penman-Monteith adapted to satellite data were employed to create ETc maps describing ETc spatially. The Penman–Monteith adapted to satellite data algorithm for ETc includes all the main environmental variables affecting ETc as well as stomatal and canopy conductance terms related to plant physiological status and architecture. But for its application detailed meteorological records are needed. What is not needed compared to SEBAL is the Thermal Band of a satellite. Thus satellites that do not carry a thermal band could also be used in such an application while for SEBAL this is not possible. An advantage, over SEBAL, is the resolution of the ETc maps produced. The Thermal Band of Landsat satellites, which is a prerequisite in SEBAL, has lower resolution (60 m x 60 m) and thus affect ETc maps in a negative optical way. Of course this does not affect the information in the pixels but the map produced is not so clear compared to the map produced from the Penman–Monteith adapted to satellite data algorithm. The advantage of the SEBAL approach is that it does not require detailed field information such as crop or land use type, moisture status or area specific crop coefficients (K_c), which are essential to compute ET_c using conventional techniques. Another advantage of SEBAL is the internal calibration that is applied for compensating atmospheric effects on satellite images. While for Penman–Monteith adapted to satellite data algorithm atmospheric corrections procedure is inevitable, for SEBAL there is an internal calibration procedure for removing atmospheric effects. For the needs of this study and in order to investigate the general effect of canopy factors to ETc algorithms, we decided to use the statistical relations which proved to have the higher correlation (R^2) values, when compared with the experimental data. In that sense, the generality of the relations used needs to be fatherly tested, in a future step of our work, especially when applied to regions of the possible range of the estimated parameters where no experimental data exist. This approach will result with better and more well-behaved statistical semi-empirical relations. However, given the fact that even the simplest linear relations show very large correlations we would expect that the general picture of our results will not be modified by slight future modifications. Furthermore, the outcomes of our study should be considered as a first step on a newly-

proposed methodology, aiming to prove the efficiency and physical justification of our technique.

The direct application of the two ETc algorithms has provided results which have a significant difference between them. t-test has revealed that by applying the algorithms as given in literature this could provide users with close results of ETc but with statistically significant difference, for all the crops. The algorithms were then modified with the semi-empirical models, developed earlier for each crop. The results, after the modification, have been found to have no significant difference which means that the two algorithms have boosted accuracy. The null hypothesis that the two algorithms should provide the same results for each crop has been proven. The increased accuracy is attributed to the fact that each semi-empirical model takes into account the special characteristics of each crop, created for. Unlikely, in the classic approach, a single model is used for estimating crop canopy factors which can lead to results with deviations to the real ones.

The methodology as described in this Thesis is novel and can support decision makers of Water Authorities. The methodology was applied for Landsats' images but it can easily be adapted for other satellites. The use of spectroradiometer can facilitate the procedure since it provides a spectrum which can be adapted to satellites' bands by simple transformation, using RSR filters of each satellite. The methodology followed can be applied for any place since it can be considered as 'algorithm adaptation' to local conditions. The models developed though can be used only in Cyprus, since they refer to its conditions.

The author recommends as a future work, for potential users of this novel method, the generation of a spectral library where all spectral signatures of the main agricultural crops will be included. Using the spectral signatures, semi-empirical models for each crop could be created in order to use them for estimating ETc using any ETc algorithm from the literature. In this way, there can be a systematic estimation of ETc which can support decision making procedures for irrigation water management. Future work can also consist of automation of the method by developing a software where all these models could be inserted and used when needed for systematic monitoring of irrigation water.

6.2. Conclusions

6.2.1. Literature review conclusions

Remote sensing has widened the opportunities for irrigation water management through ETc estimation. It is a tool that provides accurate ETc values spatially distributed over a satellite image on a pixel basis. Reliable regional ETc estimates are essential to improve spatial crop water management. Land surface energy balance (EB) algorithms, using remote sensing data from ground, airborne or satellite platforms at different spatial resolutions, have been found to be promising for mapping daily and seasonal ETc at a regional scale. Although remote sensing based ETc models have been shown to have the potential to accurately estimate regional ETc, there are opportunities to further improve these models by amending the equations used to estimate LAI and crop height for their accuracy under current agro-meteorological/environmental conditions. As it was shown recently, improving the quality of the models used to describe the canopy factors such as LAI and Crop Height can increase the accuracy of the algorithms. The procedure can be considered as a modification of the algorithm since the idea is to adapt the algorithm to the local conditions.

6.2.2. Ground data and modelling of LAI/ CH to remotely sensed data (vegetation indices) conclusions

Ground data have been found to be necessary in the procedure of modifying ETc algorithms. Time series of spectroradiometric data, LAI and CH were created in order to create models based on theory, called semi-empirical models. For each crop a semi empirical model is developed and used to retrieve the values of ETc from the satellite images.

Study results demonstrated that spectral information can provide acceptable estimates of LAI and CH of the specific area under the current geo-morphological and meteorological conditions. Quantification of the canopy leaf area index (LAI) and its spatial distribution provides an avenue to improve the interpretation of remotely sensed data over vegetated areas. The work in the Chapter 4 was carried out to test existing vegetation indices for LAI and crop height prediction from remotely sensed data. One of the main conclusions of this study is the important role of modelling of canopy. Moreover, these crop canopy models are essential to the development of predictive algorithms that can not be efficiently designed from measurements and observations in the field and/or laboratory. Such an approach of algorithm development from purely simulated data, together with its successful application to real remotely sensed data holds a strong potential for operational quantification of canopy

parameters. Models produced from the modeling procedure for LAI and CH cover the whole crop cycle and can serve as a basis for developing satellite-based monitoring systems. Correlation coefficients were found to be very high, even higher of those reported in the literature, illustrating the strength of these models. The models have also shown high accuracy when tested in field scale which is very important in practical applications.

6.2.3. Application of SEBAL and Penman-Monteith adapted to satellite data algorithms

The direct application of the two algorithms has shown that there is a statistically significant difference between the results of the two algorithms. The results have indicated that if the two methods are applied directly, then there will be a deviation on the results. While they have the same background on theory (energy balance theory) they use a different approach for estimating ETc, although they should provide identical results. Thus, the models – algorithms must be modified to provide more accurate results.

6.2.4. Modification of SEBAL and Penman-Monteith adapted to satellite data algorithms

Employing the semi-empirical models and integrating them into the algorithm sequence, the algorithms have responded with high accuracy results. The significant difference reported in the direct application of the two algorithms has been diminished. The procedure has shown that for the best possible results the ETc algorithms must be modified with ground data regarding crop canopy factors (Figure 6.1).

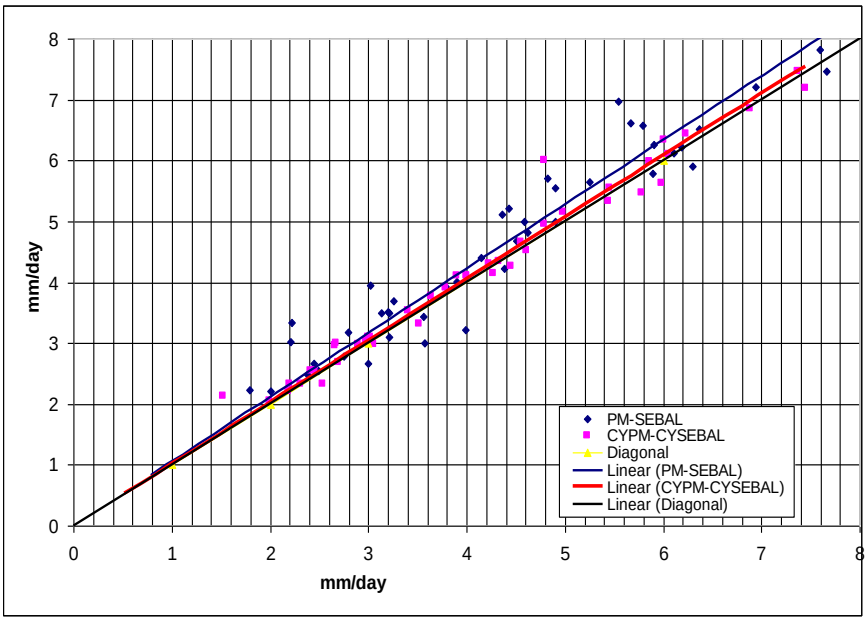

Figure 6.1. Statistical difference of classic (PM-SEBAL) and modified (CYPM-CYSEBAL) algorithms shown graphically

What is also concluded regarding the procedure is that when employing the specific method, a different crop canopy model for each crop should be used unlikely to the direct (classic) application where a single crop model is used for all the crops. That means extra work since for each satellite image ETc values of one crop can be retrieved.

6.3. Thesis original research contribution

Thesis has provided to scientific community original work which could be employed from other researchers for strengthening and broadening of their work. The development of spectral signatures of each crop for their whole phenological cycle is innovative since it has never been referred in literature for spectral signatures of each phenological stage. A single value for each crop may be given but never a value of reflectance for all the phenological stages. This very important since these spectral signatures may be used for identifying the specific crops in satellite images (image classification).

The Methodology itself is original and illustrates how researchers can be directed in estimating accurately evapotranspiration. As indicated, through algorithms modification with canopy characteristics it is possible to strengthen the algorithms accuracy and have more accurate results. The methodology can be applied to other countries with similar climatic conditions.

The Thesis has also provided innovative models regarding crop canopy characteristics. These semi-empirical models have been developed using remotely sensed data and ground data time series and can be integrated into the algorithms to support them. For each crop a semi empirical model was developed regarding its crop height and its leaf area index.

Finally the modification of the algorithms, for crop characteristics, is innovative since the specific algorithms were modified for their physical parameters and not for the crop parameters. The specific modifications have filled up the gap in the literature regarding ETc algorithms modifications.

REFERENCES

Aaron M. Beutler, BS and Andrew A. Keller. 1996. Implementation of FAO-56 Penman-Monteith Evapotranspiration in a Large Scale Irrigation Scheduling; Water and Environmental Resources Congress, Anchorage, Alaska.

Agam N., Kustas W.P., Anderson M.C., Li F. and Neale C.M.U. 2007. A vegetation index based technique for spatial sharpening of thermal imagery. Remote Sensing Environ. 107(4): 545-558.

Agapiou A., Papadavid G. and Hadjimitsis D.G. 2009. Integration of wireless sensor network and remote sensing for monitoring and determining irrigation demand in Cyprus. Remote Sensing for Agriculture, Ecosystems, and Hydrology XI, Proc. of SPIE Vol. 7472, 74720F · © 2009 SPIE · CCC code: 0277-786X/09/$18 doi: 10.1117/12.830554.

Agapiou, A., Hadjimitsis, D., Themistocleous, K., Papadavid, G., Toulios, L., 2010. Detection of Archaeological Crop Marks in Cyprus Using Vegetation Indices from Landsat TM/ETM+ Satellite Images and Field Spectroscopy Measurements, Proc. of SPIE Vol. 7831, 78310V.

Ahlrichs, J.S. and M.E. Bauer. 1983. Relation of agronomic and multispectral reflectance characteristics of spring wheat canopies. Agronomy Journal 75: 987– 993.

Ahmad M.D., Turral H., Nazeer A. 2008. Diagnosing irrigation performance and water productivity through Remote Sensing and secondary data in a large irrigation system of Pakistan. AGWAT 2689 No of pages 14.

Alexandridis T. 2003. Effect of scale on hydrological and vegetation parameters estimation using remote sensing techniques and GIS, PhD study, Aristotle University of Thessaloniki, Greece.

Allen R.G., Pereira L.S., Raes D., Smith M. 2000. Crop evapotranspiration. Irrig. and Drain paper No 56.

Allen R.G., Tasumi M. and Trezza R. 2007a. Satellite-based energy balance for mapping evapotranspiration with internalized calibration (METRIC): Model. ASCE J. Irrig. Drain. Eng. 133(4): 380-394.

Allen R.G., Tasumi M. and Trezza R. 2007b. Satellite-based energy balance for mapping evapotranspiration with internalized calibration (METRIC): Applications. ASCE J. Irrig. Drain. Eng. 133(4): 395-406.

Allen R.G. 1996. Assessing integrity of weather data for use in reference evapotranspiration estimation. Irrig. and Drain. Engng. Div., ASCE 122(2): 97-106.

Allen R.G., Pereira L.S., Raes D. and Smith M. 1998. Crop evapotranspiration, guidelines for computing crop water requirements. FAO Irrigation and Drainage Paper 56, Food and Agricultural Organization of United Nations (FAO) Rome, Italy, pp 300.

Ambast S.K., Ashok K, Keshari, Gosain A.K. 2006. Satellite remote sensing to support management of irrigation systems: concepts and approaches. Irrigation and Drainage systems 51:p 25-39.

Anderson K., Milton E.J. and Rollin E.M. 2006. Calibration of dual-beam spectroradiometric data. International Journal of Remote Sensing, 27, 975−986.

Atkinson P.M. and Beisl U. 2001. Correction of bidirectional effects in imaging spectrometer data. Remote Sensing Series, Vol. 37. Zürich, Switzerland Remote Sensing Laboratories, University of Zürich.

Azzali S., Bastiaanssen W.G.M., Menteti M., De Brower H., Meijerink A.M.J., Mza J. and Zevenbergen A.W. 1991. Remote sensing and watershed modeling. Report 48, Wagenigen.

Bannari A., Morin D., Huette A.R. and Bonn F. 1995. A review of vegetation indices. Remote Sensing Reviews, 13, 95-120.

Barbosa P.M., Casterad M.A. and Herrero J. 1996. "Performance of several Landsat 5 Thematic Mapper ™ image classification methods for crop extent estimates in an irrigation district" Int. J. of Remote Sensing, 17(18), pp. 3665-3674.

Baret F., Jacquemoud S., Hanocq J. F. 1993. About the soil line concept in remote sensing, Advances in Space Research, 13, 5, 281-284.

Baret F. and Guyot G. 1991. Potentials and limits of vegetation indices for LAI and APAR assessment, Remote Sens. Environ., 35, 161–173.

Barnes E.M., Sudduth K.A., Hummel J.W., Lesch S.M., Corwin D.L., Yang C., Daughtry C.S.T. and Bausch W.C. 2003. Remote- and ground-based sensor techniques to map soil properties, Photogrammetric Engineering & Remote Sensing, 69(6):619–630.

Bastiaanssen W.G.M., Brito Bos M.G., Souza K.A., Cavalcanti E.B. and Bakker M.M. 1998. Low cost satellite data for monthly irrigation performance monitoring: Irrigation and Drainage systems 15 : p 53-79.

Bastiaanssen W.G.M., Noordman E.J.M., Pelgrum H., David G., Thoreson B.P. and Allen R.G. 2005. SEBAL model with remotely sensed data to improve water-resources management under actual field conditions. ASCE J. Irrig. Drain. Eng. 131(1): 85-93.

Bastiaanssen W.G.M., Menenti M., Feddes R.A. and Holtslag A.A.M. 1998. A remote sensing surface energy balance algorithm for land (SEBAL), part 1: formulation, Journal of Hydrology. 212-213: 198-212.

Bastiaanssen W.G.M. 1995. Regionalization of surface flux densities and moisture indicators in composite terrain, Doctoral thesis, Agricultural University, Wageningen, The Netherlands, pp 273.

Bastiaanssen W.G.M. 2000. SEBAL-based sensible and latent heat fluxes in the irrigated Gediz Basin, Turkey. Journal of Hydrology 229:87-100.

Bastiaanssen W.G.M. and Ali S. 2003. A new crop yield forecasting model based on satellite measurements applied across the Indus Basin, Pakistan. Agriculture, Ecosystems and Environment, 94:321-340.

Bausch, W.C. and Neale, C.M.U. 1987. Crop coefficients derived from reflected canopy radiation: a concept. *Transactions American Soc. Agric. Engin.* **30** (3): 703-709.

Beisl, U. (2001). Correction of bidirectional effects in imaging spectrometer data. Remote Sensing Series, Vol. 37. Zürich, Switzerland Remote Sensing Laboratories, University of Zürich.

Berbel J., Calatrava J. and Garrido A. 2007. 'Water Pricing and Irrigation: A Review of the European Experience', in: Molle, F. and Berkoff, J. (eds). Irrigation Water Pricing: The Gap Between Theory and Practice. CABI: Oxford.

Boegh E., Soegaard H. 2004. Remote Sensing based estimation of Evapotranspiration rates. International Journal of Remote Sensing, Vol.25, No 13, p.2535-2551.

Bojinski S., Schaepman M., Schläpfer D. and Itten K. 2003. SPECCHIO: A spectrum database for remote sensing applications. Computers & Geosciences, 29, 27−38.

Bradley A.B, Jacob W.R., Hermance F.J., Mustard F.J. 2007. A curve fitting procedure to derive inter-annual phenologies from time series of noisy satellite NDVI data, Remote Sensing of Environment, 106 (2), 137-145.

Brest, C.L. and Goward, S.N. 1987. Deriving surface albedo measurements from narrow band satellite data. *Int. J. Remote Sensing* **8** (3): 351-367.

Brown K.W. 1974. Calculations of evapotranspiration from crop surface temperature. Agric. Meteorol. 14: 199-209.

Brown K.W. and Rosenberg N.J. 1973. A resistance model to predict evapotranspiration and its application to a sugar beet field. Agron. J. 65: 341-347.

Brown, L., Jin, M. C., Lablanc, S. G., & Cihlar, J. 2000. A shortwave infrared modification to the simple ratio for LAI retrieval in boreal forests: An image and model analysis. Remote Sens. Environ., 71, 16– 25.

Brown, J.F., Wardlow, B.D., Tadesse, T., Hayes, M.J., and Reed, B.C., 2009. The vegetation drought response index (VegDRI): A new integrated approach for monitoring drought stress in vegetation, *GIScience and Remote Sensing* , 45(1):16-46

Bruegge C.J., Chrien N. and Haner D. 2001. A Spectralon BRF database for MISR calibration applications. Remote Sensing of Environment, 76, 354−366.

Bruggeman A., Hadjinicolaou P., Lange M., Zoumides C., Pashiardis S. and Zachariadis T. 2011. Effect of climate variability and climate change on crop production and water resources in Cyprus, Nicosia, Cyprus (in press).

Brutsaert W., Sugita M. 1992. Application of self-preservation in the diurnal evolution of the surface energy budget to determine daily evaporation. J Geophys Res 97:18377-18382.

Brutsaert W. 1975. On a derivable formula for long-wave radiation from clear skies. Water Resources Res. 11(5): 742-744.

Campbell J.B. 1996. Introduction to Remote Sensing, Second edition, Taylor and Francis, London.

Carlson T.N. and Buffum M.J. 1989. On estimating total daily evapotranspiration from remote sensing surface temperature measurements. Remote Sensing of Environment Vol.29, No. 2: 197-207.

Caselles V. and Delegido J. 1989. Simple model to estimate the daily value of the regional maximum evapotranspiration from satellite temperature and albedo images. International Journal of Remote Sensing Vol. 8, No. 8: 1151-1162, (1987).

Castro-Esau K.L., Sánchez-Azofeifa G.A. and Rivard B. 2006. Comparison of spectral indices obtained using multiple spectroradiometers. Remote Sensing of Environment, 103, 276−288.

Chave P. 2001. 'The EU Water Framework Directive: An Introduction', International Water Association Publishing.

Chavez J.L. and Neale C.M.U. 2003. Validating airborne multispectral remotely sensed heat fluxes with ground energy balance tower and heat flux source area (footprint) functions. ASAE Paper No. 033128. St. Joseph, Mich.: ASAE.

Chavez J.L., Neale C.M.U., Hipps L.E., Prueger J.H. and Kustas W.P. 2005. Comparing aircraft-based remotely sensed energy balance fluxes with eddy covariance tower data using heat flux source area functions. J. Hydrometeorology, AMS 6(6): 923-940.

Chavez P.S., Berlin G.L. and Mitchell W.B. 1977. Computer Enhancement Techniques of Landsat MSS Digital Images for Land Use / Land cover assessment, Proceedings of the sixth Annual Remote Sensing of Earth Resources Conference, 259-276.

Chen, J. M., and Cihlar, J. (1996), Retrieving leaf area index of boreal conifer forests using Landsat TM images. *Remote Sens. Environ.* 55:153–162

Chen J, Pavlic G, L. Brown, J. Cihlar, S. G. Leblanc, P. H. White, R. J. Hall, D. R. Peddle, D. J. King, J. A. Trofymow, E. Swift, J. Van der Sanden, and P. K. E. Pellikka. 2002. "Derivation and validation of Canada-wide coarse-resolution leaf area index maps using highresolution satellite imagery and ground measurements," Remote Sens. Environ. 80, 165–184.

Chiroro D., Milford J., Makuvaro V. 2006. An investigation on the utility of Sunscan in estimating LAI of a sucarcane canopy. Proceed. S. Afr. Sug. Tech. Assesm., p.143-149

Choudhury, B.J., 1994. Synergism of multispectral satellite observations for estimating regional land surface evaporation. Remote Sensing of Environment 49: 264-274.

Chrysoulakis, N.; Abrams, M.; Feidas, H.; Arai, K. 2010. Comparison of Atmospheric Correction Methods Using ASTER Data for the Area of Crete: The ATMOSAT Project. *International Journal of Remote Sensing*, 31, 6347–6385

Clevers J.G.P.W. 1989. The application of a weighted infrared-red vegetation index for estimating leaf area index by correcting for soil moisture, Remote Sensing of Environment, 29, 25-37.

Clevers J.G.P.W. 1988. "The derivation of a simplified reflectance model for the estimation of leaf area index, _Remote Sensing of Environment_, vol 35., pp. 53-70.

Courault D., Seguin B. and Olioso A. 2005. Review on estimation of Evapotranspiration from remote sensing data: from empirical to modeling approaches. Irrigation and Drainage systems 19: p. 223-249.

Crago R.D. 2000. Conservation and variability of the evaporative fraction during the daytime. J Hydrol 180(1–4):173–194.

Crippen R.E. 1987. The regression intersection method of adjusting image data for band rationing, International Journal of Remote Sensing, 8(2), 137-155.

Crist E. P. 1984. A spectral haze diagnostic feature for normalizing Landsat Thematic Mapper data, Proc Eighteenth International Symp Remote Sens Environ, Paris, France 1-5 Oct 1984, 735-744.

Crist E. P. and Cicone R.C. 1984. Application of the Tasseled Cap concept to simulated Thematic Mapper data, Photogrammetric Eng Remote Sens Vol. 50(3), 343-352.

Crist E.P. and Kauth R.J. 1986. The Tasseled Cap demystified, Photogrammetric Eng Remote Sens Vol. 52(1), 81-86.

Curran P. J. Multispectral remote sensing for the estimation of green leaf area index. *Phil. Trans. R. Soc. Lond*. A, 1983, 309, 257-270 .

Curran P.J., Williamson H.D. 1986. Sample size for ground and remotely sensed data. Remote Sensing of Environment, 20, 31-41.

Curran P.J. and Williamson H.D. 1985. The accuracy of ground data used in remote sensing investigations. International Journal of Remote Sensing, 6, 1637–1651.

Cyprus Meteorological Service. 2010. Cyprus average annual precipitation 1901-2008. Available from http://www.moa.gov.cy/moa/MS/MS.nsf/DMLclimet_reports_en/DMLclimet_reports

Cyprus Meteorological Service. 2011. Monthly rainfall in Cyprus during the hydrometeorological year 2008-2009 and 2009-2010. Available from: http://www.moa.gov.cy/moa/MS/MS.nsf/DMLmeteo_reports_en/DMLmeteo_reports

D'Urso G., Querner E.P. and Morabito J.A. 1992. Integration of hydrological simulation models with remotely sensed data: an application to irrigation management. Leuven, Belgium , p:463-472.

D'Urso G., Calera Belmonte A. 2006. Operative approaches to determine crop water requirements from Earth Observation data: methodologies and applications. In D'Urso G., Osann Jochum M.A., Moreno J. (Eds.): Earth Observation for vegetation monitoring and water management", Conference Proceedings Naples. 2005. 9-10 Nov., published by American Inst. Physics, Vol. 852: 14-25.

D'Urso G., Menenti M. 1995. Mapping crop coefficients in irrigated areas from Landsat TM images; Proceed. European Symposium on Satellite Remote Sensing II, Europto, Paris, sett.'95; SPIE, Intern. Soc. Optical Engineering; 2585: 41-47.

D'urso G. 2001. Simulation and management of on-demand irrigation systems: A combined agro-hydrological and remote sensing approach. Doctoral Thesis, Wageningen University. pp 17-20.

Dadhwal V.K., Parihar J.S. and Medhavy T.T. 1996. "Comparative performance of thematic mapper middle-infrared bands in crop discrimination" Int. J. of Remote Sensing, 17(9), pp. 1727-1734.

Dangel S., Kneubühler M., Kohler R., Schaepman M., Schopfer J., Schaepman-Strub G., et al. 2003. Combined Field and Laboratory Goniometer System — FIGOS and LAGOS. International Geoscience and Remote Sensing Symposium (IGARSS), 7, 4428−4430.

Darvishzadeh, R**.,** A. Skidmore, M. Schlerf, C. Atzberger, F. Corsi and M. Cho**.** 2008**.** LAI and chlorophyll estimation for a heterogeneous grassland using hyperspectral measurements. *ISPRS Journal of* Photogrammetry & Remote Sensing 63(4): 409- 426.

Daughtry C.S.T., Kustas W.P., Moran M.S., Pinter P.J., Jr., Jackson R.D., Brown P.W., Nichols W.D. and Gay L.W. 1990. Spectral estimates of net radiation and soil heat flux. Remote Sensing Environ. 32(2-3): 111-124.

Dekker A.G., Malthus T.J. and Hoogenboom, H.J. 1995. The remote sensing of inland water quality, In: Advances in Environmental Remote Sensing (ed. F.M. Danson and S.E. Plummer), Wiley, 123-142.

Demetriou C. and Georgiou A. 2004. 'Management of groundwater resources in Cyprus – Harmonisation with the EU Water Framework Directive', Presentation at the BALWOIS 2004 conference, Ohrid, FYROM.

Duanjun Lu and Jie Song, 2004. A Simplified Atmospheric Correction Procedure for Estimating Surface Temperature from AVHRR Thermal Data, Vol. 41: Issue - 1, p.81-94, DOI - 10.2747/1548-1603.41.1.81

Edward G., Pamela N., Alfredo H. 2010. VI methods for estimating evapotranspiration by remote sensing. Surv Geophys (2010) 31:531–555.

E.E.A. 2007. 'Climate change and water adaptation issues', European Environment Agency: Copenhagen.

Eliades G., Metochis C. and Papachristodoulou S. 1995. 'Technoeconomic analysis of irrigation in Cyprus' (in Greek), Agricultural Research Institute, Nicosia, Cyprus.

Elvidge C.D. and Chen Z. 1995. Comparison of broadband and narrow-band red and near infrared vegetation indices, Remote Sens. Environ. 54, 38–48.

European Communities. 2000. 'Directive 2000/60/EC of the European Parliament and the Council of 23 October 2000 establishing a framework for Community action in the field of water policy', Luxembourg: Official Journal of the European Communities.

FAO. 1998. Crop evapotranspiration – Guidelines for computing crop water requirements. FAO Irrigation and Drainage Papers 56. Food and Agriculture Organization of the United Nations.

Fassnacht, K. S., Gower, S. T., MacKenzie, M. D., Nordheim, E. V., & Lillesand, T. M. (1997). Estimating the leaf area index of north central Wisconsin forest using Landsat Thematic Mapper. Remote Sens. Environ., 61, 229–245.

Feddes R.A., Kabat P., Van Bakel P.J.T., Bronswijk J.J.B. and Halbertsma J. 1988. Modelling soil water dynamics in the unsaturated zone. State of the art. J. Hydrology 100: 69-111.

Foken T. 2006. 50 Years of the Monin-Obukhov similarity theory. Boundary-Layer Meteorology, 119(3), 431 - 447.

Fourty T. and Baret F. 1998. On spectral estimates of fresh leaf biochemistry, International Journal of Remote Sensing, 19(7):1283-1297.

Franklin, S. E., Lavigne, M. B., Deuling, M. J., Wulder, M. A., and Hunt, JR, E. Estimation of forest Leaf Area Index using remote sensing and GIS data for modelling net primary production, International Journal of Remote Sensing, 1997, 18, 3459–3471.

French A.N., Hunsaker D., Thorp K., Clarke T. 2008. Evapotranspiration over a camelina crop at Maricopa, Arizona. INDCRO 5170. No of pages 12.

Funk C., Budde E.M. 2009. Phenologically-tuned MODIS NDVI-based production anomaly estimates for Zimbabwe, Remote Sensing of Environment, 113 (1), 115-125.

Gamon J.A., Rahman A.F., Dungan J.L., Schildhauer M. and Huemmrich K.F. 2006a. Spectral Network (SpecNet) - what is it and why do we need it? Remote Sensing of Environment, 103, 227−235.

Gilabert, M. A., Gandia, S., Melia J. 1996. Analyses of spectral – biophysical relationships for a corn canopy, *Remote Sens. Environ.*, 55, 11– 20.

Giorgi F. 2006. Climate change hot-spots. Geophysical Res. Letters 33, L87070.

Glenn E.P., Huete A.R., Nagler P.L. and Nelson S.G. 2008. Relationship Between Remotely-sensed Vegetation Indices, Canopy Attributes and Plant Physiological Processes: What Vegetation Indices Can and Cannot Tell Us About the Landscape. Sensors, 8, 2136-2160.

Goel, P.K., S.O. Prasher, J.A. Landry, R.M. Patel and A.A. Viau. 2003. Estimation of crop biophysical parameters through airborne and field hyperspectral remote sensing. Transactions of the ASAE 46(4): 1235–1246.

Goetz A.F.H. 1975. Portable field reflectance spectrometer. JPL Technical Report (pp. 183−188). Pasadena, California Jet Propulsion Laboratory, California Institute of Technology.

Gómez-Limón J.A. and Riesgo L. 2004. 'Irrigation water pricing: differential impacts on irrigated farms', Agricultural Economics, Vol. 31, pp. 47–66.

Gouranga K., Harsh N.V. 2005. Phenology based irrigation scheduling and determination of crop coefficient of winter maize in rice fallow of eastern India, Agricultural Water Management, 75 (3), 169-183.

Groeneveld D.P., Baugh W.M. 2007. Correcting satellite data to detect vegetation signal for eco-hydrologic analyses. J Hydrol 344:135–145.

Gu X.F. and Guyot G. 1993. Effect of diffuse irradiance on the reflectance factor of reference panels under field conditions. Remote Sensing of Environment, 45, 249−260.

Haboudance D., Miller J.R., Pattey E., Zarco-Tejada P.J. and Strachan I.B. 2004. Hyperspectral vegetation indices and novel algorithms for predicting green LAI of crop canopies: Modeling and validation in the context of precision agricultural. Remote Sens.Environ., 90, 337-352.

Hadjimitsis D.G., Clayton C.R.I., Retalis A. and Spanos K. 2000. Investigating the potential of using satellite remote sensing for the assessment of water quality in large dams, and irrigation demand, in Cyprus' Proceedings 26th Annual Conference and Exhibition of the Remote Sensing Society, RSS2000 , University of Leicester.

Hadjimitsis D.G., Clayton C.R.I. and Hope V.S. 2004. An assessment of atmospheric correction algorithms through the remote sensing of some reservoirs. International Journal of Remote Sensing, Vol. 25, 18, 3651-3674

Hadjimitsis D.G., Papadavid G. and Kounoudes A. 2008. Integrated method for monitoring irrigation demand in agricultural fields in Cyprus using satellite remote sensing and wireless sensor network, 4th International Conference on Information & Communication Technologies in Bio & Earth Sciences, 18-20 September 2008, Athens, Greece.

Hadjimitsis, D. G.; Clayton, C. R. I., Retalis, A., 2009. The use of selected pseudo-invariant targets for the application of atmospheric correction in multi-temporal studies using satellite remotely sensed imagery. *International Journal of Applied Earth Observation and Geoinformation*, 11 (3), 192-200, doi: 10.1016/j.jag.2009.01.00.

Hadjimitsis D.G., Papadavid G., Agapiou A., Themistocleous K., Hadjimitsis M.G., Retalis A., Michaelides S., Chrysoulakis N., Toulios L. and Clayton C.R.I. 2010. Atmospheric correction for satellite remotely sensed data intended for agricultural applications: impact on vegetation indices, Nat. Hazards Earth Syst. Sci., 10, 89-95.

Hadjimitsis, D. G.; Clayton, C. R. I. 2011. Field Spectroscopy for Assisting Water Quality Monitoring and Assessment in Water Treatment Reservoirs Using Atmospheric Corrected Satellite Remotely Sensed Imagery. *Remote Sens*., 3, 362-377,doi:10.3390/rs3020362

Hiler E.A. and Clark R.N. 1971. Stress day index to characterize effect of water stress on crop yields, Transactions of the American Society of Agricultural Engineering (ASEA) 14:757-761.

Hoedjes J.C.B., Chehbouni A., Jacob F., Ezzahar J. and Boulet G. 2008. Deriving daily Evapotranspiration from remotely sensed evaporative fraction over olive orchard in Morocco. Journal of Hydrology: 53-64.

Huete A.R. 1988. A soil-adjusted vegetation index (SAVI), Remote Sensing of Environment, 25, 295–309.

Huete A.R. and Warrick A.W. 1990. Assessment of vegetation and soil water regimes in partial canopies with optical remotely sensed data. Remote Sensing Environ. 32:155-167.

Huete A.R. 1989. Soil influences in remotely sensed vegetation-canopy spectra. In: Asrar, G. (Ed.), Theory and Application of Optical Remote Sensing. Wiley, New York, pp. 107–141.

Iacovides I. 2005. 'Water resources management and patterns of water use in Cyprus', in: Lange M.A., Poszig D. and Herrmann A. (Eds.), 'Water on Mediterranean Islands – Sustains Course'. Centre for Environmental Research, University of Münster.

Inoue, Y., S. Morinaga and A. Tomita. 2000. A blimp–based remote sensing system for low–altitude monitoring of plant variables: A preliminary experiment for agriculture and ecological applications. *International Journal of Remote Sensing* 21(2): 379– 385.

Idso S.B., Schmugge T.J., Jackson R.D. and Raginato R.J. 1975. The utility of surface temperature measurements for the remote sensing of the soil water status. J. Geophysical Res. 80(21): 3044-3049.

Jackson R.D., Reginato R.J. and Idso S.B. 1977. Wheat canopy temperature: A practical tool for evaluating water requirements. Water Resources Res. 13(3): 651-656.

Jackson R.D., Idso S.B., Reginato R.J. and Pinter Jr, P. J. 1981. Canopy temperature as a crop water stress indicator. Water Resources Res. 17(4): 1133-1138.

Jackson R.D., Clarke T.R. and Moran M.S. 1992. Bi-directional calibration results for 11 Spectralon and 16 BASO4 reference reflectance panels, Remote Sensing of Environment, 40, 231-239.

Jensen J.R. 1996. Introductory digital image processing, Prentice Hall, New Jersey.

Karavokiris and partners. 2010. Water Policy Report 7 on the Implementation of Articles 11, 13 and 15 of the WFD 2000/60/EC. WDD, Nicosia, Cyprus.

Justice, C.O. , Townshend, J.R.G. , Holben, B.N., Tucker, C.J., 1984. Analysis of the phenology of global vegetation using meteorological satellite data, International Journal of Remote Sensing 6 (8). 1271–1318.

Karnieli, A., Kaufman, Y. J., Remer, J., and Wald, A., 2001. AFRI – aerosol-free vegetation index, Remote sensing of environment, 77, pp. 10-21.

Kaufman Y.J. and Tanre D. 1992. Atmospherically resistant vegetation index (ARVI) for EOS-MODIS. IEEE Trans. Geosci. Remote Sens. 30:261–270.

Kauth R.J., Thomas G.S. 1976. The tasseled Cap - A Graphic Description of the Spectral-Temporal Development of Agricultural Crops as Seen by LANDSAT. In Proceedings of the Symposium on Machine Processing of Remotely Sensed Data, Purdue University of West Lafayette, Indiana, 4B,44-51.

Kim H.H., and Elman G.C. 1990. Normalisation of satellite imagery, International Journal of Remote Sensing, 11(8), 1331-1347.

Kimes D.S. and Kirchner J.A. 1982. Irradiance measurement errors due to the assumption of a Lambertian reference panel. Remote Sensing of Environment, 12, 141−149.

Kramber W.J., Morse A., Allen R.G., Tasumi M., Trezza R. and Wright J.L. 2002. Developing surrogate pixels for comparing SEBAL ET with lysimeter ET measurements. Geoscience and Remote Sensing Symposium, 2002, IGRASS '02, 2002 IEEE International, 1, 119-121.

Kross A., Fernandes R., Seaquist J., Beaubien E. 2011. The effect of the temporal resolution of NDVI data on season onset dates and trends across Canadian broadleaf forests, Remote Sensing of Environment, 115 (6), 1564-1575.

Kundzewicz Z.W., Mata L.J., Arnell N.W., Doll P., Kabat P., Jimenez B., Miller K.A., Oki T., Sen Z., Shiklomanov I.A. 2007. Freshwater resources and their management. Climate Change 2007: Impacts, Adaptation and Vulnerability. Contribution of Working Group II to the Fourth Assessment Report of the Intergovernmental Panel on Climate Change, Parry M.L., Canziani O.F., Palutikof J.P, Van der Linden P.J. and Hanson C. E., Eds. Cambridge University Press, Cambridge, UK, 173-210.

Kustas W.P. and Norman J.M. 2000. A Two-Source Energy Balance Approach Using Directional Radiometric Temperature Observations for Sparse Canopy covered Surfaces, Agron J, 92, 847-854.

Kustas W.P., Li F., Jackson T.J., Prueger J.H., MacPherson J.I. and Wolde M. 2004. Effects of remote sensing pixel resolution on modeled energy flux variability of croplands in Iowa. Remote Sensing Environ. 92(4): 535-547.

Kustas W.P., Norman J.M., Anderson M.C. and French A.N. 2003. Estimating subpixel surface temperatures and energy fluxes from the vegetation index-radiometric temperature relationship. Remote Sensing Environ. 85(4): 429-440.

Kustas W.P., Jackson R.D. and Asrar G. 1989. Chapter 16: Estimating surface energy-balance components from remotely sensed data. In Theory and Applications of Optical Remote Sensing, 605-627. G. Asrar, ed. New York, N.Y.: John Wiley and Sons.

Lambert R., Peeters A., Toussaint B. 1999. LAI evolution of perennial ryegrass crop estimated from the sum of temperatures in spring time. Agric. Forest Meteo. 58: 79-92.

Lang A., McMutrie R., Benson M. 1991. Validity of surface area indices of Pinus Radiata estimated from transmittance of the sun's beam. Agric. Forest Meteo. 57: 157-170.

Lawson, M., B. Leavitt, D. Rundquist, N. Emanuel, R. Perk, J. Keck, and M. Hauschild, 2006. Compensating for irradiance fluxes when measuring the spectral reflectance of corals in-situ. *GIScience & Remote Sensing*, 43:2, 181-197

Lee, K.S., W.B. Cohen, R.E. Kennedy, T.K. Maiersperger and S.T. Gower. 2004. Hyperspectral versus multispectral data for estimating leaf area index in four different biomes. *Remote Sensing Environment* 91(3-4): 508–520.

Liang S. 2000. Narrowband to broadband conversions of land surface albedo –Algorithms, Remote Sens. Environ., 76, 213-238.

Lietb H. 1974. Purposes of a phenology book. pages 3-22, in Phenology and seasonality modeling. Springer-Verlag, New York, NY, Ecological Studies 8.

Loukas, A. and L. Vasiliades (2004). "Probabilistic Analysis of Drought Spatiotemporal Characteristics in Thessaly Region, Greece". Natural Hazards and Earth Systems Sciences, 4, 719-731.

Loukas, A., N. Mylopoulos and L. Vasiliades, (2007). "A Modeling System for the Evaluation of Water Resources Management Scenarios in Thessaly". Water Resources Management, 21(10), 1673-1702.

Loukas, A., L. Vasiliades and J. Tzabiras (2008). "Climate Change Impacts on Drought Severity" Advances in Geosciences, 17, 1-7.

Maier S.W. 2000. Modeling the radiative transfer in leaves in the 300 nm to 2.5 μm wavelength region taking into consideration chlorophyll fluorescence - The leaf model SLOPE, PhD Thesis, Deutsches Fernerkundungstagsdatenzentrum, Technische Universidad München, Oberpfaffenhofen (Germany), 110 pp.

Markham B.L. and Barker J.L. 1987. Thematic Mapper bandpass solar exo-atmospheric irradiances, International Journal of Remote Sensing, 8 (3), 517-523.

Markou M. and Papadavid G. 2008. 'Norm Input-Output Data for the main crop and livestock enterprises of Cyprus', Agricultural Research Institute. Nicosia, Cyprus.

Massarutto A. 2003. 'Water Pricing and Irrigation Water Demand: Economic Efficiency versus Environmental Sustainability', European Environment. Vol. 13, pp. 100–119.

Mather P. 1999. Computer Processing of Remotely-Sensed Images, second edition, John Wiley, Chichester, UK.

Mather P. and Koch M. 2011. Computer Processing of Remotely-Sensed Images, fourth edition, John Wiley, Chichester, UK.

McCabe M.F. and Wood E.F. 2006. Scale influences on the remote estimation of evapotranspiration using multiple satellite sensors. Remote Sensing Environ. 105(4): 271-285.

McCloy K.R. 2010. Development and Evaluation of Phenological Change Indices Derived from Time Series of Image Data, Remote Sensing, 2, 2442-2473.

McLoy K.R. 1995. Resource Management information systems, Taylor and Francis, London, 244-281.

Menenti M., Jia L. and Su Z. 2003. On SEBI-SEBS validation in France, Italy, Spain, USA and China. In Proc. Workshop on Use of Remote Sensing of Crop Evapotranspiration for Large Regions. R. G. Allen and W. Bastiaanssen, cochairs. International Commission on Irrigation and Drainage (ICID).

Meneti M., Visser T.N.M., Morabito JAovandi A. 1989. Appraisal of irrigation performance with satellite data and georeferenced information. Irrigation theory and practice, London, :785-801.

Miller D.R., Sammis T.W., Simmons L.J., Gutschick V.P. and Wang J. 2005. Water use efficiency and net carbon assimilation in a mature irrigated pecan orchard. Applied Engineering in Agriculture.

Milton E.J. et al. 2007. Progress in field spectroscopy, Remote Sensing of Environment, doi:10.1016/j.rse.2007.08.001.

Milton E.J., Rollin E.M. 2006. Estimating the irradiance spectrum from measurements in a limited number of spectral bands, Remote Sensing of Environment, 100, 348-355.

Milton E.J., Schaepman M.E., Anderson K., Kneubühler M, Fox N. 2009. Progress in Field Spectroscopy. Remote Sensing of Environment, 113, 92-109.

Milton E.J., Lawless K.P., Roberts A. and Franklin S.E. 1997. The effect of unresolved scene elements on the spectral response, Canadian Journal of Remote Sensing, 23, 3252-256.

Milton E.J. 1987. Principles of field spectroscopy, International Journal of Remote Sensing, 8, 1807-1827.

Minacapilli M., Iovino M., D'Urso G. 2008. A distributed agro-hydrological model for irrigation water demand assessment. Agricul t u r a l water management 95, 123 – 132.

Monteith J.L. 1981. Evaporation and surface temperature. Quarterly J. Royal Meteorological Soc. 107(451): 1-27.

Monteith J.L. and Unsworth M.H. 1990. Principles of Environmental Physics, Second Edition, Butterworth Heinemann. ISBN 0-7131-2931- X.

Monteith J.L. 1965. Evaporation and the environment. In: The state and movement of water in living organisms. 19th Symp. Soc. Biol., pp. 205 – 234.

Moran M.S., Inoue Y. and Barners E.M. 1997. Opportunities and limitations for image-based remote sensing in Precision Crop Management: in RS Environment 61, p 319-349.

Moran M.S., Jackson R.D., Slater P.N. and Teilett P.M. 1992. Evaluation of simplified procedures for retrieval of land surface reflectance factors from satellite sensor output, Remote Sensing of Environment, 41, 169-184.

Nagler P., Cleverly J., Lampkin D., Glenn E., Huete A., Wan Z. 2005a. Predicting riparian evapotranspiration from MODIS vegetation indices and meteorological data. Rem Sens Environ 94:17–30.

Neckel H. and Labs D. 1984. The solar radiation between 3300 and 12500 Å, Solar Physics, 90, 250258.

Newnham G.J. and Burt T. 2001. Validation of a leaf reflectance and transmittance model for three agricultural crop species, in Proc. International Geoscience and Remote Sensing Symposium (IGARSS'01), Sydney (Australia), IEEE, Vol. 7, pp. 2976 -2978.

Nicodemus F.F., Richmond J.C., Hsia J.J., Ginsberg I.W. and Limperis T.L. 1977. Geometrical considerations and nomenclature for reflectance. National Bureau of Standards Monograph, Vol. 160 (pp. 20402) Washington D.C U.S. Govt. Printing Office.

Oetter D.R., Warren B.C., Berterretche M., Maiersperger T.K. and Kennedy R.E. 2000. "Land cover mapping in an agricultural setting using multiseasonal thematic mapper data" Remote Sensing of Environment, 76, pp. 139-155.

Okamoto K. and Fukuhara M. 1996. "Estimation of paddy field area using the area ratio of categories in each mixel of Landsat TM" Int. J. of Remote Sensing, 17(9), pp. 1735-1749.

O'Leary G.J., Connort D.J., White D.H. 1985. A Simulation Model of the Development, Growth and Yield of the Wheat Crop, Agricultural Systems 17, 1-26.

Papadavid G., Agapiou A., Michaelides S. and Hadjimitsis D.G. 2009. The integration of remote sensing and meteorological data for monitoring irrigation demand in Cyprus. Nat. Hazards earth syst. Sciences, 9, 2009-2014.

Papadavid G. and Hadjimitsis D.G. 2009. Spectral signature measurements during the whole life cycle of annual crops and sustainable irrigation management over Cyprus using remote sensing and spectro-radiometric data: the cases of spring potatoes and peas**.** Proc. of SPIE, Remote Sensing for Agriculture, Ecosystems, and Hydrology XI, Vol. 7472, 747215, doi: 10.1117/12.830552.

Papadavid G., Hadjimitsis D., Themistocleous K., Toulios L. 2010. Spectral vegetation indices from field spectroscopy intended for evapotranspiration purposes for spring potatoes in Cyprus, Proc. of SPIE Vol. 7824, 782410.

Papadavid G., Hadjimitsis D.G., Michaelides S. 2011. Effective irrigation management using the existing network of meteorological stations in Cyprus. Advances in Geosciences Journal, 9, 7-16.

Papadavid G., Hadjimitsis D.G., Perdikou S., Michaelides S., Toulios L., Seraphides N. 2011. Use of field spectroscopy for exploring the impact of atmospheric effects on Landsat 5 TM / 7 ETM+ satellite images intended for hydrological purposes in Cyprus, GIScience and Remote Sensing, 48, No 2, p. 280—298, DOI: 10.2747/1548-1603.48.2.280.

Papadavid G, Hadjimitsis D., Toulios L., Michaelides S. 2011. Mapping Potatoes Crop Height and LAI through Vegetation Indices using Remote Sensing, in Cyprus Journal of Applied Remote Sensing 5, 053526 (2011), DOI:10.1117/1.3596388

Penman H.L. 1948. "Natural evaporation from open water, bare soil and grass." Proc. Roy. Soc. London, A193, 120-146.

Penndorf R. 1956. Luminous and spectral reflectance as well as colors of natural objects. U.S. Air Force Cambridge Research Center, Bedford, Massachusetts.

Potter E., Wood J., Nicholl C. 1996. Sunscan Canopy Analysis System, User Manual, Delta-T devices, Cambridge, UK.

Price, J.C. 1992. *Estimating Leaf Area Index from Remotely Sensed Data.* Proc. IGARSS '92 (Houston). Vol. 1. pp. 1500-1502.

Qi J., Kerr Y. and Chehbouni A. 1994. External Factor Consideration in Vegetation Index Development, in_Proc. of Physical Measurements and Signatures in Remote Sensing, ISPRS, 723-730.

Qi, J., Kerr, Y. H., Moran, M. S., Weltz, M., Huete, A. R., Sorooshian, S., & Bryant, R. 2000. Leaf area index estimates using remotely senseddata and BRDF models in a semiarid region. Remote Sens. Environ., 73, 18– 30.

Ramsey E.W. and Jensen J.R. 1990. The derivation of water volume reflectances from airborne MSS data using in situ water volume reflectances, and a combined optimisation technique and radiative transfer mode, International Journal of Remote Sensing, 11(6), 979-998.

Richards John A. and Jia X. 2006. Remote Sensing Digital Image Analysis, Springer book, ISBN: 978-3-540-25128-6, P. 45.

Richardson A.J. and Wiegand C.L. 1977. Distinguishing vegetation from soil background information, Photogrammetric Engineering & Remote Sensing. 43:1541–1552.

Rijtema P.E. 1965. An analysis of actual evapotranspiration. Agric. Res. Rep., 659, Pudoc, Wageningen, pp107.

Roerink G.J., Su B. and Menenti M. 2000. S-SEBI: A simple remote sensing algorithm to estimate the surface energy balance. Physics and Chemistry of the Earth, Part B 25(2): 147-157.

Roerink G.J., Bastiaanssen W.G.M., Chambouleyron J. and Menenti M. 1997. Relating crop water consumption to irrigation water supply by remote sensing. Water Resources Management 11: 445-465.

Rogers D. and Alan M. 2007. An Evapotranspiration Primer. Irrigation Management Series. Kansas.

Rollin E.M., Milton E.J. and Emery D.R. 2000. Reflectance panel anisotropy and diffuse radiation — Some implications for field spectroscopy. International Journal of Remote Sensing, 21, 2799−2810.

Rosenberg N.J., Blad B.L. and Verma S.B. 1983. Microclimate: The Biological Environment. 2nd ed. New York, N.Y.: John Wiley and Sons.

Rossel F. 2001. Changes in recorded precipitation, in Re-Assessment of the water resources and demand of the island of Cyprus. 2002. Water Development Department (WDD) and Food and Agriculture Organization of the United Nations (FAO), Ministry of Agriculture, Natural Resources and Environment, Nicosia.

Rouse J.W., Haas Jr. R.H., Schell J.A., Deering D.W. 1974. Monitoring Vegetation Systems in the Great Plains with ERTS. In: NASA SP-351, 3rd ERTS-1 Symposium, Washington, DC, pp. 309–317.

Running, S. W., and Coughlan, J. C., 1988, A general model of forest ecosystem processes for regional applications. I. Hydrological balance, canopy gas exchange and primary production processes. Ecological Modelling, 42, 125–154.

Santini, A. 1992. Modelling water dynamics in the soil-plant-atmosphere system for irrigation problems. *Excerpta* no. 6. 1991/92.

Sakamoto T., Yokozawa M., Toritani H., Shibayama M., Ishitsuka N., Ohno H. 2005. A crop phenology detection method using time-series MODIS data, Remote Sensing of Environment, 96 (3-4), 366-374.

Schaepman M.E. 2007. Spectrodirectional remote sensing: From pixels to processes. International Journal of Applied Earth Observation and Geoinformation, 9(2), 204−223.

Schott J.R. 1997. Remote Sensing: The image chain approach, Oxford University Press, New York.

Schowengerdt R.A. 1997. Remote Sensing: Models and methods for image processing, second edition, Academic Press, New York.

Schultz G. and Engman E. 2001. Present use and future perspective of remote sensing in hydrology and water management.

Scott R.L., Cable W.L., Huxman T.E., Nagler P.L., Hernandez M., Goodrich D.C. 2008. Multiyear riparian evapotranspiration and groundwater use for a semiarid watershed. J Arid Environ 72:1232–1246.

Seguin B. and Itier B. 1983. Using middy surface temperature to estimate daily evaporation from satellite thermal IR data, Int. J. Remote Sens., 4:371-383.

Serrano, L., I. Filella and J. Penuelas. 2000. Remote sensing of biomass and yield of winter wheat under different nitrogen supplies. Crop Science 40: 723–731.

Shaykewich C.F. 1994. An appraisal of cereal crop phenology modelling, Canadian Journal of Plant Science, 329-341.

Sheeler P. and Bianchi D.E. 1987. Cell and Mollecullar biology. Third edition. John Wiley and sons Inc. Book.

SIWI (Stockholm International Water Institute). 2002. 'Water Management in the Enlarged European Union', Stockholm Water Front Magazine, Stockholm: Stockholm International Water Institute.

Slater P.N. 1980. Remote Sensing: Optics and Optical Systems, Reading, Massachusetts, Adison-Wesley Publishing company, Inc.

Smith M. 1992. CROPWAT, a computer program for irrigation planning and management. Irrigation and Drainage Paper 46, FAO, Rome, Italy.

Socratous G. 2005. 'The Cyprus water pricing policy and the implications of the Water Framework Directive (WFD)', in: Lange, A. M., Poszig, D. and Herrmann, A. (Eds.), 'Water on Mediterranean Islands – Sustains Course', Centre for Environmental Research, University of Münster.

Song, J.; Duanjun, L.; Wesely, M.L. 2003. A simplified Atmospheric Correction Procedure for the Normalized Difference Vegetation Index. *Photogrammetric Engineering & Remote Sensing*, 69, 521–528.

Stancalie G., Nertan A. and Toulios L. 2010. Satellite based methods for the estimation of Leaf Area Index. In "Satellite data availability, methods and challenges for the assessment of climate change and variability impacts on agriculture", Toulios L. and Stancalie G., editors,

© COST Office, ESF. Formalpublisher: Emm. Lavdakis O.E. publishers, Larissa, Greece, p. 49-74.

Stone L.R. and Horton M.L. 1974. Estimating evapotranspiration using canopy temperatures: Field evaluation. Agron. J. 66(3): 450-454.

Su H., McCabe M.F., Wood E.F., Su Z. and Prueger J.H. 2005. Modeling evapotranspiration during SMACEX: Comparing two approaches for local and regional scale prediction. J. Hydrometerology 6(6): 910-922.

Su Z. 2002. The surface energy balance system (SEBS) for estimation of turbulent fluxes. Hydrol. Earth Systems Sci. 6(1): 85-99.

Su Z., Schmugge T., Kustas W.P. and Massman W.J. 2001. An evaluation of two models for estimation of the roughness height for heat transfer between the land surface and the atmosphere. J. Applied Meteorology 40(11): 1933-1951.

Tassan S. 1992. An algorithm for the identification of benhtic algae in the Venice lagoon from Thematic Mapper data, International Journal of Remote Sensing, 13 (150, 2887-2909).

Tasumi M., Trezza R., Allen R., Wright J. 2003. Validation tests on the SEBAL Model for evapotraspiration via satellite: ICID Workshop on Remote sensing of ET.

Tasumi M., Allen R.G. and Trezza R. 2006. Calibrating satellite based vegetation indices to estimate evapotranspiration and crop coefficients. In Proc. 2006 USCID Water Management Conference: Ground Water and Surface Water under Stress: Competition, Interaction, and Solutions. D. Wichelns and S. S. Anderson, eds. Denver, Colo.: U.S. Committee on Irrigation and Drainage.

Teillet P.M. 1986. Image correction for radiometric effects in remote sensing, International Journal of Remote Sensing, 7(12), 1637-1651.

Telis A. and Koutsogiannis D. 2007. Estimation of Evapotranspiration in Greece. PhD Thesis, Athens.

Thenkabail, P. S., Smith, R. B., and De Pauw, E., 1999. Hyperspectral vegetation indices for determining agricultural crop characteristics, CEO research publication series No. 1. Center for Earth Observation, Yale University Press, New Haven, CT.

Thiruvengadachari S. and Sakthivadivel K. 1997. Satellite remote sensing for assessment of irrigation system performance. Research Report 9, IWMI Colombo, Srilanka.

Toulios L., Stancalie G., Savin E., Danson F.M., Struzik P., Dunkel Z. and Mika J. 2010. Satellite-derived NDVI for monitoring climate impacts on European agriculture, Idojaras journal 114, No 3, pp 169-185.

Tiktak, A., and Van Grinsven, H. J. M., 1995, Review of sixteen forest–soil–atmosphere models. Ecological Modelling, 83, 35–53.

Tsouni A. and Koutsogiannis D. 2003. The contribution of remote sensing techniques to the estimation of Evapotranspiration : the case of Greece. PhD Thesis, Athens.

Tucker, C. J., 1979. Red and photographic infrared linear combinations for monitoring vegetation, Remote Sens. Environ. 8:127–150.

UNESCO. 2006. 'Water: a Shared Responsibility', United Nations 2nd World Water Development Report, United Nations Educational: New York.

United Nations. 2002. 'Global Challenge, Global Opportunity: Trends in Sustainable Development', UN Department of Economic and Social Affairs: New York.

Vakakis and Associates. 2010. The consequences of EU accession and the future of the agricultural sector in Cyprus. Department of Agriculture, Ministry of Agriculture, Natural Resources and the Environment, Nicosia.

Van Bussel L.G.J., Ewert F., Leffelaar P.A. Effects of data aggregation on simulations of crop phenology, Agriculture, Ecosystems & Environment, Article in Press.

Waters R., Allen R., Bastiaanssen W., Masahiro Tasumi , Ricardo Trezza. 2002. SEBAL manual. Advanced Training and Users Manual. Unpublished.

Wang L., Wang W., Dorsey J., Yang X., Guo B. and Shum H.Y. 2005. Real-time rendering of plant leaves, in Proc. ACM SIGGRAPH 2005, Los Angeles (USA), 31 July - 4 August 2005, pp. 167-174.

Watson, D. J., 1947. Comparative physiological studies on growth of field crops: I.Variation in net assimilation rate and leaf area between species and varieties, and within and between years. Annals of Botany, 11, 41–76.

WDD (Cyprus Water Development Department). 2008. 'Total unit cost of irrigation water supplied by the Government through the Government Water Works', Report prepared by a Consortium consisting of WL Delft Hydraulics, ENVECO S.A. and D. Argyropoulos & Associates, under contract No. 39/03/61, Nicosia.

Welles and Norman. 1991. Instrument for measurement of canopy architecture. Agron J. 83: 818-825.

Wiegand, C. J., Richardson, A. J., Escobar, D. E., and Gerber- mann, A. H., 1991. Vegetation indices in crop assessments, Remote Sens. Environ. 35:105–119.

Wilson A.K. 1988. The critical dependence of remote sensing on sensor calibration and atmosphere transparency, In: Proceedings of the NERC 1987 Airborne Campaign Workshop, NERC, Swindon-UK, 29-58.

Yang F., White M., Michaelis A., Ichii K., Hashimoto H., Votava P., Zhu S., Nemani R. 2006. Prediction of continental-scale evapotranspiration by combining MODIS and Ameriflux data through support vector machine. IEEE Trans Geosci Rem Sens 44:3452–3461

Zoumides and Zachariades. 2009. Irrigation Water Pricing in Southern Europe and Cyprus: The effects of the EU Common Agricultural Policy and the Water Framework Directive, Cyprus Economic Policy Review, Vol.3, No. 1, pp. 99-122 (2009) 1450-4561.

Zoumides C. and Bruggeman A. 2010. Temporal and spatial analysis of blue and green water demand for crop production in Cyprus. Report presented at the WDD, 9 Nov. 2010, Nicosia. Available from http://www.cyi.ac.cy/node/698.

References from the Internet

1. http://www.demeter-ec.net

2. http://www.pleiades.es

3. http://www.eea.europa.eu

4. http://www.seos-project.eu

PUBLICATIONS DERIVED AND ASSOCIATED WITH THIS THESIS

JOURNAL PAPERS

1. **Papadavid G**., Agapiou A., Michaelides S. and Hadjimitsis D.G. 2009. The integration of remote sensing and meteorological data for monitoring irrigation demand in Cyprus. Nat. Hazards earth syst. Sciences, 9, 2009-2014.
2. Hadjimitsis D.G., **Papadavid G**., Agapiou A., Themistocleous K., Hadjimitsis M.G., Retalis A., Michaelides S., Chrysoulakis N., Toulios L. and Clayton C.R.I. 2010. Atmospheric correction for satellite remotely sensed data intended for agricultural applications: impact on vegetation indices, Nat. Hazards Earth Syst. Sci., 10, 89-95.
3. **Papadavid G**., Hadjimitsis D. 2010. An integrated approach of Remote Sensing techniques and micro-sensor technology for estimating Evapotranspiration in Cyprus. Agricultural Engineering International: CIGR Journal, Manuscript 1528, Vol. 12, No. 3.
4. **Papadavid G.,** Hadjimitsis D.G., Michaelides S. 2011. Effective irrigation management using the existing network of meteorological stations in Cyprus. Advances in Geosciences Journal, 9, 7-16.
5. **Papadavid G.,** Hadjimitsis D.G., Kurt Fedra and Michaelides S. 2011. Smart management and irrigation demand monitoring in Cyprus, using remote sensing and water resources simulation and optimization. Advances in Geosciences Journal, 9, 1-7, doi:10.5194/adgeo-9-1-2011.
6. **Papadavid G**., Hadjimitsis D., Toulios L., Michaelides L. 2011. Mapping Potatoes Crop Height and LAI through Vegetation Indices using Remote Sensing, in Cyprus Journal of Applied Remote Sensing 5, 053526 (2011), DOI:10.1117/1.3596388.
7. **Papadavid G**., Hadjimitsis D.G., Perdikou S., Michaelides S., Toulios L., Seraphides N. 2011. Use of field spectroscopy for exploring the impact of atmospheric effects on Landsat 5 TM / 7 ETM+ satellite images intended for hydrological purposes in Cyprus, GIScience and Remote Sensing, 48, No 2, p. 280—298, DOI: 10.2747/1548-1603.48.2.280.
8. **Papadavid G.,** Hadjimitsis D. and Toulios L. 2011. Estimating evapotranspiration of groundnuts using remote sensing; a modified SEBAL model under the current Cypriot conditions, HSJ-2011-0055 (submitted for publication).

PROCEEDING PAPERS OF INTERNATIONAL CONFERENCES

1. Hadjimitsis D., **Papadavid G,** and Kounoudes A. «Integrated method for monitoring irrigation demand in agricultural fields in Cyprus using remote sensing and wireless sensor network technology» ; HAICTA Athens proceedings, Vol.3, p.212-220.
2. Hadjimitsis D., **Papadavid G**, Kounoudes A, Themistocleous K. Toulios L. 2008. «Estimating irrigation demand using satellite remote sensing: a case study of Paphos District area in Cyprus» SPIE Cardiff proceedings, Vol. 7107: ISSN 0277-786.
3. Hadjimitsis D.G., Themistocleous K. and **Papadavid G**. 2008. 'The application of atmospheric correction algorithms for monitoring atmospheric pollution using Landsat TM images', Proceedings of SPIE Europe Remote Sensing, 15 - 18 September 2008 University of Wales Institute, Cardiff, UK : Vol. 7104: ISSN 0277-786.
4. Hadjimitsis D.G, Agapiou A. and **Papadavid G**. 2009. Surface reflectance retrieval from Landsat TM/ETM+ images for monitoring irrigation demand in Cyprus. Conference- 29th EARSeL Symposium: Imagine Europe. Chania, Crete, Greece, 15-18/6/2009.
5. **Papadavid G**. and Hadjimitsis D. 2009. Estimating Evapotranspiration using Remote Sensing Techniques for the sustainable use of irrigation water in Agriculture, 29th EARSeL Symposium,, Chania, Crete, Proceedings, DOI: 10.3233/978-1-60750-494-8-166.
6. **Papadavid G**., Hadjimitsis D. 2009. Surface reflectance retrieval from Landsat TM/ETM+ images for monitoring irrigation demand in Cyprus, 29th EARSeL Symposium, Chania, Crete, DOI: 10.3233/978-1-60750-494-8-166.
7. **Papadavid G**. and Hadjimitsis D.G. 2009. Remote sensing as an alternative tool for monitoring water consumption over agricultural areas of Cyprus. Proceedings of the 2nd International CEMEPE & SECOTOX Conference, Mykonos, June 21-26 2009, ISBN978-960-6865-09-1, p.1697-1703.
8. **Papadavid G**. and Hadjimitsis D.G. 2009. Spectral signature measurements during the whole life cycle of annual crops and sustainable irrigation management over Cyprus using remote sensing and spectroradiometric data: the cases of spring potatoes and peas. Proceedings of SPIE Vol. 7472, 747215,p. 1-10, Cardiff.

9. **Papadavid G.,** Agapiou A. and Hadjimitsis D.G. 2009. Integration of wireless sensor network and remote sensing for monitoring and detrmining irrigation demand in Cyprus. Proceedings of SPIE Vol. 7472, 74720F,p. 1-8,Cardiff.
10. **Papadavid G**. and Hadjimitsis D.G. 2009. Integration of satellite remote sensing, gis, modeling and wireless sensor network for monitoring and determining irrigation demand in Cyprus. EWRA Seventh International Conference, Proceedings 2009, Limassol Cyprus. p. 973-980.
11. **Papadavid G**., Agapiou A., Hadjimitsis D.G., Themistocleous K. 2009. Estimating Evapotranspiration of spring potatoes in Paphos, Cyprus using remote sensing, spectroradiometric and meteorological data. Proceedings of RSPSoc 2009 Annual conference, September, Leicester, UK, p. 289-295.
12. **Papadavid G**., Agapiou A. and Hadjimitsis D.G. 2010. Validation of remote sensing vegetation indices, indented for hydrological purposes, through field spectroscopy, 10thInternational Conference on Meteorology – Climatology and Atmospheric Physics (10thCOMECAP), organized by: The Laboratory of Atmospheric Physics of the University of Patras and the Hellenic Meteorological Society, 15-21/5/2010, University of Patras.
13. **Papadavid G**., Agapiou A., Nisantzi A., Hadjimitsis D.G and Michaelides. 2010. Exploring the need of using existing meteorological stations for the effective monitoring of irrigation demand in Cyprus, 10th International Conference on Meteorology – Climatology and Atmospheric Physics (10th COMECAP), organized by: The Laboratory of Atmospheric Physics of the University of Patras and the Hellenic Meteorological Society, 15-21/5/2010, University of Patras.
14. **Papadavid G**., Hadjimitsis D.G., Themistocleous K., Toulios L. 2010. "Spectral vegetation indices from field spectroscopy intended for evapotranspiration purposes for spring potatoes in Cyprus," Proceedings of SPIE Vol. 7824, 782410.
15. **Papadavid G**., Hadjimitsis D., Agapiou A., Alexakis D. and Papoutsa C. 2011. Irrigation water management using geoinformatics and remote sensing techniques: the case of Mandria, SW Cyprus, Proceedings of 6th EWRA International Symposium, Water engineering and Management in a changing environment, Catania, 1-3 July 2011.
16. Χατζημιτσής Δ., Αγαπίου Α., **Παπαδαυίδ Γ.** 2011. Ταξινόμηση χρήσεων γης για σκοπούς υπολογισμού της εξατμισοδιαπνοής με τη χρήση δορυφορικών δεδομένων

και έλεγχος με τη χρήση επίγειων φασματοραδιομετρικών δεδομένων. 11ο Πανελληνιο Συνέδριο Οπορокηπευτικών, Λεμεσός, Κύπρος.(Poster)

17. **Παπαδαυίδ Γ**., Χατζημιτσής Δ. και Κούντιος Γ. 2011. Η συμβολή της δορυφορικής τηλεπισκόπισης στη διαχείριση του νερού άρδευσης - Τεχνοοικονομική μελέτη. Περιοδικό 'Γεωπονικά' τεύχος 56, Επιστημονικές εργασίες, ISSN 0367 5009.
18. **Papadavid G**., Hadjimitsis D. G., Michaelides S. , Toulios L., Agapiou A. 2012. A comparison of a hydrological and an energy balance model for estimating evapotranspiration of chickpeas at Paphos (SW Cyprus) agricultural area. (Submitted for COMECAP proceedings Athens 2012).
19. Hadjimitsis M.G., **Papadavid G.C.**, Perdikou S., Hadjimitsis D.G., Agapiou A. 2012. Smart management and monitoring of irrigation demand in Cyprus using satellite remote sensing and third generation mobile phones. (Submitted for EARSEL proceedings 2012).

APPENDICES

The attached compact disc contains Appendices 1 to 5. Each Appendix is in a folder/directory.

Appendix 1	Spectroradiometric measurements (including Relative spectral response values for Landsat-5 TM and Landsat-7 ETM+)
Appendix 2	Satellite images for ETc
Appendix 3	SEBAL assisting files (ECXEL files)
Appendix 4	Statistical analysis for models evaluation (SPSS files)
Appendix 5	Statistical analysis for results inter-comparison